Spring 2013

Plant water use and canopy-fog interactions across a land use change trajectory of pasture to pine reforestation in a seasonally dry tropical montane cloud belt

Maria Susana Alvarado Barrientos
University of New Hampshire, Durham

PLANT WATER USE AND CANOPY-FOG INTERACTIONS ACROSS A LAND USE CHANGE TRAJECTORY OF PASTURE TO PINE REFORESTATION IN A SEASONALLY DRY TROPICAL MONTANE CLOUD BELT

BY

MARIA SUSANA ALVARADO BARRIENTOS

BS, Universidad del Valle de Guatemala, 2003

MS, VU University Amsterdam, 2007

DISSERTATION

Submitted to the University of New Hampshire

in Partial Fulfillment of

the Requirements for the Degree of

Doctor of Philosophy

in

Natural Resources and Earth Systems Science

May, 2013

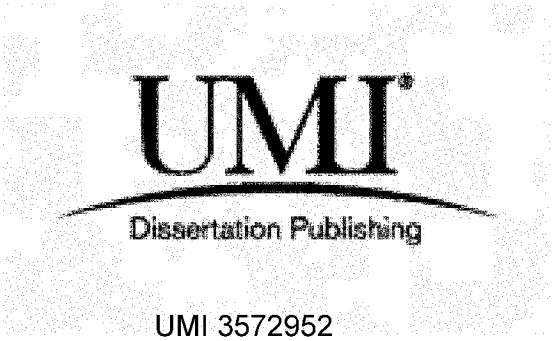

ProQuest LLC
789 East Eisenhower Parkway
P.O. Box 1346
Ann Arbor, MI 48106-1346

This dissertation has been examined and approved.

Dissertation Director, Heidi Asbjornsen,
Associate Professor of Natural Resources

L.A. (Sampurno) Bruijnzeel,
Professor of Land Use and Hydrology,
VU University Amsterdam

Todd E. Dawson,
Professor of Plant Physiological Ecology,
University of California at Berkeley

Mark J. Ducey,
Professor of Forest Biometrics
and Management

Scott V. Ollinger,
Professor of Ecosystem Ecology

Date: 4/29/2013

DEDICATION

I dedicate this dissertation to my grandfather, Julio Vicente *El Sarampagüilo* Barrientos, from whom I undoubtedly inherited the wanderlust gene that moved me to explore and wonder; and to all the mountains and forests I have been fortunate to experience, because while trekking I too, found that "if there is magic in this world, is contained in water" (Loren Eiseley).

ACKNOWLEDGEMENTS

I am indebted to all the mentors and friends I have been fortunate to meet ever since I decided to study forests and water. I am grateful to my dissertation advisor, Heidi Asbjornsen, and to members of my doctoral committee, for all their time, support, guidance, mentoring, enthusiasm and encouragement. I have learned very much from all of you! Thanks to Sampurno Bruijnzeel and Todd Dawson for all your help, knowledge, inspiration, and your sense of humor. Thanks to Mark Ducey, for taking the time to fill a whiteboard with thoughts on radial profiles of sap velocity and statistics. Thanks to Scott Ollinger for mentoring and making me think about modeling ecological processes, which I hope to start putting in practice in the near future. I would like to extend special thanks to Tom Sauer for his support and advice as member of my committee for the first years of my doctorate degree in Iowa State University.

This dissertation would not have been possible without the additional mentoring, training and help I had from postdoctoral researchers under the supervision of my advisor. I am particularly indebted with Friso Holwerda for all the help in the field, many productive discussions, meteorological and canopy interception data and friendship. I would like to also gratefully acknowledge Virginia Hernández-Santana for mentoring, many productive (and unproductive) discussions and sisterhood. This research was possible also thanks to the hard work, support, friendship and great sense of humor of field technicians Adán Hernández Hernández and Sergio Cruz Martínez.

Many other people contributed to this research. To David Bouck, Laura Luna Maira and Rosalinda Castillo Hernández: Thanks a lot for your help in the field! Thanks

to Martín Gómez Cárdenas and David Williams for help with sapflow equipment and guide the construction of sapflow probes. Special thanks to all the students that meticulously constructed sapflow probes: Agustina Sánchez, Jose Antonio López, Eric Redmond and Lori Andrews. Many thanks to Daniel Geissert, Alberto Gómez-Tagle and Conrado Tobón and Edgar Hincapié for all your help with installing and calibrating soil moisture probes, characterizing soil horizons, and many productive discussions. I would like to acknowledge many other scientists and students I met (some only virtually) along the way and from whom I have learned much too: Lyssette Muñoz-Villers, Greg Goldsmith, Jeff McDonnell, Kelly Caylor, Danilo Dragoni, Vilma Mateos Remigio, Jason Scullion, Floortje van Osch, Reinert Karlsen, Beatriz Marin and Sybil Gotsch.

I would like to gratefully acknowledge the operational support that was provided by the Instituto de Ecología, A.C., Xalapa, Veracruz (Mexico), through Daniel Geissert, Guadalupe Williams-Linera, and Oscar Briones. Also, the support provided by equipment and materials from the VU University Amsterdam (The Netherlands), and from the National Laboratory for Agriculture and the Environment, USDA, Iowa (USA).

Thanks to the Municipality of Coatepec, Veracruz, and the inhabitants of Loma Alta and Tierra Grande for allowing fieldwork in their land properties. Particularly, I would like to extend special thanks to Leonides, Eusebia, Paulina, Sabino and José Luis Martínez for always being welcoming in their home and making my time in the field a great experience.

I am grateful to friends and family for their support and encouragement, even from the distance, and for listening about my research, adventures, complains and many grievances. Thanks specially for being there at particular moments to Vilma Mateos

Remigio, Tim Mitchell, Kathleen Eggmeyer, Katie Jennings, Eric Zentmyer, Alex Guerra, René Zamora, Virginia, Adán, Friso and Lyssette. Thanks to my UNH officemate, Nicholas Warren, for listening all my random thoughts. Double-special thanks to Benjamin Halsey for all your patience and (pretending) interest in my research, but mostly, for making my life easy while I write this. And triple-special thanks to Boily, the dog, for walking along my side, keeping livestock away from precious measuring devices, sitting patiently below my desk, and resting your head in my lap all these years. Thanks to my mother, father, sister, brother and all my family for your love, support, encouragement, and for being always excited to hear about my adventures in the "wild".

Finally, I would like to thank the funding sources that made this work possible: National Science Foundation's Ecosystem Science Panel (grant DEB-0746179 to Heidi Asbjornsen, Todd E. Dawson and Jeffrey J. McDonnell), Consejo Nacional de Ciencia y Tecnología of Mexico (CONACyT grant 106788 to Daniel Geissert), Iowa State University graduate and travel support, the NRESS First Year Fellowship from the Univeristy of New Hampshire, and several travel grants from the Farrington Fund and UNH Graduate School.

TABLE OF CONTENTS

LIST OF TABLES

LIST OF FIGURES

ABSTRACT

PLANT WATER USE AND CANOPY-FOG INTERACTIONS
ACROSS A LAND USE CHANGE TRAJECTORY OF
PASTURE TO PINE REFORESTATION IN A
SEASONALLY DRY TROPICAL MONTANE CLOUD BELT

by

María Susana Alvarado Barrientos

University of New Hampshire, May, 2013

Understanding evapotranspiration (ET) variation associated with land use change is critical for assessing impacts on water resources and improving the applicability of climate models to predict water availability under future climate scenarios. The overall objective was two-fold: i) to examine ET variation associated to a land use change trajectory foreseen to increase in tropical mountains, and ii) to assess fog effects on tree transpiration (E_t) and the potential implications of projected diminishing fog occurrence. An actively grazed pasture (PAS) represented the land use change baseline, and young (YREF) and mature (MREF) *Pinus patula* plantations represented typical reforestation efforts and subsequent local forest management. A combination of process-based measurements of near-surface climate and plant physiology were used to derive rates of E_t and ET over a 1.5-year period in the seasonally dry tropical montane cloud belt of central Veracruz, Mexico. Four stand-alone articles are presented. In the first chapter, sap

velocity radial profiles are studied in detail as a critical initial step in up-scaling point measurements to whole-tree sapflow and deriving reliable estimates of stand-level E_t. The second chapter presents ET estimations for the three land cover types. Ranking of ET normalized by available energy (net radiation) was: PAS (0.80) = YREF (0.80) > MREF (0.42). Results suggest that in this high radiation and non-water limited environment, planting *P. patula* on former pasture uplands would not result in substantial increases in ET after >10 years of planting. Next, the E_t suppression effect of fog was examined in the third chapter. Given relatively low fog frequency under current climate, if all fog occurrences are replaced by overcast conditions, the potential change in annual E_t for YREF was estimated as a 2% increase; for sunny conditions, the increase was 17%. Lastly, in chapter 4, examination of nighttime E_t in relation to the dynamics of fog occurrence revealed a slight increase in hourly rates during dry nights following fog events. These findings suggest that climate change-related decreases in dry-season precipitation, more than diminishing fog occurrence alone, presents a worrisome prospect for the study area due to potential reductions in soil water reserves.

INTRODUCTION

Ecosystems of tropical montane regions vary widely in appearance, structure and composition not only due to gradients of microclimate, edaphic conditions and natural disturbances (Bruijnzeel et al., 2011; Martin et al., 2007), but also due to past and present human intervention (Foster et al., 2003). Consequently, these landscapes are typically patchy, consisting of different types of montane forests of varying degrees of conservation or regeneration, pastures, crops and agroforestry systems, tree plantations, and human settlements (Aide et al., 2010; Muñoz-Villers and Lopez-Blanco, 2008; Sarmiento and Frolich, 2002; Williams-Linera, 2007). The structure and species composition of a particular land cover has a substantial influence on the magnitude and rate of water moving through the soil-plant-atmosphere continuum; consequently, the replacement of one land cover with another may modify the fluxes of water and energy (Lambers et al., 2008; Monteith and Unsworth, 2007).

There are multiple potential consequences of land-cover alterations at different scales. For instance, the amount of precipitation available for infiltration, runoff production, and ultimately, for streamflow generation, is affected by the magnitude of total plant water use of a certain land cover (evapotranspiration –ET), as the hydrological cycle is intrinsically coupled to vegetation (Shuttleworth, 2012). Also, latent heat (i.e. ET in units of heat flux density) is a major driver of climate (Andre et al., 1989; Niyogi et al., 2009; Pielke et al., 1998). Drastic alterations in structure and species composition may lead to important changes in surface net radiation and its partitioning into latent and sensible heat flux, as well as changes in the aerodynamic roughness of the land surface

(Monteith and Unsworth, 2007), ultimately impacting climate forcing. The anthropogenic influence on regional and global climate via land-use changes is much less understood than that from the changes in the chemical composition of the atmosphere (Bonan, 2008; IPCC, 2007), and consequently, poorly taken into account in climate change models (Pielke et al., 2011; Pitman, 2003).

Therefore, understanding the variation in ET associated to alterations in land use is critical not only for the assessment of land-use change impacts on water resources (Bosch and Hewlett, 1982; Farley et al., 2005; Zhang et al., 2001) but also to elucidate the influence and feedbacks of land-use change on the weather and climate (Pielke et al., 2011; Pitman, 2003) and, ultimately, improve predictions of water availability scenarios (Jackson et al., 2001). Moreover, without reliable estimates of ET for different land covers at the same operational scale that land management practices are conducted (i.e. parcel-scale), it is not possible to develop local and sound land management policies (Betts, 2000; Calder, 2007; Kaimowitz, 2005; Tallis et al., 2008).

While in principle, the processes that drive and limit ET given a set of land surface characteristics are well understood, predicting changes in ET associated with land-cover variation is complex in practice (Zhang et al., 2010). Surface parameters required by models are oftentimes applied to a wider range of vegetation conditions from which they were derived in the first place, increasing prediction uncertainty particularly for tropical and mountainous regions (Zhang et al., 2010), from where hydrometeorological and plant physiological data are mostly lacking (Manley and Askew, 1993). Furthermore, the lack of local ground data limits the validation of modeling results (Pielke et al., 2011).

On the other hand, ET and its components (i.e. plant transpiration and the evaporation of precipitation intercepted by vegetation and soil surfaces) are also affected by prevailing weather conditions (Shuttleworth, 2012). Frequent immersion in ground-level clouds, or fog, is a ubiquitous feature of ecosystems located within mountain cloud belts (Bruijnzeel et al., 2010). The direct hydrological effect of fog on the water budget of forest ecosystems (i.e. cloud water canopy interception) has been researched extensively (cf. Bruijnzeel et al., 2011; cf. Giambelluca and Gerold, 2011), but the indirect effects of foggy conditions, such as the suppression of plant transpiration, has been largely overlooked and not routinely quantified. This restricts a complete understanding of the net hydrological effect of fog. Also, it limits the understanding and predictability of the consequences of the projected reductions in ground-level cloud immersion under future drier and warmer climate in tropical montane regions (Barradas et al., 2010; Karmalkar et al., 2011; Lawton et al., 2001; Richardson et al., 2003; Van der Molen et al., 2006; Williams et al., 2007).

Given the importance of generating data and analyses that advance the understanding of complex ecohydrological interactions in tropical montane ecosystems, the purpose of the present dissertation was twofold: (i) **to examine the variation of ET associated to a land-use change trajectory foreseen to increase in tropical uplands**; **and** (ii) **to assess the effect of fog occurrence on tree transpiration and the potential implications of the projected diminishing cloud immersion**. The seasonally dry tropical montane cloud belt of central Veracruz, eastern Mexico, was selected as the study area because most attention has been given to ecosystems in wetter tropical cloud belts (e.g. Costa Rica, Hawaii, and Puerto Rico; cf. Bruijnzeel et al., 2010). Also because

understanding the hydrological impacts of both land-cover and climate change are very important for sites that present seasonality with respect to rainfall. For the particular case of the study area, 80% of annual precipitation falls during 6 months of the year (May–October) and fog occurs more frequently during the dry season (Nov–April; Holwerda et al. 2010). Thus the present study area also enables the exploration of the notion that the hydrological role of fog may be more important for seasonally dry environments compared to wetter (Bruijnzeel et al. 2010).

The conversion of old-growth forests to pasture or other crops such as shaded coffee plantations has been the main land-use change trajectory in tropical uplands (Aide et al., 2010; Muñoz-Villers and Lopez-Blanco, 2008). During the past decade however, there has been an increase, albeit small, of forested land cover worldwide (FAO, 2010). Natural forest recovery in tropical uplands is limited mainly by invasive species competition (e.g. grasses and ferns) and poor seed dispersal of native tree species (c.f. (Aide et al., 2010; Muniz-Castro et al., 2006). For this reason, the main tool available to restore degraded tropical lands is tree planting, as it has the potential to catalyze forest regeneration (Parrotta et al., 1997; Pedraza and Williams-Linera, 2003). Indeed, tree planting is actively promoted as a solution for a wide variety of problems, from improving water quality and supply to mitigating climate change and alleviating rural poverty (Calder, 2007; Kaimowitz, 2005; van Dijk and Keenan, 2007). Therefore, tree plantations are foreseen to expand in tropical uplands with the increase of direct incentive programs (e.g. Pro-Arbol in Mexico; Valtierra Pacheco et al., 2008) including the establishment of plantations in the context of markets to offset carbon emissions (SEMARNAT, 2010; UNEP, 1998). Other important drivers of the expansion of forested

land cover in tropical montane regions are land-use policies and/or socio-economic causes that incentivize abandonment of pasture and crop lands and eventual forest regeneration (e.g. Aide and Grau, 2004; Calvo-Alvarado et al., 2010; Grau et al., 2003).

In the case of Mexico, the most widely used tree species in reforestation projects are conifers, and in central Veracruz, this includes the Mexican weeping pine (*Pinus patula*; Valtierra Pacheco et al., 2008). Pine reforestations established on former introduced pasture in the uplands are foreseen to expand (Carabias et al., 2007; Sánchez-Velásquez et al., 2009; SERMARNAT 2010) and stakeholders from lower-lying areas are eager for information about the hydrological impacts of these plantations (Pérez-Maqueo et al., 2005; Scullion et al., 2011). Energy and water fluxes from old-growth lower montane cloud forest (LMCF), 20-year-old regenerating LMCF, and shaded coffee plantation have been examined recently (Goldsmith et al., 2012; Holwerda et al., 2013; Holwerda et al., 2010; Muñoz-Villers et al., 2012; Muñoz-Villers and McDonnell, 2012). With the aim to add to this growing body of knowledge and improve our understanding of the hydrological consequences of different land-use change trajectories in tropical montane regions, the present study focused on the estimation of ET from pasture and *P. patula* plantations at two different stages of stand development: a young (10-year-old) reforestation near canopy closure, and a mature heterogeneous forest dominated by *P. patula* (canopy trees age ranging from 17 to >60 years). Both forested sites were formerly managed as pasture for grazing livestock with some scattered trees as remnants of previous old-growth forested land cover. The approximate years since establishment of the current land use for the mature pine forest was 30 years (local inhabitants, pers. comm.). This work also addresses the response of tree transpiration to the occurrence of

ground-level cloud occurrence (or fog). Specifically, the suppressive effect of fog occurrence and the effect of prior fog immersion on nocturnal transpiration rates was assessed in detail for the young pine reforestation.

The present dissertation is organized as a collection of four independent research articles that build upon each other and address specific questions and objectives under the overarching twofold purpose described above. In Chapter 1, the characterization of sap velocity radial profiles for *P. patula* is presented as a critical initial step in up-scaling point measurements of sap velocity to whole-tree sap flow. This in turn, is necessary to reliably estimate stand-level tree transpiration, which is generally the main component of ET from forests (Shuttleworth, 2012). Chapter 2 addresses the estimation and comparison of ET across the land-use change trajectory of pine reforestation. Next, the effect of fog on stand-level tree transpiration is examined in Chapter 3. The implications of a projected rise of the cloud base on the annual amounts of transpiration from a young pine plantation are also addressed in Chapter 3. The interesting phenomenon of nighttime pine transpiration was examined in the context of diminishing fog occurrence and presented in Chapter 4. Lastly, a series of supplemental information and figures are presented in the Appendix.

CHAPTER I

VARIABILITY OF THE RADIAL PROFILE OF SAP VELOCITY IN *PINUS PATULA* FROM CONTRASTING STANDS WITHIN THE SEASONAL CLOUD FOREST ZONE OF VERACRUZ, MEXICO [1]

Abstract

Characterizing the variability of the radial profiles of sap velocity (v_S) is a critical step to improve upscaling point measurements of v_S to whole-tree sap flow. One promising approach is the use of a probability distribution function (pdf) to model radial profiles of v_S, because shape parameters could potentially be generalized to trees of the same species based on the premise that the shape remain consistent regardless of the tree size and age, and over time, even though the magnitude of v_S may vary with environmental conditions. The objective of this study was to characterize and assess the variability of the radial profile and to examine the validity of the premises underlying this approach by applying it to *Pinus patula*, one of the most widely planted tree species in the uplands of central-eastern Mexico. We measured v_S with the Heat Ratio method at various sapwood depths in 18 *P. patula* trees with a dbh between 7.3-59.7 cm and age between of 10-34 years, over a period of 1.5 years. Trees were growing in two stands: a mature forest stand and a young plantation. By fitting the Beta-pdf to hourly radial profiles of v_S, we derived a

[1] Reproduced (with permission) from copyrighted material:
Alvarado-Barrientos, M.S., Hernández-Santana, V., Asbjornsen, H., 2013. Variability of the radial profile of sap velocity in Pinus patula from contrasting stands within the seasonal cloud forest zone of Veracruz, Mexico. *Agricultural and Forest Meteorology* 168: 108-119

lumped shape parameter (ρ) to denote the radial position relative to sapwood depth with average v_S and a scaling parameter (c_S). The typwas unimodal, asymmetrical and with peak v_S generally within the outermost 20-33% of the sapwood depth. However, tree-to-tree variability in ρ was considerable among trees within the same stand and also across stands. Long-term and day-to-day variation of ρ was marginal. The hourly dynamics of the radial profile, characterized by c_S, can be explained by a linear combination of incoming shortwave radiation, vapor pressure deficit, the hour of day and their interaction (r^2=0.74). An independent field evaluation confirmed that a radial profile of fixed shape can be effectively used to estimate whole-tree sap flow with relatively low bias (4-26% underestimation) relative to cut-tree water uptake, particularly for trees for which v_S observations covered at least 60% of the sapwood depth. Our findings emphasize the importance of conducting multiple v_S point measurements covering most of the sapwood depth for accurate characterization of the radial profile, and demonstrate the utility of fitting a pdf to point v_S measurements in order to assess the variability of v_S radial profiles as well as to compute sap flow at the whole-tree level.

1. Introduction

Sap flow techniques that use needle-like probes inserted in tree stems using heat as a tracer for sap ascent, such as heat pulse velocity methods (Burgess et al., 2001; Huber and Schmidt, 1937; Marshall, 1958) are now widely used to derive estimates of whole-tree sap flow, which in turn, is used to upscale transpiration to the stand level (Asbjornsen et al., 2010; Čermák et al., 2004). Whole-tree sap flow is computed by multiplying sap velocity (v_S) by the cross-sectional area of sapwood at the measurement

height in the stem. As v_S typically varies radially with sapwood depth (Cohen et al., 2008; Gebauer et al., 2008; Jimenez et al., 2000; Mark and Crews, 1973; Phillips et al., 1996), an accurate characterization of the radial profile of v_S is critical to scaling point measurements to the whole-tree level (Delzon et al., 2004; Ford et al., 2004b; Hatton et al., 1990; Nadezhdina et al., 2002; Wullschleger and King, 2000), and ultimately, to stand transpiration (Fiora and Cescatti, 2006; Hatton et al., 1995; Poyatos et al., 2007). Several approaches have been used to characterize the radial variability of v_S and to integrate the radial profile across the sapwood depth and around the stem, including an area-weighted average (Hatton et al., 1990; Pausch et al., 2000) and a curve to fit several point measurements of v_S (e.g. a second or higher degree polynomial (Cohen et al., 2008; Edwards and Warwick, 1984), a combination of a modified growth function with a decay function (Luttschwager and Remus, 2007), a four-parameter Weibull probability density function –pdf- (Gebauer et al., 2008; Kubota et al., 2005), a three-parameter Gaussian-pdf (Ford et al., 2004b), or the Beta-pdf (Caylor and Dragoni, 2009)).

Recently, an analytical framework was presented in which instantaneous v_S at any point into the sapwood is defined as the product of a time-invariant and a time-varying term related to a species' specific hydraulic architecture of the trunk and to bulk atmospheric and soil moisture controls on transpiration, respectively (Caylor and Dragoni, 2009). This approach uses a bounded function, namely the Beta-pdf, to characterize the radial profile of v_S and provide parameters to describe the time-invariant and time-varying terms. Furthermore, these authors proposed that the shape of the radial profile (i.e. the time-invariant term), among trees of the same species, is consistent if the location into sapwood of v_S measurements is expressed in normalized units relative to the

tree's size. They presented evidence of the consistency of the shape of the radial profile among trees of varying sizes for two diffuse porous species (Caylor and Dragoni, 2009). Furthermore, Dragoni et al. (2009) showed that the time-variant term of the radial profile can be strongly correlated to meteorological conditions such as atmospheric water demand and local soil water availability. An important implication of this framework is that a characteristic radial profile can potentially be generalized to trees of the same species regardless of their size, and the short-term dynamics of the radial profile modeled with meteorological variables. Moreover, it opens the possibility to model the radial profile, and consequently whole-tree sap flow, for periods of time with few or no v_S point data. Given its promising applications, this framework deserves further examination, not only for more species including conifers, but also to determine the extent to which the 'time-invariant' component remains invariant over longer periods of time, which was not addressed in (Caylor and Dragoni, 2009). Furthermore, an independent evaluation of sap flow estimates at the whole-tree level derived from this approach has not been reported.

Pinus patula is one of the most widely planted tree species in reforestation projects in the uplands of southeastern Mexico, a trend that has sparked concern over potential hydrological impacts of extensive plantations on downstream water supply (Muñoz-Villers et al., 2012). Assessing such hydrologic impacts requires accurate information about whole-tree and stand water use of this species, currently lacking. Earlier sap flow studies on *P. patula* plantations were conducted in South Africa (Dye et al., 1991; Dye et al., 1996) and presented some insight into the radial profile of v_S for this species. However, temporal and spatial variation was confounded in the characterization

of the radial profile as short-term dynamics were largely ignored (Nadezhdina et al., 2002) casting doubts on the radial shape of v_S reported for this species.

With the present study we aimed to characterize the radial profile of v_S in *P. patula* within its native distribution range in Mexico, assess its variability and to determine whether a simple model can be formulated to estimate whole-tree sap flow based on a characteristic radial profile and measured meteorological variables. Specifically, we addressed the following questions:

- Is there a consistent shape amongst the radial profiles of v_S in *P. patula* trees of differing sizes/ages and stand development stage, and over an extended time period?
- Does the shape of the radial profiles characterized with point observations of v_S made in the outermost portion of the sapwood change when deeper observations are included?
- To what extent do meteorological conditions, namely incoming shortwave radiation (R_s) and vapor pressure deficit (D), explain the short-term (hourly) dynamics of the radial profile?
- How do whole-tree sap flow estimates derived by assuming a variable or fixed radial profile shape compare to direct empirical measurements of water uptake?

2. Materials and Methods

2.1 Study sites and sample trees

The study was conducted within the seasonal tropical montane cloud forest zone of central Veracruz, Mexico (19° N, 97° W), which has a temperate humid climate with an

average temperature of 12-18°C and a mean annual precipitation (MAP) of 2000-3000 mm (García, 1973). Approximately 80% of MAP occurs between May and October consisting of frequent showers and thunderstorms, while a relatively dry season occurs between November to April characterized by an alternation of stable dry weather and cloud immersion events consisting of mixtures of rain, drizzle and fog (Holwerda et al., 2010). A detailed description of the climate of this zone can be found in Holwerda et al. (2010) and Goldsmith et al. (2012).

Our sample of *Pinus patula* trees consisted of 18 individuals: 10 trees from a young plantation (dbh range: 7.3-11.8 cm), and 8 from a mature forest stand dominated by *P. patula* (dbh range: 28.7-59.7 cm). The young stand (19.4931° N, 97.0422° W; 2,180 m a.s.l.) was planted in 2000 within the natural reserve "La Cortadura" of the Municipality of the city of Coatepec, Veracruz, with a density of 3,783 stems ha^{-1} and had not received any thinning treatments at the time of this study. Formerly this site was covered with mature lower montane cloud forest, locally known as "bosque mesófilo de montaña" (García Franco et al., 2008). Further topographical and soil characteristics of this site are provided by Muñoz-Villers et al. (2012). The mature stand (19.5054° N, 97.0559° W; 2470 m a.s.l) was located near the locality of "Tierra Grande", approximately 2 km from the young stand. The original pine-oak forest was cleared approximately 70 years ago and managed as pasture for grazing livestock with some remnant trees (*P. patula, P. pseudostrobus* and *Quercus* spp.) and later was both reforested with *P. patula* and allowed to regenerate naturally (local inhabitants, personal communication). At the time of this study, the mature stand was comprised of multi-cohort patches of *P. patula* and other species, predominantly *P. pseudostrobus* and

Quercus spp., with an estimated density of 580 stems ha^{-1}. The two study sites had similar aspect (South-East) and slope (20-26°). Sample trees were located within a 20 m radius at each study site, with the exception of 3Y and 4Y (located ca. 300 m from other young trees, but planted the same year and at the same elevation) and 18M and 20M (located ca. 100 m from other mature trees and located at the same elevation).

2.2 Meteorological measurements

Meteorological stations were installed in open grassy and shrubby patches with SE exposure and located at 350 m and 450 m from the young and mature stands, respectively. The following parameters were available as 10 min averages from 30 s sampling intervals: i) incoming shortwave radiation (R_s) [W m^{-2}] measured with a CMP3 pyranometer (Kipp & Zonen, Netherlands) at 3 m above the ground; ii) vapor pressure deficit (D) [kPa] calculated as the difference between actual vapor pressure derived from psychrometric data (dry- and wet-bulb thermocouples, VU University, Netherlands) and saturation vapor pressure derived as in Lowe (1976) using air temperature from a HMP45C (Vaisala, USA) installed at a height of 2m; iii) precipitation [mm] measured with a tipping bucket rain gauge (ARG100, Environmental Measurements) installed at a height of 1.15 m; and iv) horizontal visibility [m] obtained with a Mini Optical Fog sensor (Optical Sensors, Sweden) installed at 3m above the ground. The occurrence of cloud immersion (or fog) was defined as instances with visibility < 1000 m (Glickman, 2000), and in order to avoid very short and isolated occurrences, cloud immersion events were defined as periods with at least 4 observations with visibility < 1000 m within 6 consecutive 10-min observations (Tardif and Rasmussen, 2007).

2.3 Sap velocity measurements

The Heat Ratio method (Burgess et al., 2001) was used to obtain point measurements of v_S within the sapwood of the sample trees. Probe sets were custom-made in the laboratory following (Burgess et al., 2001). For the entire study period (Nov 2008 – May 2010) all trees had one probe set with three copper-constantan thermocouples, such that heat pulse velocity was measured at three depths into the sapwood (0.5, 1.7 and 3 cm from the cambium). These probe sets were installed into the stem at breast height (1.40 m from the ground) at the north facing side and following standard installation guidelines as described in Hernández-Santana et al. (2010). To avoid introduction of bias due to long-term wounding effects, fresh installations where conducted every three months always on the north facing side of each stem, but 10 cm above or below and 3-5 cm to the left or right of the previous probe set (hereafter referred to as "Dataset I"). A second dataset (hereafter "Dataset II") was obtained for a period of two weeks during May 2010 with longer probe sets installed into the stem of mature trees (with thermocouples at 3.4, 4.6, 5.8 and 7.1 cm from the cambium), 5 cm to the right and 10 cm below the north side probe set. Both the original and longer probes were simultaneously measuring, as the purpose of Dataset II was to obtain v_S data at deeper sapwood depths than those provided by Dataset I in larger individuals. Due to probe malfunction, not all thermocouple positions of these larger probes provided data for all mature trees, thus the total number of v_S data points in Dataset II varied per tree (i.e. one to four additional points, with the exception of no additional points for tree 20M; Fig. 1.1). "Dataset I+II" hereafter refers to all available v_S data points within the sapwood of a mature tree. For further analysis, the

position into the sapwood where v_S point observations were expressed relative to tree size, in this case, the sapwood depth (Fig. 1.1).

Each individual thermocouple junction circuit was connected with a 10 m long extension cable to AM16/32 multiplexers and CR1000 dataloggers (Campbell Scientific, USA).

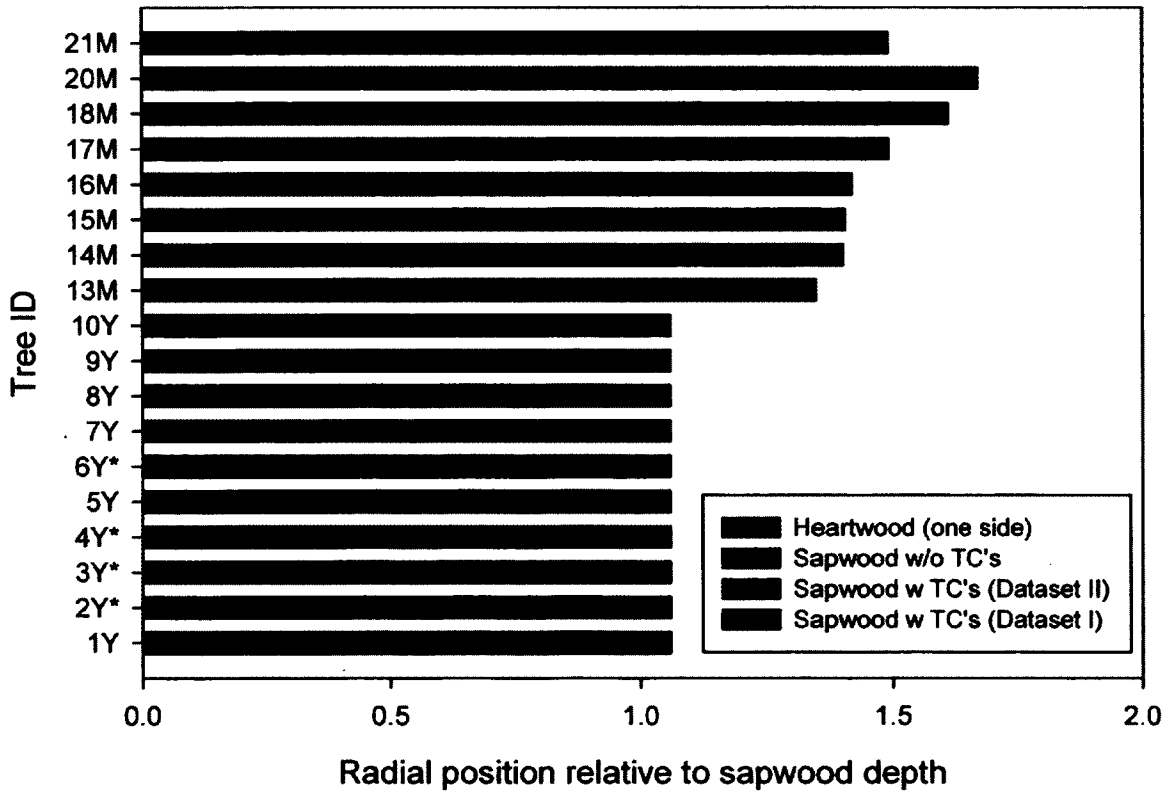

Figure 1.1 Radial position of sap velocity point measurements within the sapwood of sample *Pinus patula* trees. ID = tree identification were Y=young, M= Mature and * = cut-tree; TC's = thermocouples. Sapwood depth is depicted in gray, where light and dark gray show depth with and without sap velocity point observations, respectively. Hatched light gray area shows the additional extent of point measurements in mature trees that was achieved by installing longer probes for a short period of time (Dataset II). Heartwood depth (one sided) is shown in black. Sapwood and heartwood depths are normalized by sapwood depth such that zero is the cambium-sapwood interface and one is the sapwood-heartwood interface.

The datalogger recorded 10-min averages of initial temperature (n = 8 in 10 sec), controlled a heater bank to send a heat pulse of 3 sec, and recorded average temperature after the heat pulse (n = 25 in 40 sec). These data were then processed to compute heat pulse velocity using the nominal value of thermal diffusivity of green wood: 2.5 x 10^{-3} cm^2 h^{-1} (Marshall, 1958; Burgess et al., 2001), as well as to correct for "true zero (see below), verify misalignment, correct for wounding effects, and finally convert to v_S following Burgess et al. (2001). Wood density and water content of the sapwood were measured empirically from sapwood cores as in Burgess et al. (2001). Following completion of the measurement period, the reference heat pulse velocity (or "true zero") was determined by cutting the flow of sap by drilling a hole of 11.5 mm diameter with an increment borer (Suunto, Finland) a couple of cm above and below the probes and to a depth exceeding the length of each probe. These values and reference heat pulse velocities obtained at the end of cut-tree evaluations (see section 2.5) were used to compute offsets (mean of absolute values: 0.33 cm h^{-1}; 95%CI: 0.17-0.49 cm h^{-1}) to correct all heat pulse velocity data (Burgess et al., 2001; Dawson et al., 2007).

2.4 Characterization of sap velocity radial profiles

We adopted the approach proposed by Caylor and Dragoni (2009) to characterize the v_S profiles using a unimodal and bounded function, the Beta-pdf. As an initial simplification we also assumed circumferential homogeneity of the radial profile. By using a bounded function such as the Beta-pdf, the resulting radial profile is constrained at x = 0 and x = 1, that is, v_S is zero at these locations by definition. We modified Caylor and Dragoni's approach by normalizing the radial locations of v_S point measurements by sapwood depth

rather than by the stem radius (i.e. x = 1 in our case was the sapwood-heartwood interface, not the stem center as in the original approach). We introduced this variant because as pine trees increase in diameter and age, the proportion of radius that is composed of sapwood does not remain constant (Fig. 1.1; Delzon et al. (2004)), and thus the radial pattern of v_S, in principle, would not remain invariable between trees of different sizes relative to the total stem radius as the proportion of non-conducting tissue (heartwood) would increase with tree diameter. Furthermore, Caylor and Dragoni (2009) added an additional zero velocity point at x that, for their analysis, represented the sapwood-heartwood interface relative to the stem center. With our modification we had no other radial position between the cambium-sapwood and the sapwood-heartwood interface in which it was reasonable to assume sap velocity to be zero. Consequently we did not add any additional zero velocity points. Hourly daytime radial profiles of v_S were thus fitted with the non-linear least-squares method to (Eq. (16) in Caylor and Dragoni (2009)):

$$v_S = c_S \ (1 / B(\alpha, \beta)) \ (r / L_S)^{\alpha - 1} (1 - (r / L_S))^{\beta - 1} \quad (1)$$

where r is the radial position of the measurement (i.e. depth below the cambium-sapwood interface at which a thermocouple was placed) [cm]; L_S is the sapwood depth[cm] measured from visual inspection of a core taken at breast height at the end of the study period; c_S is a scaling parameter or the time-variant component of the radial profile of v_S ("stem conductance" *sensu* Caylor and Dragoni (2009)) [cm h^{-1}]; and B is the Beta-pdf with shape parameters α and β [dimensionless]. A lumped shape parameter, ρ, can be derived for each hourly radial profile which denotes the radial location relative to the sapwood depth at which average v_S is found, namely the mean of the Beta-pdf: $\alpha / (\alpha + \beta)$.

In addition, the radial location with peak v_S can be derived, ρ_{max}, from the two shape parameters as the mode of the Beta-pdf: $(\alpha - 1) / (\alpha + \beta - 2)$. We used the Curve Fitting Toolbox of Matlab R2008a (The MathWorks, Inc.) to derive maximum likelihood estimates of α, β and c_S.

2.5 Independent evaluation of whole-tree sapflow estimates

We performed an independent evaluation of whole-tree sap flow estimates to contrast the use of a constant against a variable shape to integrate the radial profile, that is, a constant or variable ρ across trees and seasons, by performing a cut-tree procedure similar as described in Dye et al. (1996). We also used this independent field evaluation to assess the predictive performance of our model of the short-term dynamics of the radial profile of v_S (see section 2.6). Trees 2Y, 3Y, 4Y and 6Y were secured with ropes to nearby trees and a small area surrounding their stem was flooded using a plastic skirt secured to the stem near the ground, and stakes placed away from the stem forming a temporary basin. Shortly before dusk, a sharp hand saw was used to cut the trees under water, and immediately, a bucket was set under the cut stem such that the cut section remained under water. Next, the water level in the bucket was fixed and marked using a metallic pin attached to the wall of the bucket such that its tip was breaking the water meniscus. A plastic cover was used to prevent evaporation from the bucket. While automated v_S measurements were taking place, we used a graduated cylinder to refill the bucket every hour (i.e. replenish the water lost by tree water uptake); since the cylinder was graduated it was possible to measure the volume of water required to bring the water level up to the initial marked level. All trees were cut during a sunny or partially cloudy late-dry season

day (3Y and 4Y on April 24 and May 5, 2009, respectively; 2Y and 6Y on May 12, 2010).

The hourly and total accumulated water depleted from the bucket (Q_B; [L]) was used as an independent evaluation of estimated whole-tree sap flow derived from Heat Ratio probes at corresponding time scales (i.e. hourly instantaneous (F_S; [L h^{-1}]) and cumulative (Q_S; [L]). F_S was calculated using the following expression (Eq. (10) in Caylor and Dragoni (2009)):

$$F_S(t) = 2 \pi L_S^2 (\alpha / (\alpha + \beta)) c_S(t) \quad (2)$$

where all terms are as defined earlier. Q_S was computed as the sum of F_S throughout the evaluation period (7-11 hours).

Three different estimates of F_S, and corresponding Q_S, were computed to be compared with Q_B: i) $F_S\_varshape$ computed using maximum likelihood estimates of α, β and c_S, or in other words allowing the shape of the radial profile to vary fitting the v_S data points as described earlier; ii) $F_S\_fixshape$ using the median radial profile shape of all young trees, that is, a fixed value of ρ, and finding maximum likelihood estimates of c_S; and iii) $F_S\_modeled$ using a fixed value of ρ but in this case using a modeled term c_S from a mixed effects model as described in the following section. Table 1.1 shows the median and ranges of the parameters used to compute these three F_S estimates. Additionally, the area-weighted average of v_S data points (Hatton et al., 1990), which is the simplest approach to integrate the radial profile, was calculated for comparison with Q_B (i.e. F_H and corresponding Q_H).

Table 1.1. Median shape parameters (α, β and ρ) and scaling parameter ranges (c_S) used to compute three different whole-tree sap flow estimates derived from the characterization of the radial profile of sap velocity (v_S) by the Beta-pdf (*F_S_varshape*, *$F_S$fixshape* and *F_S_modeled*). Median absolute deviations are given, when appropriate, between parentheses.

		Tree ID			
		2Y	3Y	4Y	6Y
F_S_varshape	α	1.35 (0.03)	1.84 (0.01)	2.16 (0.09)	1.75 (0.14)
	β	1.70 (0.02)	2.35 (0.01)	2.96 (0.09)	1.97 (0.02)
	ρ	0.44 (0.00)	0.44 (0.00)	0.43 (0.00)	0.47 (0.02)
	c_S [cm h^{-1}]	1.36 - 12.69	4.81 - 9.67	3.97 -30.65	5.25 -11.64
F_S_fixshape	α	1.49	1.49	1.49	1.49
	β	1.87	1.87	1.87	1.87
	ρ	0.44	0.44	0.44	0.44
	c_S [cm h^{-1}]	1.30 - 12.54	4.90 - 9.79	4.14 - 31.72	5.38 - 11.66
F_S_modeled	α	1.49	1.49	1.49	1.49
	β	1.87	1.87	1.87	1.87
	ρ	0.44	0.44	0.44	0.44
	c_S [cm h^{-1}]	1.36 - 12.69	6.49 - 10.63	3.63 - 11.80	4.72 - 11.15

2.6 Statistical analyses

To avoid being affected by outliers, ρ for each sample tree within each dataset was characterized by its median value, and its variability was quantified with the median absolute deviation (MAD). Significant differences of ρ among all sample trees using only Dataset I were tested with the Kruskal-Wallis one way analysis of variance on ranks and the Dunn's method for pairwise multiple comparisons (Dunn, 1964). We examined the effect that additional v_S point observations deeper into the sapwood have on the characterization of the radial profile previously determined with only a few shallow points (20-40% of the sapwood depth) in mature trees by comparing median ρ from Dataset I with that from Dataset I+II using the Mann-Whitney rank sum test. We repeated

the test for significant differences of median ρ amongst all sample trees by substituting Dataset I with Dataset I+II for mature trees to assess whether the earlier result changed. Linear regression analysis was used to examine trends over an extended period of time of ρ with a serial time value and daily median ρ as the independent and dependent variable, respectively. Due to technical difficulties arising from working in an inaccessible and humid montane environment, only a selected subset of eight trees was used in this analysis (four young and four mature), for which Dataset I included data spanning more than two weeks of complete days and covering at least 50% of the entire study period. The above statistical analyses were conducted with the Statistics Toolbox of Matlab R2008a (The MathWorks, Inc.).

A linear mixed effects model for nested data was constructed in which the response variable was c_S and the explanatory variables (fixed effects) examined for inclusion in the model were D, R_s, hour of day, month and all possible interactions. Tree identity nested within stand (young or mature) was a random factor in the model specification per study design. The protocol described in Zuur et al. (2009) was followed to determine the optimal model structure for nested data, which uses the Akaike's information criterion (AIC) to select the best random effects structure and the likelihood ratio to test for the significance of each fixed factor. The selected model thus included the fixed factors that significantly better explained the data variability (Zuur et al. 2009). The hour of day was incorporated as a fixed effect to take into account the hysteresis in the relationship of c_S and both D and R_s, and month was included to examine possible seasonal effects. The coefficient of determination (r^2) of the linear relationship of predicted versus observed c_S data was used to determine the amount of variance

explained by this model. The nlme R package version 3.1-102 (Pinheiro et al., 2011) was used to perform these analyses.

As a measure of agreement between each hourly instantaneous whole-tree sap flow estimate evaluated (i.e. $F_{S\_}varshape$, $F_{S\_}fixshape$, $F_{S\_}modeled$ and F_H) and hourly values of cut-tree water uptake (Q_B), the coefficient of determination (r^2) of the linear relationships between these values was calculated for individual cut-trees as well as altogether. Also, a % bias was used to evaluate the performance of each cumulative whole-tree sap flow estimate (i.e. $Q_{S\_}varshape$, $Q_{S\_}fixshape$, $Q_{S\_}modeled$ and Q_H) relative to total Q_B, calculated as: % bias = $(\sum^{n}_{i=1} (Q_i - Q_{B,i}) / \sum^{n}_{i=1} Q_{B,i}) * 100$, where the index i refers to each hourly value and Q is the estimate for which the % bias relative to Q_B is being calculated for. The % bias was calculated for each individual cut-tree as well as altogether.

3. Results

3.1 Meteorological setting

Our observations encompassed two contrasting dry seasons and a wet season (Fig. 1.2a-f). Monthly precipitation at both sites followed a markedly seasonal pattern (Fig. 1.2a), but in spite of this, the soil at both sites remained wet throughout the study period (Fig. 1.2b). Incoming solar radiation, air temperature and vapor pressure deficit from the automated tower near the young plantation (Fig. 1.2c-e) were in the range of values reported previously for this site (Holwerda et al., 2010; Muñoz-Villers et al., 2012), with the particularity that the dry season of 2010 was wetter and with higher frequency of cloud immersion events (Fig. 1.2f) than previous years.

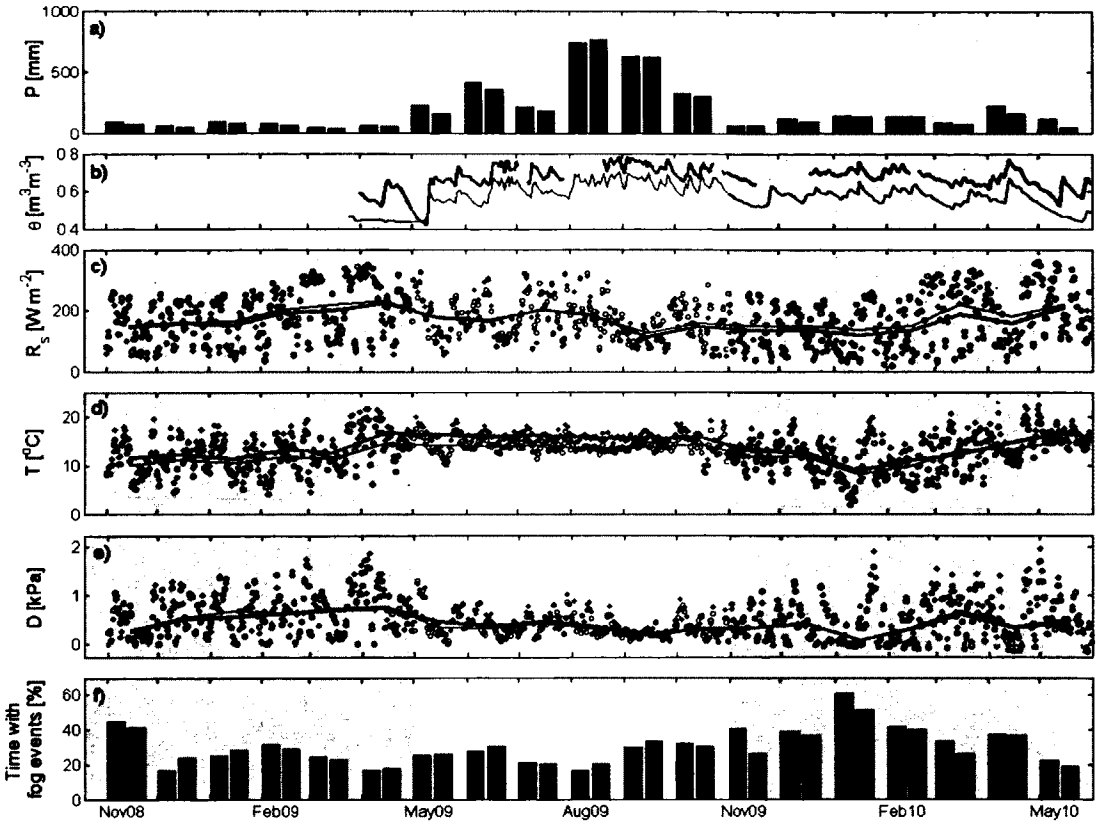

Figure 1.2 Meteorological conditions during the study period: a) monthly precipitation totals (P); b) daily mean volumetric soil moisture at a depth of 20cm (θ); c) monthly (solid lines) and daily (dots) mean incoming solar radiation (R_s); d) monthly (solid lines) and daily (dots) mean air temperature (T); e) monthly (solid lines) and daily (dots) mean vapor pressure deficit (D); and f) percent time with cloud immersion (or fog) events. Black bars, thick solid lines, and black dots depict data from the young *Pinus patula* plantation, while gray bars, thin solid lines and empty dots refer to data from the mature *P. patula* forest stand. Light-gray shaded areas indicate dry season periods.

3.2 Tree-to-tree variability in the shape of sap velocity radial profile

A total of 18,405 daytime (7:00–17:00 hours) hourly radial profiles composed Dataset I, of which 59% and 41% were from young and mature trees, respectively. We did not find a consistent value of ρ amongst all young or all mature trees, or between all young and mature trees by analyzing Dataset I (Kruskal-Walis test, $p < 0.001$; Fig. 1.3).

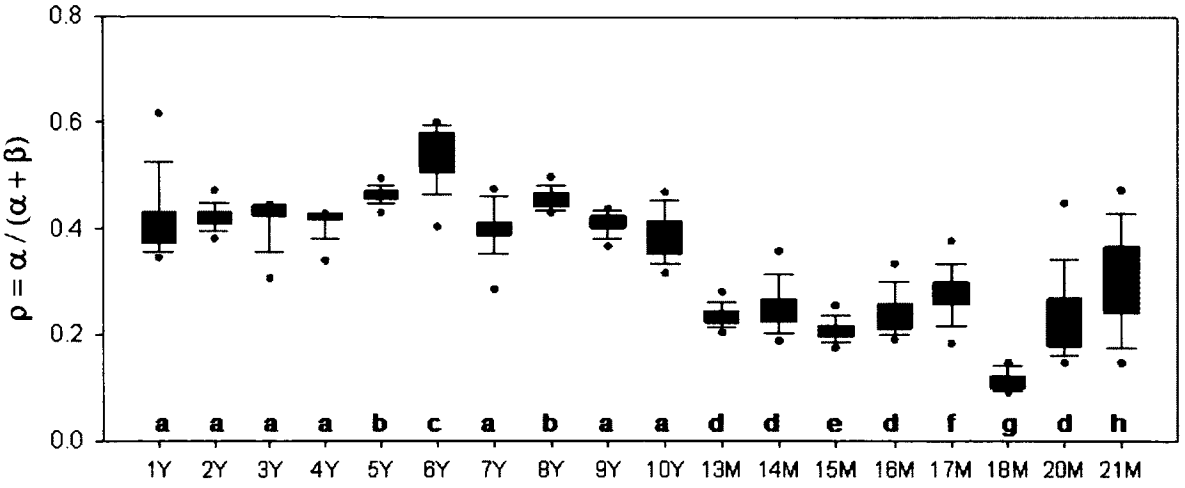

Figure 1.3. Distribution of the lumped shape parameter (ρ) characterizing the radial profile of sap velocity for each sample young and mature *Pinus patula* trees (Dataset I). Each box shows the 5th, 25th, 50th (median), 75th and 95th percentile as lower dot, bottom whisker end, bar near middle of box, upper whisker end and upper dot, respectively. Different letters indicate statistically different median ρ (Dunn's pairwise multiple comparisons, $p < 0.05$).

Despite the high degree of tree-to-tree variation, a greater similarity of ρ was found among young trees than among mature trees (Dunn's pairwise multiple comparisons, $p < 0.05$; Fig. 1.3). The radial profiles of young trees generally showed both average and maximum v_S at a radial position nearer the center of the sapwood (median ρ: 0.44 ± 0.03, median ρ_{max}: 0.33 ± 0.09; Fig. 1.3 and 1.4a) compared to mature trees again when examining only Dataset I (median ρ: 0.24 ± 0.03, median ρ_{max}: 0.14 ± 0.02; Fig. 1.3 and 1.4c). However, median ρ for each mature tree examined changed significantly (Mann-Whitney test, $p < 0.001$) when v_S observations made deeper into their sapwood were included in the characterization of their radial profiles. For most cases, deeper v_S observations increased the value of ρ compared to values obtained with observations made only in the outermost portion of the sapwood (median ρ: 0.28 ± 0.08; Fig. 1.4c-d and Appendix A1). Also, for Dataset I+II peak v_S shifted more towards the center of the

sapwood depth of mature trees compared to Dataset I (median ρ_{max}: 0.20 ± 0.08). Moreover, the variation among mature trees and between all trees was reduced, and in fact, there was not enough evidence to reject the null hypothesis of equal median ρ for 16% of the pairwise comparisons between young and mature trees (Fig. 1.5).

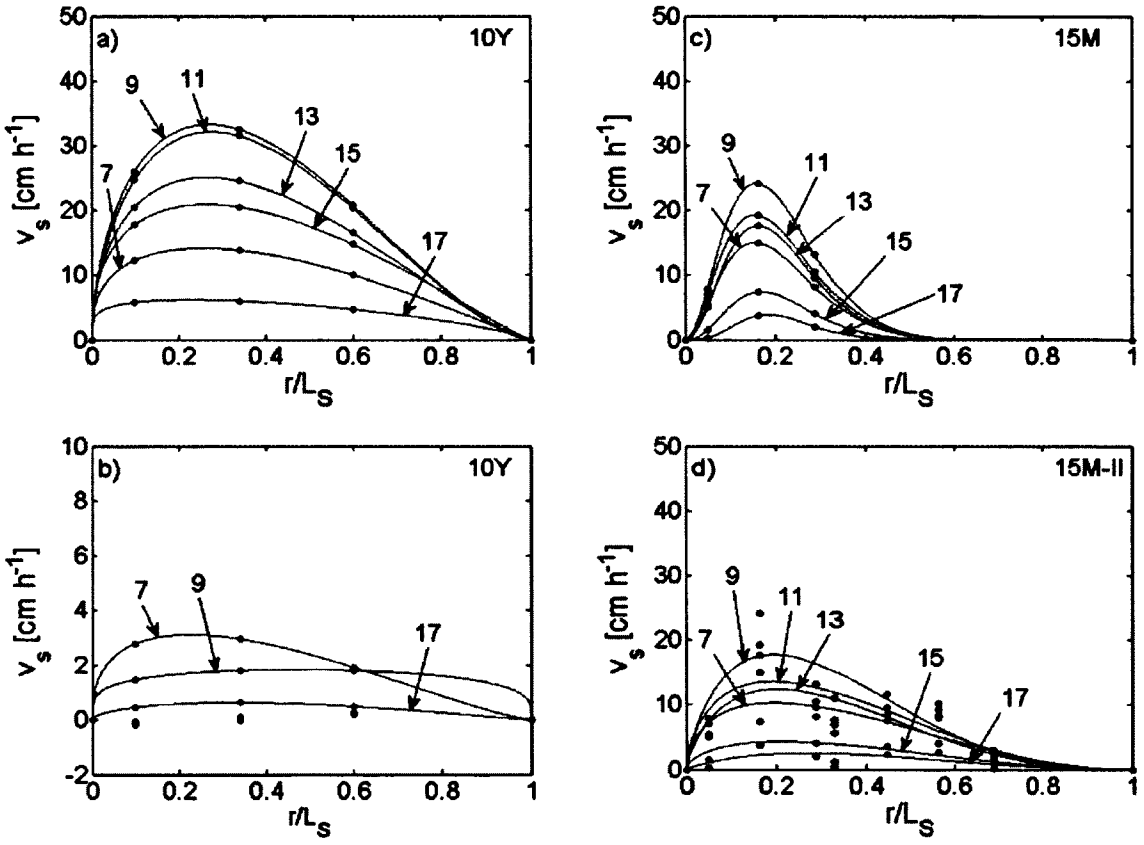

Figure 1.4. Representative hourly dynamics of the radial profile of sap velocity (v_s) of *Pinus patula* trees. Profiles of a young tree during: a) a sunny dry-season day (28 Feb 2009), and b) during the following day in which a cloud immersion event occurred from 9 am. Profiles of a mature tree also during a sunny dry-season day (30 May 2010) characterized by: c) using only three v_S data points (Dataset I), and d) after additional points deeper into the sapwood were included (Dataset I+II). Tree ID's are shown in each panel. Numbers with arrows indicate the hour of the day and dots depict v_S data points and added zero velocity points at the cambium-sapwood (r/L_S=0) and sapwood-heartwood (r/L_S =1) interfaces. Lines show the fitted Beta-pdf to data points where r^2 was ≥ 0.90. Light-gray shaded areas depict MAD ranges of ρ for each particular tree and dataset.

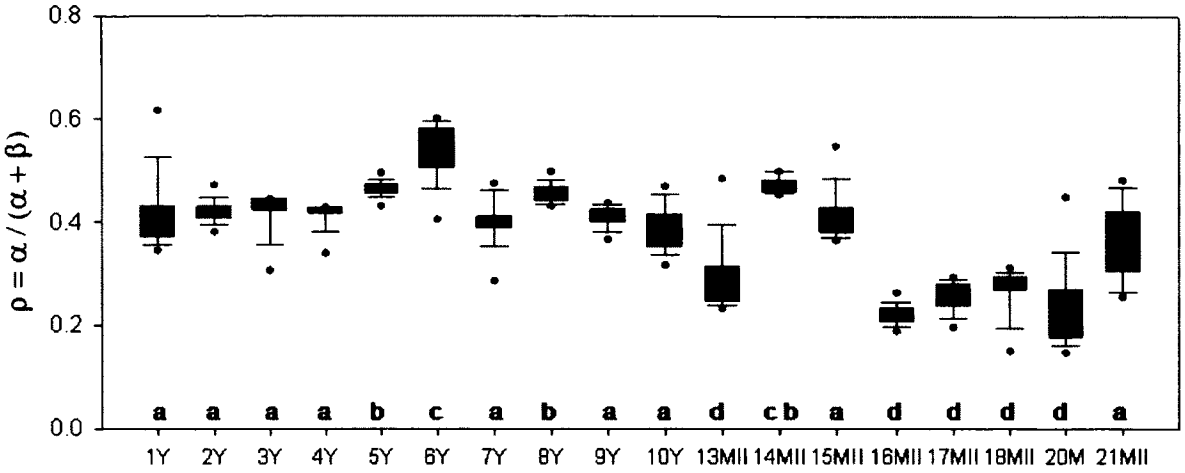

Figure 1.5. Distribution of ρ of each sample young (Dataset I) and mature *Pinus patula* trees (Dataset I+II, except for tree 20M). Each box shows the 5th, 25th, 50th (median), 75th and 95th percentile as lower dot, bottom whisker end, bar near middle of box, upper whisker end and upper dot, respectively. Different letters indicate statistically different median ρ (Dunn's pairwise multiple comparisons, $p < 0.05$).

3.3 Short and long-term consistency of sap velocity radial profiles

Generally, ρ was consistent during the day with slight variations at early and late hours of the day (Fig. 1.6a) and during rainy and cloud immersion conditions (Fig. 1.4b and Appendix A2). In contrast, the scaling parameter (c_S) clearly varied with the hour of day (Fig. 1.6b) as expected, being the 'time-variant' component of the radial profile. Maximum c_S, which is the maximum amplitude of the radial profile, was reached generally between 9 and 11 am during sunny days (Fig. 1.4 and 1.6b).

There was no consistent trend of daily median ρ over extended periods of time among the trees examined, and we also did not observe a clear seasonal effect (Fig. 1.7a). Linear regressions fitted to the relationship of daily median ρ and time (i.e. serial day number), although generally significant, showed only a marginal trend over time for up to 1.5 years as these slopes represented a change in ρ of ± 0.0001 per day. Moreover, the distributions of daily median ρ were generally strongly unimodal and peaked (Fig 7b),

indicating the consistency of this parameter over an extended period of time. We found a relatively larger, yet arguably still small, day-to-day variation as the MAD of daily median ρ ranged from 0.004 to 0.054 for each tree examined.

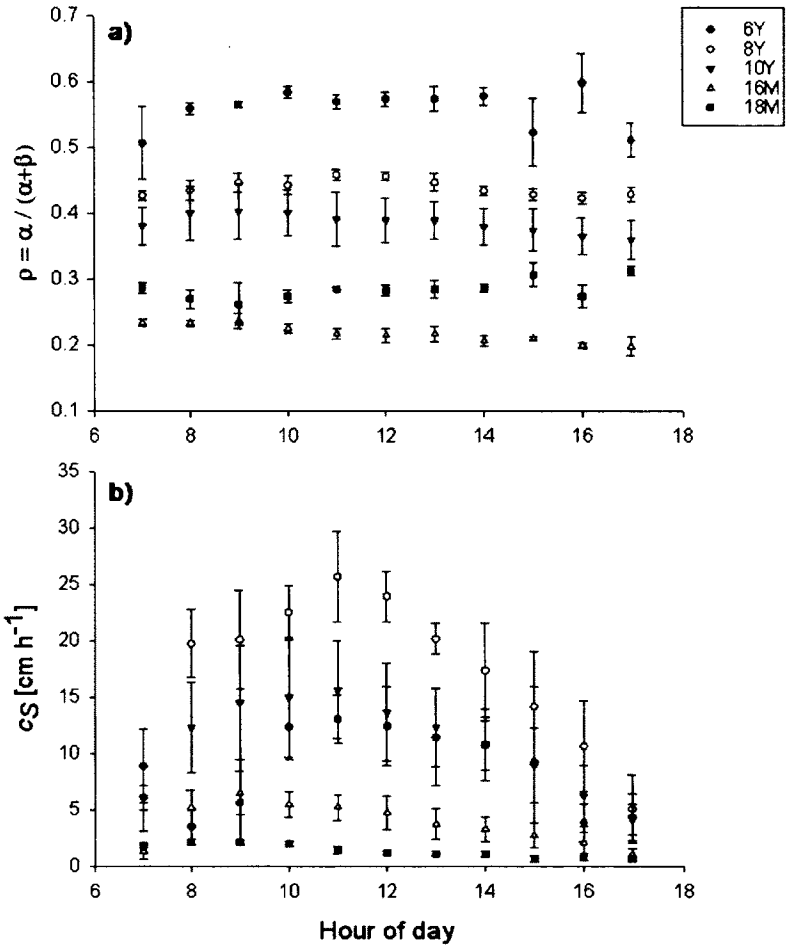

Figure 1.6. Hourly variability of a) the lumped shape parameter (ρ) and b) the scaling parameter (c_S), which characterize the radial profile of sap velocity in *Pinus patula* trees. Example young (Y; Dataset I) and mature (M; Dataset I+II) trees shown represent the overall tree-to-tree variability found in the parameters. Symbols and error bars are the medians and MAD, respectively.

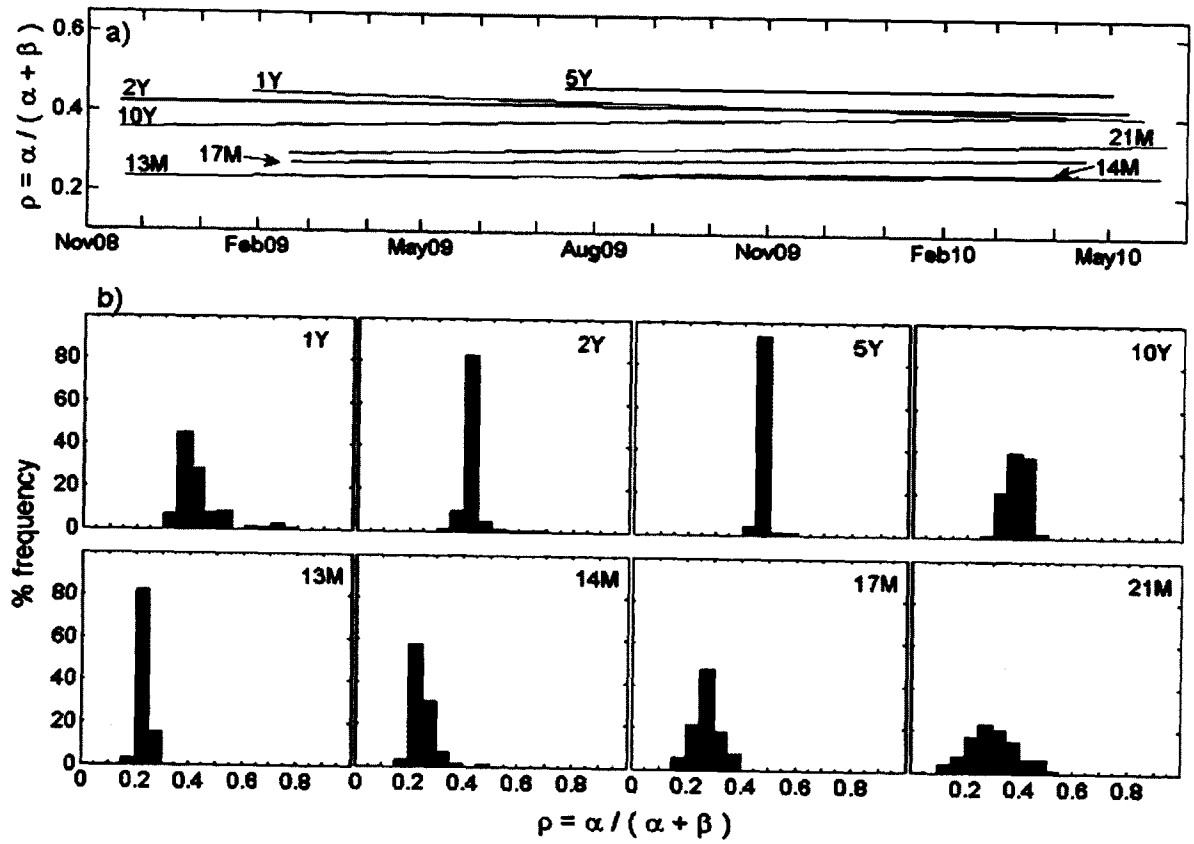

Figure 1.7. a) Trend over time of the daily median lumped shape parameter (ρ) characterizing the radial profile of sap velocity in young (Y; Dataset I) and mature (M; Dataset I) *Pinus patula* trees. For clarity, daily median ρ data points for each tree are not shown; instead, their distributions are shown below in b). Light-gray shaded areas depict daily MAD ranges.

3.4 Meteorological controls of the radial profile's short-term dynamics

The linear mixed effects model that resulted optimal for our c_S data, explaining 74% of the variation (Fig. 1.8 and Table 1.2), included incoming solar radiation (R_s), vapor pressure deficit (D) and the hour of day (H), with the interactions D^*R_s, D^*H and R_s^*H, in the fixed effects structure. Other factors examined, such as the month of the observation and higher order interactions, were found not significant ($p > 0.05$) and thus were removed from the model specification. The optimal random effects structure was a

random slope with correlated intercept for D, R_s and H for each tree. Thus, the strength of this model changes randomly between trees (L = 12,384.08; df = 10, $p < 0.001$).

Table 1.2. Estimates and statistics of the parameters of a linear mixed effects model relating the hourly dynamics of the scaling parameter of the sap velocity radial profile (c_S) with meteorological conditions (c_S*_modeled* in Figure 8). D = vapor pressure deficit; R_s = incoming shortwave radiation; H = hour of day.

Fixed effects					Random effects
Parameters	Estimate	SE	t	p	Variance
Intercept	4.172	1.568	2.660	0.008	2.567
D	4.392	0.597	7.358	0.000	1.526
R_s	0.023	0.001	23.965	0.000	0.060
H	-0.242	0.101	-2.388	0.017	0.651
D : Rs	-0.003	0.000	-20.973	0.000	
Rs : H	-0.001	0.000	-36.375	0.000	
D : H	0.136	0.023	6.029	0.000	
Residual					1.651

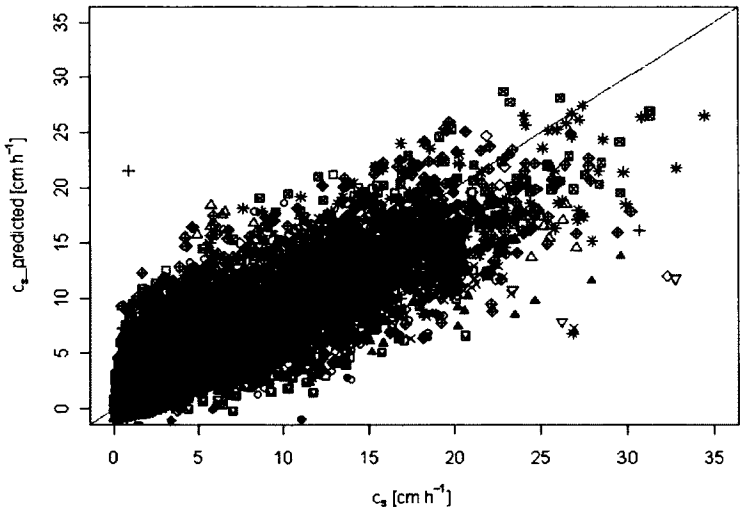

Figure 1.8. Relationship between hourly values and modeled scaling parameter (c_S and c_S*_predicted*, respectively). The former was obtained from the characterization of the radial profile of sap velocity with the Beta-pdf, while the later was determined with a linear mixed effects model based on few meteorological variables and hour of day (r^2 = 0.74, $p < 0.001$; Section 3.3 and Table 1.4). Different symbols depict different trees and the straight line included for reference represents a 1:1 relationship.

3.5 Estimates of whole-tree sap flow compared to cut-tree water uptake

In general, there was a good agreement between hourly volumes of water depleted from the bucket and $F_{S\_}varshape$ (r^2 range: 0.61-0.95; Fig. 1.9a). For three out of four cut-trees, $Q_{S\_}varshape$ underestimated the total cumulative cut-tree water uptake (Q_B; Fig. 1.9b), and while altogether $Q_{S\_}varshape$ underestimated Q_B by 7%, there was considerable variation in % bias (range: 16% to -25%; Fig. 1.9b). The effects of ignoring tree-to-tree variation in the shape of the radial profile, that is, assuming a fixed value of ρ for all cut-trees using the median ρ for young trees (0.44) when computing whole-tree sap flow, was only a slight reduction in the agreement of hourly values ($F_{S\_}fixshape$ r^2 range: 0.56-0.94; Fig. 1.9a) and a consistent underestimation of cumulative values relative to Q_B ($Q_{S\_}fixshape$ % bias range: -4% to -26%, overall: -10%; Fig. 1.9b). $F_{S\_}modeled$, which was derived from $c_{s\_}modeled$ (Table 1.2, Fig. 1.8) and a fixed ρ, produced the worse hourly agreements with cut-tree water uptake (r^2 range: 0.16-0.69; Fig. 1.9a). $Q_{S\_}modeled$ presented the widest variation in % bias (range: -52% to 12%; Fig. 1.9b), overall underestimating Q_B by 25%. Whole-tree sap flow derived from the simpler approach to integrate the radial profile (i.e. based on an area-weighted average) yielded good agreements with hourly cut-tree water uptake, similar to those obtained with $F_{S\_}varshape$ and $F_{S\_}fixshape$ (F_H r^2 range: 0.58 to 0.94; Fig. 1.9a). Q_H generally produced overestimated cumulative volumes (overall 14% bias; Fig. 1.9b). We found a sharp negative slope when contrasting % bias of $Q_{S\_}varshape$, $Q_{S\_}fixshape$ and Q_H with % sapwood depth of each cut-tree (Fig. 1.10).

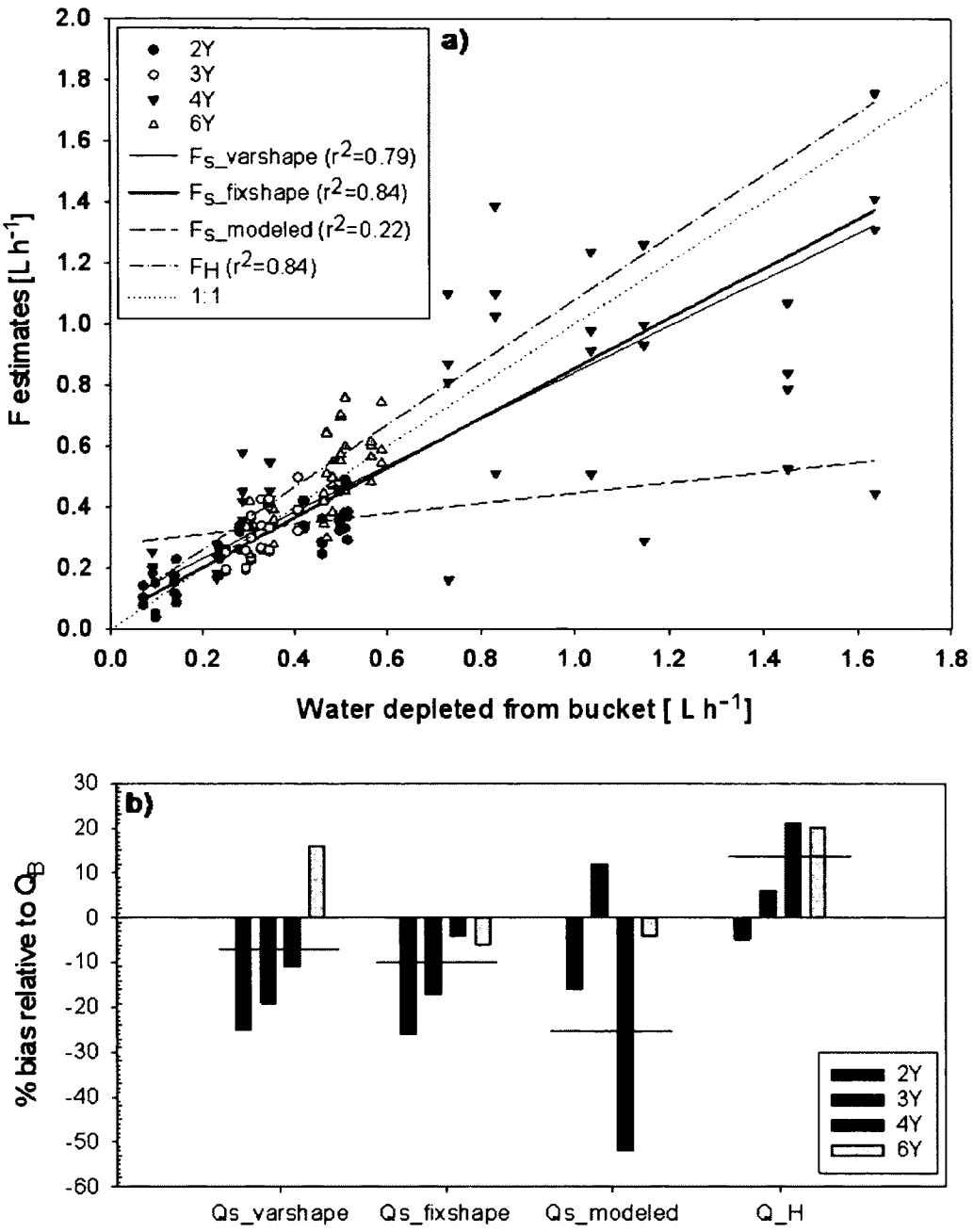

Figure 1.9. a) Relationship between cut-tree water uptake (Q_B) and hourly values of different whole-tree sap flow estimates for four young *Pinus patula* trees. Sap flow estimates were derived from the characterization of the radial profile of sap velocity (v_S) by the Beta-pdf (*F_S_varshape*, *F_S_fixshape* and *F_S_modeled*) and by the area-weighted method (F_H; Hatton et al. (1990)). Linear regressions shown were made with pooled data of all cut-trees for each estimate; r^2 ranges of tree-specific regressions are given in the text (Section 3.5). b) Percent bias of corresponding whole-tree cumulative sap flow estimates shown in the above panel relative to total cumulative Q_B for each cut-tree. The horizontal lines depict the overall % bias for each estimate.

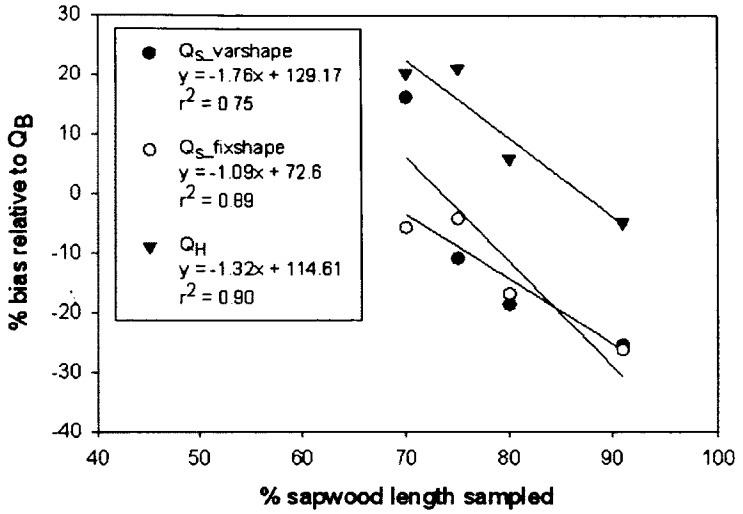

Figure 1.10. Relationship between percent of sapwood length sampled for sap velocity in four young *Pinus patula* trees and % bias relative to total cut-tree water uptake (Q_B) found with different whole-tree sap flow estimates (Q_S*_varshape*, Q_S*_fixshape* and Q_H).

4. Discussion

4.1 Shape of the radial profile characterized by the Beta-pdf

The choice of the function (or combination of functions) to characterize the radial profile of v_S should be based ideally and primarily on the physical reality of the movement of sap through the tree stem. In light of evidence that v_S approaches zero at the cambium-sapwood and sapwood-heartwood interfaces in conifers (Booker and Swanson 1979 cited by Swanson (1994)), we consider, in agreement with others (Caylor and Dragoni, 2009), that a bounded function such as, but not exclusively, the Beta-pdf, resembles closely the radial distribution of v_S within a pine tree stem. In spite of this, several different unbounded functions and combinations of functions have been used in recent studies examining the radial variability of sap velocity of coniferous tree species (Ford et al., 2004b; Nadezhdina et al., 2002). Moreover, the use of these functions requires the

estimation of many parameters creating a risk of over-fitting the data available. This was an important consideration in our case because for half of our sample trees and most of the study period v_S data were only available for three depths within the sapwood. Thus, we considered that the Beta-pdf, despite requiring the same number of parameters as v_S data points we had generally made, presented the most promising candidate for our study as it is a bounded unimodal function able to fit asymmetrical profiles with the least number of parameters required.

The use of a bounded function imposes the need to set the location of the sapwood-heartwood interface within a reasonable degree of accuracy. We did not reach this interface in any of the sample trees with sap flow probes and thus were unable to verify this location with v_S data (Čermák and Nadezhdina, 1998). However, we measured xylem water content for both sap and heartwood separately from wood cores as proposed by Kozlowski and Pallardy (1997) and Kravka et al. (1999) confirming our visual localization of the interface (data not shown) and giving us confidence in the measured sapwood depths.

In general, the Beta-pdf was a good fit to our hourly radial profiles data as 70% of all the fits had an $r^2 \geq 0.90$. One reason causing low or zero r^2 values was that during low evaporative demand (i.e. cloud immersion events or rainy conditions) v_S was almost homogenous throughout the sapwood or presenting a radial pattern not described by the Beta-pdf (e.g. negative v_S at one or more points during cloud immersion events; Fig. 1.4b and Appendix 2A). For instance, only 24% of the radial profiles during cloud immersion events had an $r^2 \geq 0.90$. It is important to point out that at very low values of v_S the uncertainty associated with setting the reference velocity or "true zero" may have

affected the fits during cloud immersion (e.g. small negative values were possibly not negative). Nevertheless, values more negative than about -0.70 cm h^{-1} (i.e. beyond the 95%CI of mean offset for reference velocity correction) may indicate the occurrence of reverse sap flow by hydraulic redistribution (Nadezhdina et al. 2010 and references therein) however, more work is needed to explore the underlying mechanisms producing the observed different radial profile patterns during cloud immersion events.

On an individual tree basis the % of radial profiles that fitted the Beta-pdf with an $r^2 \geq 0.90$ varied considerably (range: 96-20%; median: 77% ± 13%). Three out of 18 sample trees (6Y, 1Y and 18M) presented bimodal radial profiles at times such that the outer and inner portion of the sapwood had larger v_S compared to the middle portion, and consequently, the Beta-pdf did not fit their radial profiles. Many previously published reports have shown that the radial profiles in pine species present a unimodal and asymmetrical shape (Čermák et al., 2008; Cohen et al., 2008; Delzon et al., 2004; Ford et al., 2004b; Nadezhdina et al., 2002; Nadezhdina et al., 2007a), in agreement with what we generally found. However, evidence of non-unimodal radial profiles has been also reported for coniferous species (Anfodillo et al., 1993; Booker and Kininmonth, 1978; Dye et al., 1991). The only other study examining the radial profile of v_S in *Pinus patula* reported a multimodal trend where near zero v_S and multiple peaks of v_S were correlated with the location of late and earlywood rings, respectively (Dye et al., 1991). We did not observe such multimodal pattern, however the use of moving probes during mid-day hours for characterizing the radial profile in the Dye et al. (1991) study confound substantial short-term (hourly) and radial variation (Nadezhdina et al., 2002), thereby casting doubts on the reported radial variability of v_S. Furthermore, there were no visually

apparent differences between the trees with bimodal v_S radial profile shape and the others among the same stand that may have explained these divergent patterns, such as crown position and exposure to incident radiation. We do not rule out the possibility however, that unexamined sapwood characteristics or other factors that affect xylem development (e.g. vertical distribution of leaf area (Fiora and Cescatti, 2008) or root distribution differences (Čermák et al., 2008)) may have contributed to the different radial profile shapes.

The radial location at which maximum or peak v_S occurs (ρ_{max}) is an important feature of a unimodal radial profile shape. Previous studies on conifer species have found that peak v_S occurs in the outermost portion of the sapwood depth, typically $\rho_{max} < 0.2$ (Čermák et al., 1992; Mark and Crews, 1973; Phillips et al., 1996; Waring and Roberts, 1979). On the other hand, studies carried out in diffuse-porous species showed that v_S peaks within mature xylem in contrast to young xylem and thus $\rho_{max} > 0.2$ (Nadezhdina et al., 2007b; Gebauer et al., 2008). Our results indicate that generally $\rho_{max} > 0.2$ in all young and mature trees for which v_S observations covered more than 50% of the sapwood depth (Dataset II; Fig. 1.3 and 1.4). These findings contradict the general expectation that maximum v_S occurs within the youngest xylem in conifers (Phillips et al., 1996), particularly for mature trees. The values of ρ_{max} that we found for young trees are however, in agreement with previous reports if we consider that all of their xylem is still relatively young and that live branches were found down to two thirds of their stem height, thus presumably connected to actively transpiring foliage. Some authors point out that v_S peaks in deep portions of the sapwood more frequently during conditions of high evaporative demand (Domec et al., 2006; Ford et al., 2004a; Ford et al., 2004b; Medhurst

et al., 2002; Saveyn et al., 2008) as a result of the interplay between larger water potential gradient from soil to canopy (Ford et al., 2004b) and the axial and radial tension gradients within the xylem (Domec et al., 2006) compared to times of low evaporative demand, which leads to increasing flow and consequently increasing v_S in deeper portions of the sapwood. During our study, day-to-day variability in evaporative demand was often high, with daily average of vapor pressure deficits > 1.5 kPa, combined with high soil water content throughout the year despite the seasonality in rainfall and cloud immersion (Fig. 1.7a-d). Consequently, we hypothesize that these conditions contributed to the relatively deep ρ_{max} values observed in our sample trees. It is important to point out that, as we showed, discrepancies amongst reported location of peak v_S could also arise in relation to the location of v_S measurements used in the characterization of the radial profiles (Fig. 1.4).

4.2 Tree-to-tree variability in the shape of the radial profile

We found considerable tree-to-tree variability in the shape of the radial profile (Fig. 1.5), in agreement with previous studies examining trees of the same species (Delzon et al., 2004; Nadezhdina et al., 2007b; Poyatos et al., 2007). We expected that the radial profiles of v_S among trees growing in a homogenous stand (young plantation) were more consistent compared to that of trees growing in a more heterogeneous setting (mature stand). We did not find strong evidence to confirm this, and in fact, we found considerable tree-to-tree variability in both stands, contrasting the results of (Caylor and Dragoni, 2009) who found consistent radial shapes among trees both from a homogenous (apple orchard) and a heterogeneous stand (deciduous forest). It is important to point out

that small differences may have been amplified in our study given the flexibility of the Beta-pdf in instances when only three point v_S observations were included in the characterization as discussed earlier. Further, as we were able to show, had we sampled deeper into the sapwood of mature trees, or had we sampled the same % of sapwood, their profiles may have resembled more closely those of young trees (Fig. 1.3 and 1.5).

4.3 Temporal dynamics of the radial profile

The approach we used to decouple the radial profile in two terms, one relating to its shape and another to its hourly variability, proposed by Caylor and Dragoni (2009), proved helpful to investigate its short-term variability, which was largely ignored in early studies on this species (e.g. Dye 1991). Also, it allowed us to assess the meteorological controls of this short-term variability. Our finding that the hourly dynamics of v_S can be explained by a few meteorological variables, namely R_s and D, is in agreement with previous studies (Fiora and Cescatti, 2006; Ford et al., 2004a; Ford et al., 2004b; Kubota et al., 2005; Nadezhdina et al., 2002; Saveyn et al., 2008). However previous work had not taken into account the hysteresis that we (data not shown) and others have found in the relationship between v_S and these meteorological variables (Motzer et al., 2005; Saveyn et al., 2008; Zeppel et al., 2004). By including the hour of day to interact with meteorological variables into the model specification we found that a great proportion of the overall variance of c_S was explained (74%; Fig. 1.8). The month in which the radial profiles were assessed did not significantly explain the variability of c_S indicating that there were no strong seasonal effects for R_s or D affecting their relationship with c_S. We did not include in the model specification any variable indicative of the soil moisture

status, as there was no evidence of soil water limitation in our study area (Goldsmith et al., 2012). The use of a mixed effects model was a valuable tool to incorporate the overall effects of tree-to-tree variability (random effects), which was overlooked in previous studies (Dragoni et al., 2009; Ford et al., 2004a) and we found to be significant. Improvements to this model are still necessary, particularly to better predict higher c_S values. Our simple model based on linear combinations is not a mechanistic model and thus non-linear responses of c_S to some of the explanatory variables were not captured (e.g. an observed asymptotic response of c_S to D similar to what has been reported as the response of transpiration to D suggesting stomatal regulation during instances of high evaporative demand; Ford et al. 2011; Hernández-Santana et al. 2008). These improvements would augment the model's complexity however, and the development of tools to conduct more complex analyses is in the frontiers of statistical research (Zuur et al., 2009).

Most sap flow studies are not conducted over an extended time period, thus the long-term variation of the radial profiles is not generally examined. We chose to use a fixed value of sapwood depth throughout the study period to normalize our hourly radial profiles in order to avoid introducing an untested model of its increment into our analysis. Not taking into account changes in sapwood length, namely increasing sapwood depth thus decreasing the normalized location of each point measurement of v_S (r/L_S), would potentially confound changes in ρ with time. We expected a consistent decrease in ρ with time among the trees examined if only the length of the sapwood was increasing while the radial location relative to this length remained constant. We did not find a consistent decrease among the trees examined (Fig. 1.7a), and given arguably small changes and

general consistency (Fig. 1.7b), we consider that a fixed ρ can be assumed to upscale point measurements of v_S at least for a period of up to 1.5 years. Nevertheless, changes in ρ over longer time periods deserve further investigation.

4.4 Implications for point v_S sampling strategy

An important general implication of our results for designing a sampling strategy of point v_S is that it is not safe to assume that the peak or average v_S will be found strictly neither in the few outermost 20-40 mm nor strictly in the outermost 20% of the sapwood depth. Therefore, the sampling strategy for point measurements of v_S should not be geared towards only sampling shallow points without taking into account the size of the tree (and consequently, the size of the sapwood depth). Furthermore we suggest, in agreement with earlier recommendations, a sampling strategy of distant points (Ford et al., 2004b), but proportionally distributed through the sapwood depth such that most of the sapwood depth is covered as opposed to sampling intensively only in the outermost 20%. A practical disadvantage still exists in that it is difficult to construct and install long probes in the case of trees with deep sapwood (but see James et al. (2002)). However, considering the possibility of high circumferential variability (which we did not examined here but could be important (Cohen et al., 2008; Nadezhdina et al., 2007b; Saveyn et al., 2008)), a proportional distribution of sampling points within the sapwood area should consider that the deeper portion of the sapwood represents less area than the outer portion. Thus, less deep points would be needed, yet these should not be neglected. We focused most of our attention on the radial position with average v_S (ρ) because the scaling procedure of point measurements of v_S to the whole-tree level we used here was

based on this characteristic (Eq. (2)). Also, because we envisioned that once ρ was known, future sampling in *P. patula* could be adjusted to aim for this location given the typical limited resources available to sample many points within the sapwood. However, the considerable tree-to-tree and moderate temporal variability preclude precise and practical sampling at a particular location.

4.5 Implications for scaling v_S to the whole-tree level

The procedure of scaling up whole-tree sap flow to the stand level may carry considerable errors not only due to the difficulty in effectively capturing radial variability in v_S with point measurements within trees, but also if this spatial variability is not consistent among the sample trees representing the stand (e.g. substantial variation among trees of different size). Errors stemming from the initial procedure of scaling up v_S point measurements to the whole-tree level are rarely quantified. Given the considerable tree-to-tree variability shown here, we propose that the range of % bias in Q_S estimates relative to cut-tree water uptake can be used as a proxy for the expected error range of Q_S estimates derived from Heat Ratio method measurements and the characterization of the radial profile of sap velocity (v_S) by the Beta-pdf in future studies. While we did not perform cut-tree evaluations for mature trees, our results obtained for few young trees cut for the field evaluation provide a first approximation and are informative of the error range expected across trees of different sizes when this is related to the % of sapwood depth measured (Fig. 1.10).

Importantly, our results suggest that a fixed radial shape may be safely assumed for plantation *P. patula* trees to upscale point v_S measurements to the whole-tree level,

which simplifies and generalizes the procedure. The predictive performance of the simple model we constructed to determine c_S using meteorological data, which in turn was used to compute $F_s\_modeled$ and $Q_S\_modeled$, is not acceptable for high values of v_S (Figs. 8 and 9) possibly due to linear simplifications of non-linear relationships (e.g. between c_S and D). Its direct use for conditions that arguably are more important for applications such as water balance studies is therefore limited. We found considerably less overall % bias for our estimates of $Q_S\_varshape$ and $Q_S\_fixshape$ (Fig. 1.9) compared to the average overestimation of 49% reported in a previous study that performed cut-tree evaluations of Q_S estimates derived from the compensation heat-pulse method in *P. patula* (Dye et al. 1996), and also compared to the average underestimation of 35% found in a laboratory and field evaluation of the same sap flow technique, but in a diffuse-porous species (Steppe et al., 2010). Only an evaluation of Heat Ratio method-derived Q_S estimates using potted eucalyptus trees reported less % bias than all of our estimates, namely an overestimation by 2-5% relative to the water loss measured by weighing lysimeters (Bleby et al., 2004).

An alternative approach to integrate the profile to estimate whole-tree sap flow is needed for instances in which the Beta-pdf does not provide a good characterization of the radial pattern of v_S (only 30% of hourly radial profiles in this study). In the case of radially homogeneous v_S, there is no need to characterize a radial profile however, and a single point measurement of v_S or a simple average should suffice to upscale to the whole-tree level. Now, for the case of bimodal radial profiles, or profiles containing negative values as during foggy conditions, other approaches should be explored, such as using another bounded function (or combination of functions) or the area-weighted

average. Our results confirmed however, that for the simplest scaling-up approach to be effective (i.e. the area-weighted average), point v_S data must have equal areal weight otherwise large errors are expected when the portion with larger areal weight presents considerably different v_S.

5. Conclusions

In this study we applied an analytical approach to assess tree-to-tree and temporal variability of a large data set of radial profiles of v_S in a widely planted tree species. This approach proved useful to determine general characteristics of the shape of the radial profile. Despite the considerable variation in the shape of the radial profile, we conclude that a typical radial profile for *P. patula* can be generalized as unimodal, asymmetrical and with peak v_S expected within the outermost 20-33% of the sapwood depth. We show that a generalized radial shape may be assumed to upscale point v_S measurements to whole-tree sap flow with relatively low bias compared to an independent measure of whole-tree water uptake. Our findings emphasize the potential error introduced by neglecting to conduct point v_S measurements throughout the entire sapwood depth. We also show that hourly dynamics of the radial profile can be largely explained by a few meteorological variables easily obtained from routine measurements, such as R_s and D, and the hour of day. Further improvements to this model's predictive performance are necessary (e.g. incorporating non-linear features) such that it can be successfully applied to predict whole-tree sap flow under a wide range of meteorological conditions, particularly instances leading to high sap flow rates.

CHAPTER II

PLANT WATER USE VARIATION ACROSS THE LAND USE CHANGE TRAJECTORY PASTURE TO PINE REFORESTATION IN A SEASONALLY DRY TROPICAL MONTANE CLOUD BELT[1]

Abstract

Understanding evapotranspiration (ET) variation associated with land use change is critical not only for the assessment of impacts on water resources, but also to improve the applicability of climate change models. ET across a land use change trajectory of pasture-to-pine reforestation was estimated using a combination of near-surface climate and sapflow measurements for a 1.5-year period in the seasonal tropical montane cloud belt of central Veracruz, Mexico. An actively grazed pasture (PAS) dominated by *Axonopus compressus* represented the baseline land cover. A young (YREF) Mexican weeping pine (*Pinus patula*) reforestation near canopy closure and a mature pine plantation (MREF) under selective logging represented local reforestation efforts and forest management. Tree transpiration at the stand level was higher at YREF compared to MREF; however, normalized by leaf area index, the difference was minimized. The contribution of understory transpiration to total stand level transpiration for MREF was only about 5%. Rainfall interception loss (E_i) for the pine plantations was found to be low (5.4% and

[1] Report as basis for manuscript preparation. Collaborators: F. Holwerda, H. Asbjonsen, L.A. Bruijnzeel, D. Geissert, A. Gómez-Tagle, G. Goldsmith, T.E. Dawson.

7.5% of annual rainfall for YREF and MREF, respectively) and as such, did not increase ET beyond that of PAS. Land covers ranked from higher to lower ET normalized by available energy (net radiation) as: PAS (0.80) = YREF (0.80) > MREF (0.42). Similar ET per unit available energy for PAS and YREF, and higher for PAS compared to MREF, combined with similar soil hydrological properties and apparent functional rooting depth across land cover types, suggest that differences in energy partitioning and the relative importance of surface and aerodynamic conductance, may be the drivers of the observed patterns in ET across the land use change trajectory examined here. The present results further suggest that planting *P. patula* on former pasture lands in the uplands of central Veracruz, Mexico, would not substantially increase ET after >10 years of planting.

1. Introduction

The vegetation of a particular land cover modifies the exchange of water and energy between the surface of the Earth and the atmosphere by influencing evapotranspiration (ET). which consists of the combined processes of plant transpiration (i.e. soil water uptake by plants) and direct evaporation of water collected on vegetation and soil surfaces (Monteith, 1965). ET is also referred to as total plant water use. As summarized below, understanding the variation in ET associated with land use change is critical not only for the assessment of impacts on water resources (Bosch and Hewlett, 1982; Farley et al., 2005; Zhang et al., 2001), but also to elucidate the feedbacks of land use change on the weather and climate (Pielke et al., 2011; Pitman, 2003).

The amount of precipitation available for infiltration, runoff production, and ultimately, streamflow generation, is affected by the magnitude of ET as the hydrological cycle is inextricably coupled to vegetation (Shuttleworth, 2012). Therefore, reliable estimates of ET for different land covers at the same operational scale that land management practices are conducted (i.e. field, stand), are critical to developing sound land management policies (Kaimowitz, 2005; Tallis et al., 2008). Furthermore, latent heat (ET in units of heat flux density) is a major driver of climate (Andre et al., 1989; Niyogi et al., 2009; Pielke et al., 1998). Changes in land use usually involve drastic alterations in land cover structure and species composition, which in turn may lead to important changes in surface net radiation and its partitioning into latent and sensible heat flux, as well as in the aerodynamic roughness of the land surface (Monteith and Unsworth, 2007). Indeed, the processes that drive and limit ET given a set of land cover characteristics are, at least in principle, well understood (Calder, 1998; Moore and Heilman, 2011), but predicting changes in ET associated with land cover variation is complicated in practice (Zhang et al., 2010). Also, the anthropogenic influence on regional and global climate due to land use changes is more poorly understood than due to changes in the chemical composition of the atmosphere (IPCC, 2007), and consequently, rarely taken into account in climate change models (Pielke et al., 2011; Pitman, 2003). A better understanding of how ET varies with land use change will therefore improve the applicability of climate models and, ultimately, improve predictions of water availability under future climate change scenarios (Jackson et al., 2001).

ET was recently modeled at the global scale (Zhang et al., 2010) and large errors were found, particularly for tropical regions (up to 100 mm per year). Surface parameters

required by models are often applied to a wider range of vegetation conditions from which they were derived, thereby increasing prediction uncertainty (e.g. Mata-Gonzalez et al., 2005). The lack of data for many land cover types arising from complex interactions between vegetation, soil types, topography and land-use legacy also limits the potential for modeling validation (Pielke et al., 2011). This issue is especially critical for areas such as tropical montane regions, were hydrometeorological measurements are mostly lacking (Manley and Askew, 1993).

The present study focuses on estimating and comparing ET under different land cover types with the aim of adding to the recently growing body of information on plant water use from tropical montane regions (e.g. Brauman et al., 2012; Holwerda et al., 2013; Muñoz-Villers et al., 2012) and to improve our understanding of the hydrological consequences of different land use change trajectories in these regions. The conversion of old-growth forests to pasture or other crops is one of the most common land use change trajectories in tropical uplands (Muñoz-Villers and Lopez-Blanco, 2008). During the past decade, however, there has been an increase, albeit small, of forested land cover due to forest regeneration and tree planting world-wide (Aide et al., 2010; Evans, 1999; FAO, 2010). In the case of Mexico, reforestations established on former (introduced) pasture in the uplands is foreseen to increase (Carabias et al., 2007; Sánchez-Velásquez et al., 2009), and stakeholders from lower-lying areas are eager for information about the hydrological impacts of these plantations (Pérez-Maqueo et al., 2005; Scullion et. al, 2011). The most widely used tree species in reforestation projects in are conifers, and in the seasonal montane cloud belt of central Veracruz (eastern Mexico), this includes the Mexican weeping pine (*Pinus patula*; Valtierra Pacheco et al., 2008). Therefore a typical

pasture actively managed for grazing livestock was selected as the baseline land use, while two *P. patula* plantations at different stages of stand development (10-year-old reforestation reaching canopy closure and a mature plantation under selective logging) were chosen to represent local reforestation efforts and management practices. The specific objectives were:

- Estimate and compare plant water uptake at the stand level (total transpiration $-E_T$) between the two *P. patula* plantations.
- Determine and compare total plant water use (evapotranspiration –ET) among pasture and the *P. patula* plantations.

2. Material and Methods

2.1 Study sites

The study area is located in the upper La Antigua river basin (1325 km^2), at the headwaters of the Los Gavilanes watershed (30 km^2), on the eastern slopes of the Cofre de Perote volcano (4282 m a.s.l.), central Veracruz, Mexico (Fig. 2.1). The climate between 2000 and 3000 m elevation in this region is 'temperate humid with abundant rains during the summer', with an average temperature between 12 and 18°C and a mean annual precipitation (MAP) between 2000 and 3000 mm (García, 1973). The region has a seasonal rainfall and cloud immersion regime, with a wet season between May and October, in which approximately 80% of MAP falls, and a relatively dry season between November and April. Rainfall in the wet season is of convective origin, brought by frequent showers and thunderstorms, while the dry season is characterized by an alternation of stable dry weather conditions and cloud immersion events, often

accompanied by rain and/or drizzle (García-García and Zarraluqui, 2008; Holwerda et al., 2010; Muñoz-Villers et al., 2012). More details on the area's climate, geology, topography, soil characteristics and hydrology can be found in Holwerda et al. (2010), Muñoz-Villers et al. (2012), Muñoz-Villers and McDonnell (2012) and Goldsmith et al. (2012b).

Three study sites within the cloud forest zone where selected to represent three discrete stages of the land use change trajectory of pasture conversion to mature pine plantation. To represent the actively grazed land cover within the study area, a typical pasture site was selected (hereafter PAS), dominated by *Axonopus compressus* and *Alchemilla pectinata*, with remnant trees from the former land use (see below) and sparse shrubs and ferns such as *Pteridium aquilinum* (Fig. 2.2a). Two *Pinus patula* stands at different development stages were selected to represent local reforestation efforts and forest management: a 10-year-old reforestation near canopy closure (hereafter YREF; Fig. 2.2b) and a mature plantation under selective logging (hereafter MREF; Fig. 2.2d). YREF and PAS are located within the La Cortadura Forest Reserve, property of the municipality of Coatepec, Veracruz (Fig. 2.1). MREF is located near the locality of Tierra Grande, approximately 2 km from YREF (Fig. 2.1).

Both PAS and YREF were formerly (at least >30 years ago; local inhabitants, pers. comm.) covered with mature lower montane cloud forest (LMCF) locally known as "bosque mesófilo de montaña" (García Franco et al., 2008). YREF was established in 2000, after supporting marginal grazing land with remnant LMCF trees, and had not received any thinning treatments at the time of this study. MREF was formerly covered with cloud-affected pine-oak forest, which was cleared ca. 70 years ago and thereafter

managed as pasture for grazing livestock with some remnant trees (predominantly *P. patula*, *P. pseudostrobus* and *Quercus* spp.). Approximately 30 years ago, the pasture was reforested with *P. patula* and thereafter allowed to grow and regenerate naturally without further intervention other than selective logging (local inhabitants, pers. comm.). At the time of this study, MREF was comprised of multi-cohort patches dominated by *P. patula* and an understory dominated by *Miconia glaberrima* and *Dryopteris filix-max*. Table 2.1 provides further characteristics of each study site.

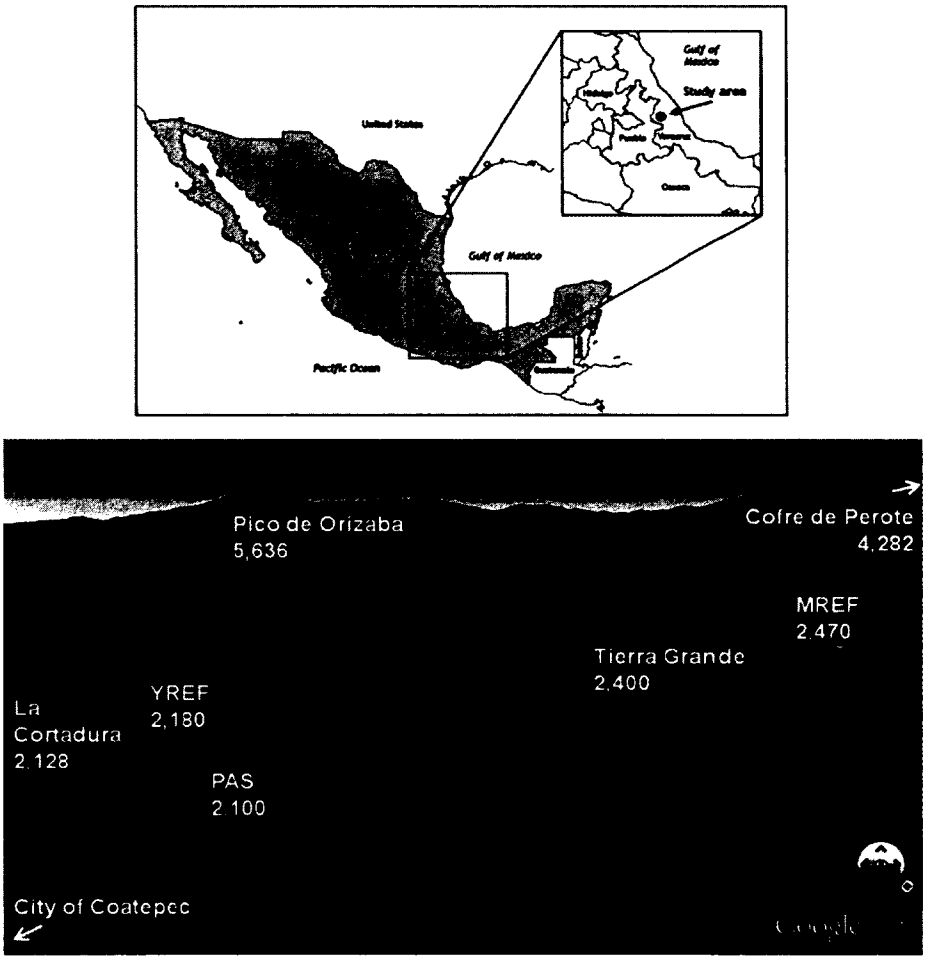

Figure 2.1. Location of study area in central Veracruz, Mexico, study sites (PAS = pasture; YREF = young *Pinus patula* plantation; MREF = mature *P. patula* forest) and automated weather stations (La Cortadura and Tierra Grande). Altitude at the sites and highest nearby points are given in m a.s.l..

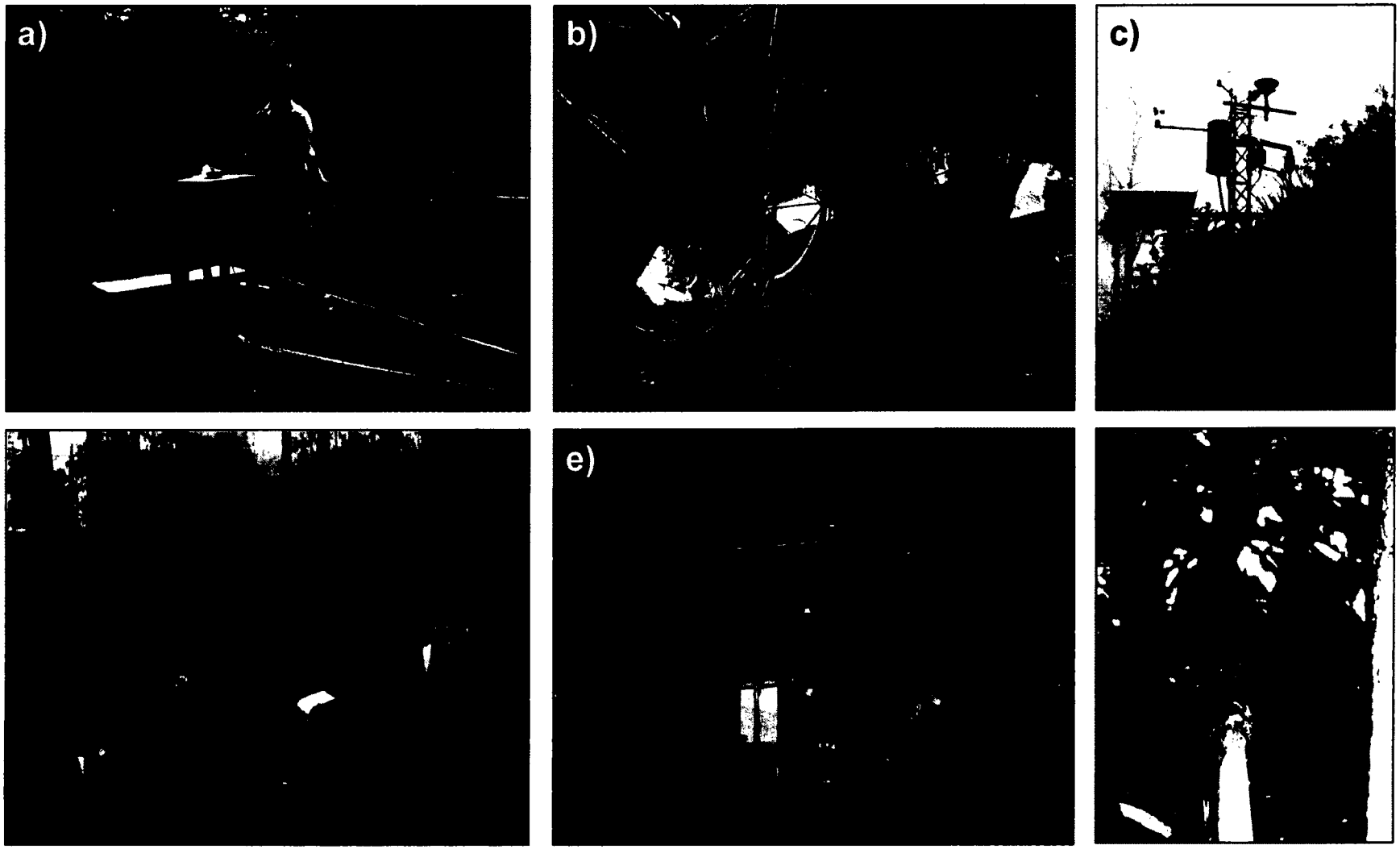

Figure 2.2. View of the study sites and selected instrumentation: (a) PAS, (b) YREF and (c) weather station at La Cortadura; (d) MREF and (e) weather station at Tierra Grande; (f) HBM sapflow sensor (prior to insulation) installed in a branch of *Miconia glaberrima* at MREF.

Table 2.1. Characteristics of the study sites a pasture dominated by *Axonopus compressus* (PAS), a 10-year-old *Pinus patula* reforestation (YREF) and a *P. patula*-dominated mature stand under selective logging (MREF). LAI = leaf area index; DBH = diameter at breast height; LUC = land use change; DS09 = dry season 2008/09; DS10 = dry season 2009/10; LMCF = lower montane cloud forest. Standard deviations are given between parentheses where available.

	PAS	YREF	MREF
Elevation [m a.s.l.]	2100	2180	2470
Coordinates	19.4956° N 97.0418° W	19.4931° N 97.0422° W	19.5054° N 97.0559° W
Area [ha]	~3	~1	~20
Plots exposure and slope	3°, SE	20°, SE	25°, SE
Mean canopy height [m]	0.05 (0.02) [a]	7 (1.5) [b]	23 (2.80) [b]
Canopy LAI [m^2 m^{-2}]	DS10: 1.2 (0.4) [c]	DS09: 6.0 (0.6) [d] DS10: 6.5 (0.2) [d]; 5.2 (0.1) [e]	DS09: 3.0 (0.8) [d] DS10: 3.0 (0.9) [d]; 3.2 (0.3) [e]
Understory LAI [m^2 m^{-2}]	-	-	DS10: 0.6 (0.3) [c]
Tree density [stems ha^{-1}] [b]	-	3,783 (652)	662 (92)
Tree basal area [m^2 ha^{-1}] [b]	-	34.3 (9.6)	46.7 (15.3)
Tree DBH range [cm]	-	9.6–11.8	20.4–61
Former land use	LMCF	remnant LMCF and PAS	remnant pine-oak forest and PAS
Years since LUC [f]	>30	10	~30

[a] Actively grazed pasture measured throughout late DS09 and DS10 in 20 random points.
[b] Hernandez-Hernandez (2010) and this study.
[c] *Miconia glaberrima* only (dominant in terms of crown area coverage per unit land area) and determined from destructive measurements (Appendix C).
[d] From photosynthetically active radiation attenuation measurements (Appendix C).
[e] From diffuse light attenuation obtained with a LAI-2000 canopy analyzer (Appendix C).
[f] Approximate years since establishment of current land use (local inhabitants, pers. comm.).

2.2 Meteorological measurements

Automated weather stations (Figs. 2c and 2e) were installed in open areas with south-east exposure at a distance of 350 m ("La Cortadura"; 2128 m a.s.l.) and 450 m ("Tierra Grande"; 2400 m a.s.l.) from YREF and MREF, respectively (Fig. 2.1). Meteorological data were available as 10-min averages from 30-s sampling intervals and during a 1.5-year period (November 2008–April 2010). Variables measured at standard height above the ground (2 m) included: incoming solar radiation (R_s [W m^{-2}]), air temperature (T [°C]), vapor pressure deficit (e [kPa]), wind speed (U [m s^{-1}]), horizontal visibility (VIS [m]), and rainfall (P [mm]).Vapor pressure deficit (D [kPa]) was computed as the difference between e and saturation vapor pressure (e_s; computed as in Lowe (1977) using T). Fog events were defined as periods with fog occurrence (VIS > 1000 m) separated by a fog-free period of at least three hours (see further details in Chapter 3).

Additionally, a metallic tower was installed at YREF and a mast at PAS, to measure R_n with a REBS Q7.1-L net radiometer at each site. The measurement height at YREF was 9 m (2 m above average canopy height) while at PAS it was 2 m. Gaps in the time series of R_n (19% and 38% of total hours for YREF and PAS, respectively) were filled with R_s data collected at the La Cortadura weather station. The linear regression for YREF was: $R_n = 0.68R_s - 27.96$ ($r^2 = 0.96$; RMSE = 43.08), and for PAS was: $R_n = 0.52R_s - 9.5$ ($r^2 = 0.83$; RMSE = 64.53). R_n for MREF was estimated from net longwave radiation (R_{nl}) calculation at daily time steps (Allen et al., 1998), daily R_s from Tierra Grande weather station and average daily albedo for clear-sky days determined for YREF ($1 - (R_n - R_{nl}) / R_s$). The use of equal albedo for YREF and MREF was an initial simplification, subject to future examination given their very different canopy LAI and

height. The tower at YREF was also instrumented with a LI-190SL quantum point sensor (LI-COR) to collect photosynthetically active radiation above the canopy (PAR_a). PAR_a at MREF was not logistically possible, and was therefore, obtained from R_s measured at the Tierra Grande weather station using an empirical linear model relating R_s and PAR_a measured at La Cortadura and YREF, respectively: $PAR_a = 1.64R_s$ (fixed bound at the origin; $r^2 = 0.90$; RSME = 192). Additionally, PAR below the canopy (PAR_b) was measured at MREF with a LI-191SL quantum line sensor (LI-COR) installed on a leveled wooden bench at ~30 cm from the ground and with a north-south orientation.

The mast at PAS was also instrumented with a RM Young 03101 Wind Sentry anemometer to measure U, and a Vaisala HMP45C probe to measure T and RH. Furthermore, D at PAS was calculated as described above but e in this case was derived from RH (Allen et al., 1998).

2.3 Soil moisture dynamics and other soil characteristics

Soil moisture was monitored continuously from April 2009 with soil moisture probes installed at five depths on an undisturbed wall of a pit dug at each site (~1.5 m deep). At MREF, two pits were dug (MREF1 and MREF2) adjacent to plots where sapflow was monitored (see Section 2.4 below). The depths at which soil moisture was monitored coincided with different soil horizons characterized at the time of sensor installation (see Appendix D for more details). In addition to other standard soil physical characteristics, field capacity and permanent wilting point were determined for each horizon and site, in collaboration with the Soil Laboratory of Instituto de Ecología A.C., Xalapa, Veracruz (Appendix Table D1). S616 probes connected to a CR1000 datalogger (Campbell

Scientific) were used at PAS and YREF, while EC5 probes connected to an Em50 datalogger (Decagon) were utilized at MREF. Volumetric water content (θ [m^3 m^{-3}]) was determined from raw data and site- and depth-specific calibration curves (Appendix Tables D2 and D3) as recommended for volcanic soils (Frumau et al., 2006).

2.4 Tree sapflow measurements and stand level tree transpiration (E_t)

Measurements of sap velocity at breast height (1.4 m above ground) were conducted in the stem of 8 and 10 trees at YREF and MREF, respectively, following the Heat Ratio method (Burgess et al., 2001). Sample trees were growing within circular plots of 10 m radius. One plot was set up in YREF, while in MREF three plots were necessary to cover the variation in DBH classes (see Appendix B). Two plots in MREF were adjacent to each other (MREF1), while the third was at a distance of ca. 100 m from the others but at the same elevation (MREF2). All plots had similar aspect (south-east) and slope (20–26°). A detailed description of sap velocity data collection, characterization of the radial profile of sap velocity for all sample trees, and calculation of whole-tree sapflow (F_s) is given in Alvarado-Barrientos et al. (2013). Transpiration at the whole-tree level was assumed equal to F_s, that is, we ignored any time lag due to stem capacitance, and considered it a reasonable assumption as discussed in more detail in Chapter 4.

Sapflow-derived stand level tree transpiration (E_t [mm h^{-1}]) for YREF was derived by averaging hourly F_s across all sample trees and multiplying by stand density (Table 2.1), as the stand was even-aged and tree spacing was fairly homogeneous (Čermák et al., 2004). Given the more complex structure of MREF, scaling up was based on quantifying sapflow for trees representing the distribution in DBH classes in the stand

(Čermák et al., 2004). Briefly, a survey of trees (DBH > 10 cm, non-suppressed trees) was conducted to determine stand characteristics such as stocking density (trees ha^{-1}). Five circular plots of 1000 m^{-2} were selected in patches were *P. patula* dominated. Data from the plots were pooled and the distribution of stocking density in DBH classes was derived. To scale F_s to the stand level (E_t), each sample tree was assigned to a DBH class (Appendix B).

The time series of hourly E_t was not complete for the entire study period due to equipment malfunction; 26% and 49% of total hours were missing for YREF and MREF, respectively. First, a complete time series of daily E_t was produced for all days having complete 24-h values (36% and 42% of the total number days for YREF and MREF, respectively) were used to derive daily totals of E_t [mm day^{-1}]. Next, these values were regressed against daily reference crop evapotranspiration (ET_o) computed with the Penman-Monteith equation (Monteith, 1965) using measured meteorological variables from the respective nearby weather stations and following (Allen et al., 1998). The Curve Fitting Toolbox 3.2 of Matlab R2011b (The MathWorks, Inc.) was used for non-linear least-squares optimization. Annual rates of E_t were computed as the sum of daily totals for the study period divided by 1.5.

The ratio of seasonal and annual E_t to ET_o was used to compare between YREF and MREF as a direct comparison of E_t would be confounded by differences in meteorological conditions associated with the altitudinal differences between the sites. Furthermore, the ratio was recalculated with E_t normalized by the LAI (derived from PAR attenuation measurements; Table 2.1 and Appendix C) of the corresponding site to account for tree age and size differences, as well as stand structural differences, between

the plantations. Because LAI data were only available for the dry seasons, LAI from the previous season was used for the wet season (i.e. dry season of 2008/2009).

Uncertainty bounds for seasonal and annual E_t totals were computed by propagating errors from: (i) up-scaling sapflow from individual trees to the stand level; and (ii) modeling daily totals of E_t. Errors stemming from (i) included the error in average F_s due to variability amongst trees, i.e. SE of the mean, and uncertainty in the scaling factor, i.e. SE of tree density (cf. Kostner et al., 1998). Thus, the total scaling error was estimated as the propagation of errors in a simple product. The modeling error, in turn, was the RMSE of the relationship between E_t and ET_o. Total errors for annual E_t totals were computed as the quadratic sum of total scaling and modeling errors (Muñoz-Villers et al., 2012).

2.5 Understory sapflow measurements

YREF did not have significant understory vegetation, in contrast to MREF (Fig. 2.2). The understory vegetation in MREF was surveyed in three transects 100 m long positioned within a quadrangular area of one hectare enclosing both sapflow monitoring plots at this site. The location of these transects was randomly chosen and the distance between transect 1 and 2 was 30 m, and 20 m between transect 2 and 3. Nine circular plots covering an area of 10 m^2 were placed every 10 meters within transects, such that the total area sampled was 270 m^2. The area covered by the crown of each understory shrub(s) was measured in each plot, as well as the % that each species covered. *Miconia glaberrima* was the dominant species, with a crown coverage estimated at 2260 ± 629 m^2

ha^{-1}, and therefore selected for sapflow monitoring. The next most dominant species was the fern *Dryopteris filix-max* covering 981 ± 279 m^2 ha^{-1}.

The heat balance method (HBM; Sakuratani, 1981) was used to collect sapflow data for *M. glaberrima.* Briefly, the HBM consists of solving the heat balance for a segment of stem constantly heated by a known amount supplied to the surface via a film heater tightly surrounding the stem, and determining the contribution of sap flux to the loss of the supplied heat, or the loss of heat upwards and downwards within the stem segment (Sakuratani, 1981). Mass flow rate of xylem sap of the understory (F_{su} [g s^{-1}]) was calculated with as follows:

$$F_{su} = \frac{Q - \lambda A \frac{(T_u - T_u') + (T_d - T_d')}{\Delta x} - kE}{c\,(T_d - T_u)} \quad (1)$$

where Q is the heat supply to the stem segment [W]; T_d and T_u are the stem temperatures measured down- and upstream from the heated segment [°C], respectively; T_u' is the stem temperature at Δx [m] downward from the measuring point of T_u; similarly, T_d' is the stem temperature at Δx upward from where T_d was measured; λ and A is the thermal conductivity [W m^{-1} $°C^{-1}$] and cross sectional area [m^2] of the heated stem segment, respectively; kE is the electromotive force [W] of the heat sensing element attached to the stem; and c is the specific heat of water (4.18 J g^{-1} $°C^{-1}$).

The HBM sensors consisted of a pair of thermocouples (upper and lower) and a thermopile, both mounted on flexible cork making a collar to wrap around a segment of a stem. Sensors for 7 mm stem diameter were constructed at Iowa State University following (Senock and Ham, 1995). In total, 5 individual shrubs were instrumented, each with one sensor on an exposed branch (Fig. 2.2f). The sensors were insulated with tube

foam insulator tied with cable ties, and lastly wrapped with tin foil. A constant power system (including a Dynamax voltage regulator) was used to supply 2.0 V for periods of 36 h in order to obtain daily courses while avoiding overheating the stems. The electrical power was supplied with two (12 V, 12 Amp) batteries that were recharged by a solar panel located next to the Tierra Grande weather station. Voltage and temperature readings were taken every 60 seconds with a data logger-multiplexer system (CR1000-AM16/32, Campbell Scientific) and stored as 10-min averages.

At the end of the measurement period all the leaves downstream of the heated stem segment from each branch were collected in separate bags and their leaf area determined with a LI-3100C leaf area meter (LI-COR). Average F_{su} per unit leaf area [L m^{-2}] was up-scaled to the stand level (E_u [mm]) by multiplying by leaf area index (LAI) of the understory (0.6 ± 0.3 m^2 m^{-2}). See Appendix C for details on understory LAI determination. For days with complete F_{su} hourly values, the ratio of mean daily E_u to daily E_t for MREF was calculated: $v = E_u / E_t$. Due to logistical limitations, data for only three full days were available during DS10 (March 29, April 3 and 4).

2.6 Total transpiration (E_T) of Pinus patula plantations

Total sapflow-derived transpiration (E_T) for MREF was computed on a daily time scale as the sum of E_t and vE_t, while for YREF it was equal to E_t. Annual rates of E_T were computed as the sum of daily totals for the study period divided by 1.5. Uncertainty bounds for seasonal and annual E_T totals in MREF were computed by propagating errors from: (i) total errors in E_t (see Section 2.4); and (ii) modeling the contribution of daily E_u. Errors stemming from (ii) included the error in average F_{su} due to variability amongst

branches (i.e. SE of the mean), uncertainty in the scaling factor (i.e. SE of understory LAI) and the RMSE of the relationship between υ and E_t.

2.7 Evapotranspiration (ET) and comparison among land uses

ET from PAS was computed by applying the Penman-Monteith equation using a daily calculation following Allen et al. (1998) and using meteorological data collected at the site. The following surface parameters were used: (i) albedo as calculated from R_n measurements on site, R_s from the La Cortadura weather station, and estimated R_{nl} (cf. Allen et al., 1998); (ii) aerodynamic resistance calculated using an average crop height of 10 cm; and, (iii) canopy resistance, using a fixed of 70 s m^{-1} (i.e. the reference value used for a 'well-watered grass'; Allen et al., 1998). Using this approach was an initial simplification as no measurements were taken to constrain surface conductance. Therefore, it must be noted that ET for PAS was conceptually not different from reference crop evapotranspiration (ETo) computed for the site (La Cortadura). Annual rates were computed as the sum of daily totals for the study period divided by 1.5.

For the forested sites, annual ET was simply the sum of its components: annual E_T, interception loss (E_i) and soil and forest floor evaporation (E_s). Estimated E_i was derived from a combination of throughfall measurements at YREF and MREF (plus stemflow at YREF) and modelling following methods described in Holwerda et al. (2010). The measurements were conducted during the same time period of the present study. E_i as a percentage of rainfall was found to be 5.4% and 7.5% for YREF and MREF, respectively (F. Holwerda, unpubl. data). Evaporative losses from the soil and forest floor (E_s) were considered negligible for YREF given its closed canopy. However,

overlooking E_s for a forested land cover structured as MREF may substantially underestimaate ET given its open canopy and high rainfall rates of the study area (Denmead, 1984). Unfortunately, direct observations that could be used to estimate E_s were not performed. Nevertheless, an indirect approach using θ data (down to a depth of ~30 cm) to determine soil moisture depletion attributable to E_T and E_s, was explored. Briefly, it involved the subtraction of E_T from the calculated volume of soil water depleted in a day (i.e. difference between the current day's θ and θ from the previous day) such that E_s is assumed to be the residual (Conrado Tobon, pers. comm.). However, this approach can only be applied for periods when θ is below field capacity (Ibid.) and according to the data available for MREF, this did not occur during the study period (Fig. 2.4). For this reason, a rough estimate of E_s for MREF was derived using the ratio E_s/E_i of 0.6, from a similarly structured mature pine plantation (*P. caribeae* planted on former grasslands in Fiji with LAI of 3 m^2 m^{-2} and tree density of 621 trees ha^{-1}; Waterloo et al., 1999). Mean annual ET normalized by R_n (in evaporation equivalent units [mm $year^{-1}$]) was used to compare the land cover types.

3. Results

3.1 Meteorological conditions and soil moisture dynamics

The study period included two contrasting dry seasons (November 2008–April 2009 and November 2009–April 2010, hereafter DS09 and DS10, respectively) and a wet season (May 2009–October 2009, hereafter WS09). DS10 was relatively wetter and foggier than DS09 as P and the % of time with fog events increased almost two-fold at the presently studied altitudes within the cloud belt (Fig. 2.3a-b). Annual P, calculated as the sum of P

for the study period divided by 1.5, was 2484 mm for La Cortadura and 2231 mm for Tierra Grande (Fig. 2.3a). The proportion of time with fog occurrence recorded at the two altitudes was similar (Fig. 2.3b). While on average fog event occurrence was the same during DS09 and WS09 (26% and 27% of the time at La Cortadura and Tierra Grande, respectively), there was a considerable increase during DS10 at both altitudes (42% and 36% of the time at La Cortadura and Tierra Grande, respectively), particularly in December, January and April, presenting a two-fold increase relative to DS09 (Fig. 2.3b).

As expected from the difference in altitude covered by the study sites (~290 m), monthly median R_s was generally higher at Tierra Grande compared to La Cortadura (Fig. 2.3c). For both altitudes, the highest monthly median R_s was observed just before the onset of the wet season, i.e. during March and April (Fig. 2.3c). Maximum T was observed during the wet season (Fig. 2.3d). Greater day-to-day variation in daily T and D were observed during the dry seasons than during the wet season at the two altitudes (Fig. 2.3d-e). Monthly median T at La Cortadura (12.5 ± 0.5 °C and 15.8 ± 0.1 °C for both dry seasons combined and WS09, respectively) was consistently higher than at Tierra Grande (11.6 ± 0.6 °C and 14.0 ± 0.2°C, for both dry seasons combined and WS09, respectively). Monthly median D was similar for both altitudes and followed the same seasonal pattern of R_s, reaching maximum daily values during the dry season up to ~2 kPa at La Cortadura and Tierra Grande (Fig. 2.3e). U did not present seasonal variation at both altitudes and was generally low, although U was consistently higher at Tierra Grande (monthly median U range: 1.6–2.5 m s^{-1}) compared to La Cortadura (monthly median U range: 1.26–1.68 m s^{-1}; Fig. 2.3f).

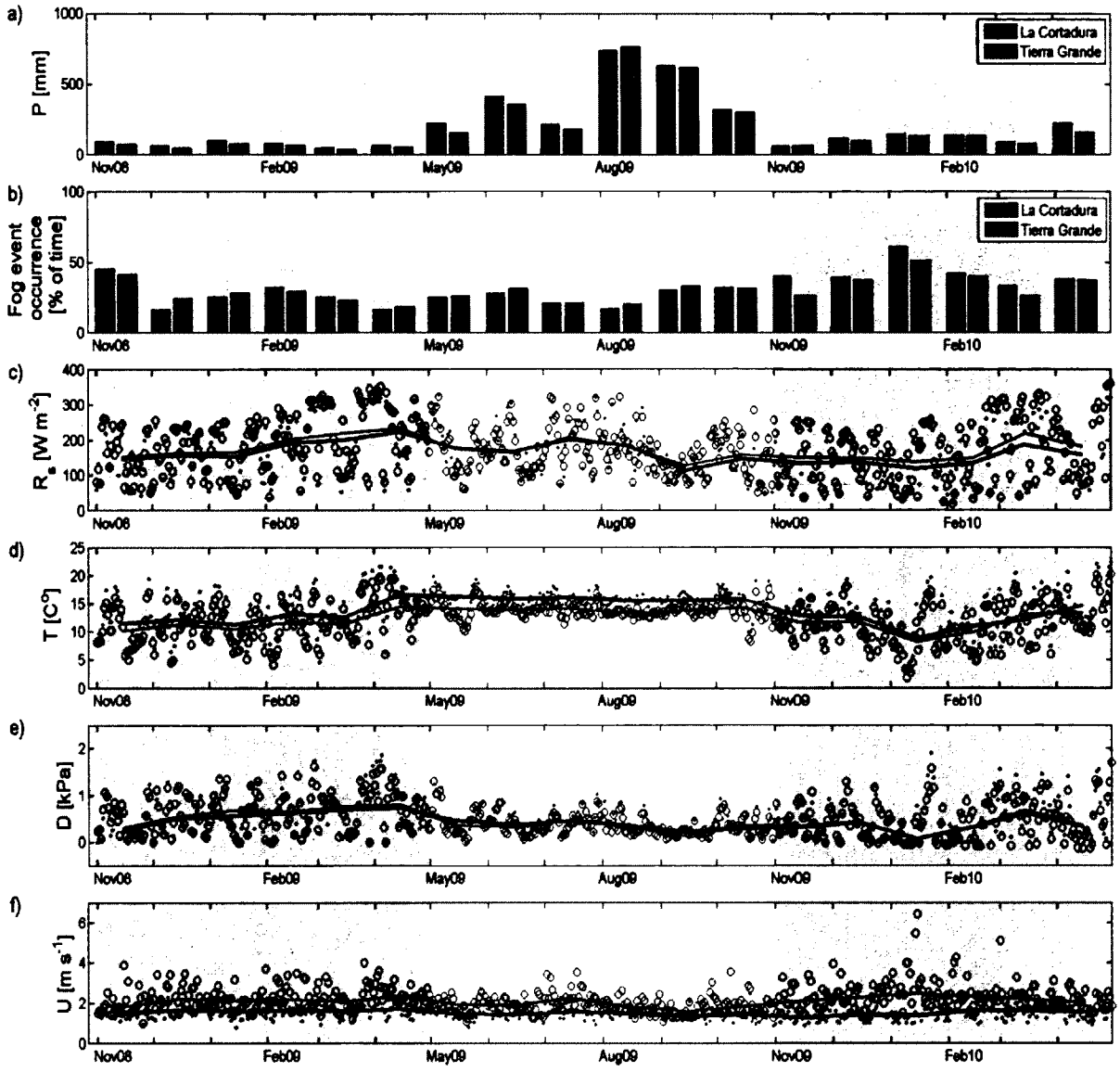

Figure 2.3. Meteorological conditions during the study period at two altitudes within the seasonally dry montane cloud belt of central Veracruz, Mexico: La Cortadura (2128 m a.s.l.) and Tierra Grande (2400 m a.s.l.). (a) Monthly rainfall totals (P). (b) Percent time with fog events. (c) Median incoming solar radiation (R_s). (d) Median air temperature (T). (e) Median vapor pressure deficit (D). (f) Median wind speed (U). Solid lines and symbols depict monthly and daily data, respectively. Thick solid lines and dots correspond to La Cortadura, while thin solid lines and empty circles correspond to Tierra Grande. Light gray shaded areas indicate the two dry seasons under study (DS09: November 2008–April 2009; DS10: November 2009–May 2010), and the white area corresponds to the wet season (WS09: May–October 2009).

Dynamics of calibrated mean daily soil moisture content (θ [m^3 m^{-3}]) at five depths, together with concurring P [mm], shown for each site in Fig. 2.4. All the sites presented relatively high θ throughout the study period. Long periods without rainfall were rare at all sites (Fig. 2.4). Considering only days with θ data, the longest rain-less period (P < 1 mm day^{-1}) had a duration of 18 days and occurred in the last weeks of DS09. The minimum value of θ was observed at the end of this period at all sites: 0.45 m^3 m^{-3} at PAS (depth: 5 cm), 0.42 m^3 m^{-3} at YREF (depth: 19 cm), 0.44 m^3 m^{-3} at MREF1 (depth: 35 cm), and 0.33 m^3 m^{-3} at MREF2 (depth: 25 cm).

Notably, the minimum θ values for all the forested sites approximated the respective field capacity θ for these shallow depths (Fig. 4b-d; Appendix Table D1), while for PAS (depth: 5cm), the minimum θ value was below the field capacity θ for 11 days during this dry period (approximating permanent wilting point θ of 0.41; Fig. 2.4a; Appendix Table D1). In fact, the pasture vegetation was observed to start wilting in patches by the end of this rainless period, but it recovered shortly following the start the wet season.

Another interesting observation for PAS was that θ at the deepest soil layer monitored (-100 cm) presented similar values as those recorded for the shallowest depth (-5 cm). This pattern was as not observed at the other sites. It should be noted that calibration of soil moisture probes yielded a different % bias (with respect to the equation provided by the manufacturer) for the depth of 100 cm compared to all other depths (Appendix Table D2).

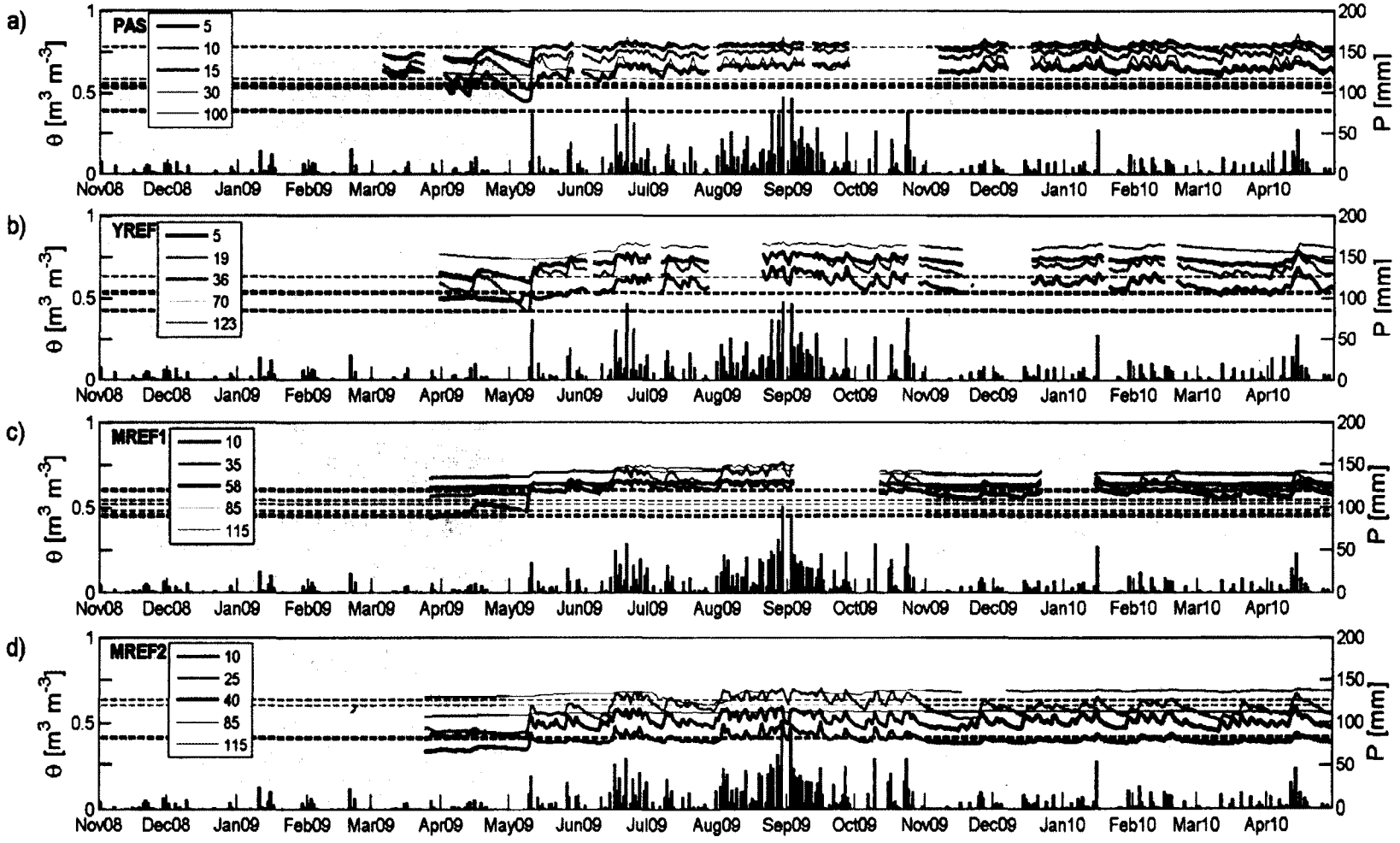

Figure 2.4. Dynamics of calibrated mean daily soil moisture content (θ [m^3 m^{-3}]; solid lines) at different measurement depths described in the legends, and daily rainfall totals (P [mm]; bars). θ at field capacity (FC; Appendix Table D1) for each depth are shown with dashed lines.

3.2 Stand-level transpiration estimates for YREF and MREF

Whole-tree sapflow (F_s) increased with tree size. An exponential function describes the relationship between F_s and tree basal area (Fig. 2.5). The derived empirical functions to predict E_t at a daily time scale from reference evapotranspiration (ETo) at the two *P. patula* plantations are presented in Fig. 2.6. Despite some scatter, exponential functions fitted the data from both plantations very well ($r^2 > 0.80$; Fig. 2.6). Mean annual E_t estimated for YREF was 645 ± 50 mm, and seasonally, DS09: 367 ± 58 mm, WS09: 302 ± 61 mm, and DS10: 299 ± 31 mm. In contrast, estimated mean annual E_t for MREF was considerably lower, at 260 ± 45 mm, and seasonally, DS09: 143 ± 39 mm, WS09: 134 ± 40 mm, and DS10: 113 ± 39 mm. The ratio E_t/ETo on a seasonal time scale was higher for YREF than for MREF for all seasons (Fig. 2.7a). Annually, E_t/ETo was 0.80 ± 0.06 for YREF, and 0.30 ± 0.05 for MREF. On a per unit leaf area, however, the differences of the ratio between plantations are minimized (Fig. 2.7b).

An example of the daily course of understory (E_u) and tree transpiration (E_t) at MREF, with concurring PAR above and below the canopy, is shown in Fig. 2.8a. It can be noted that the magnitude of E_u is relatively low compared to E_t. The ratio of daily E_u to E_t (υ) was found to change with the magnitude of E_t (Fig. 2.8b). Rather than defining a constant υ to estimate total transpiration for MREF, the following empirical model was used to derive a daily value of υ for the study period:

$$E_t < 0.40; \upsilon = -0.17E_t + 0.16 \quad (2)$$

$$E_t \geq 0.40; \upsilon = 0.04E_t^{-0.81} \quad (3)$$

were eq. (2) is the linear extrapolation to intersect with the y-axis of (3), which in turn, is the best nonlinear fit for daily mean υ against E_t (solid line in Fig. 2.8b). At an annual scale, E_u was only 5 ± 2% of annual E_T.

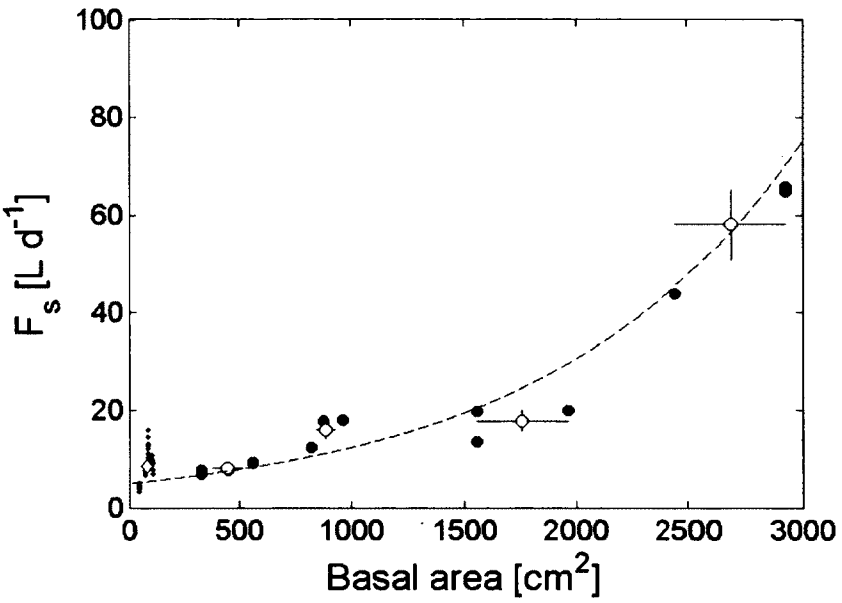

Figure 2.5. Relationship between tree size (basal area) and daily totals of whole-tree sapflow (F_s) of all sample *Pinus patula* trees for days with near clear-sky. Open circles show mean F_s for each DBH class (MREF), the open diamond show mean F_s for all sample trees at the young pine site (YREF). Closed circles and diamonds show individual tree data for MREF and YREF, respectively. The continuous line depicts the best non-linear fit through all mean values: $F_s = 5.01\exp(9.03\text{x}10^{-3}\text{basalarea})$; r^2=0.93; RMSE: 5.19.

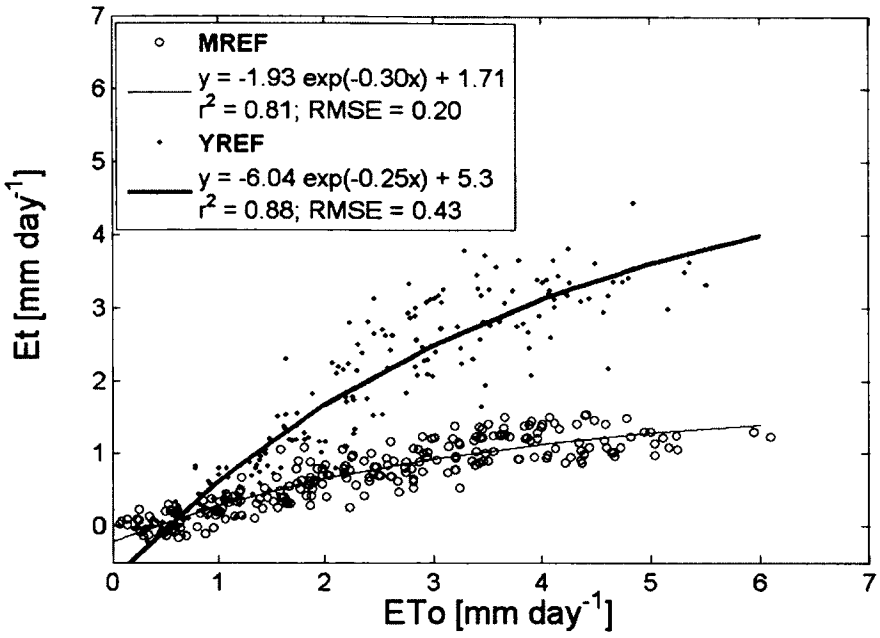

Figure 2.6. Relationship between daily reference evapotranspiration (ETo) and daily stand level tree transpiration (E_t) derived from sapflow measurements in *Pinus patula* from contrasting stands at two elevations within the montane cloud belt of central Veracruz, Mexico: a young (YREF; 2180 m a.s.l.) and a mature plantation (MREF; 2470 m a.s.l.).

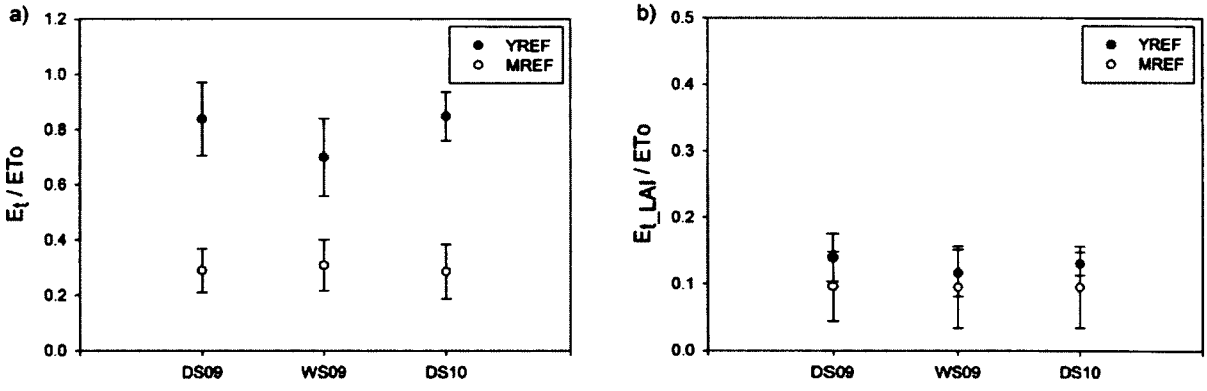

Figure 2.7. (a) Ratio of seasonal totals of stand level tree transpiration (E_t) to ETo for a young (YREF; 2180 m a.s.l.) and a mature (MREF; 2470 m a.s.l.) *Pinus patula* plantation. (b) Idem with the ratio computed using stand level tree transpiration per unit leaf area (E_{t_LAI}).

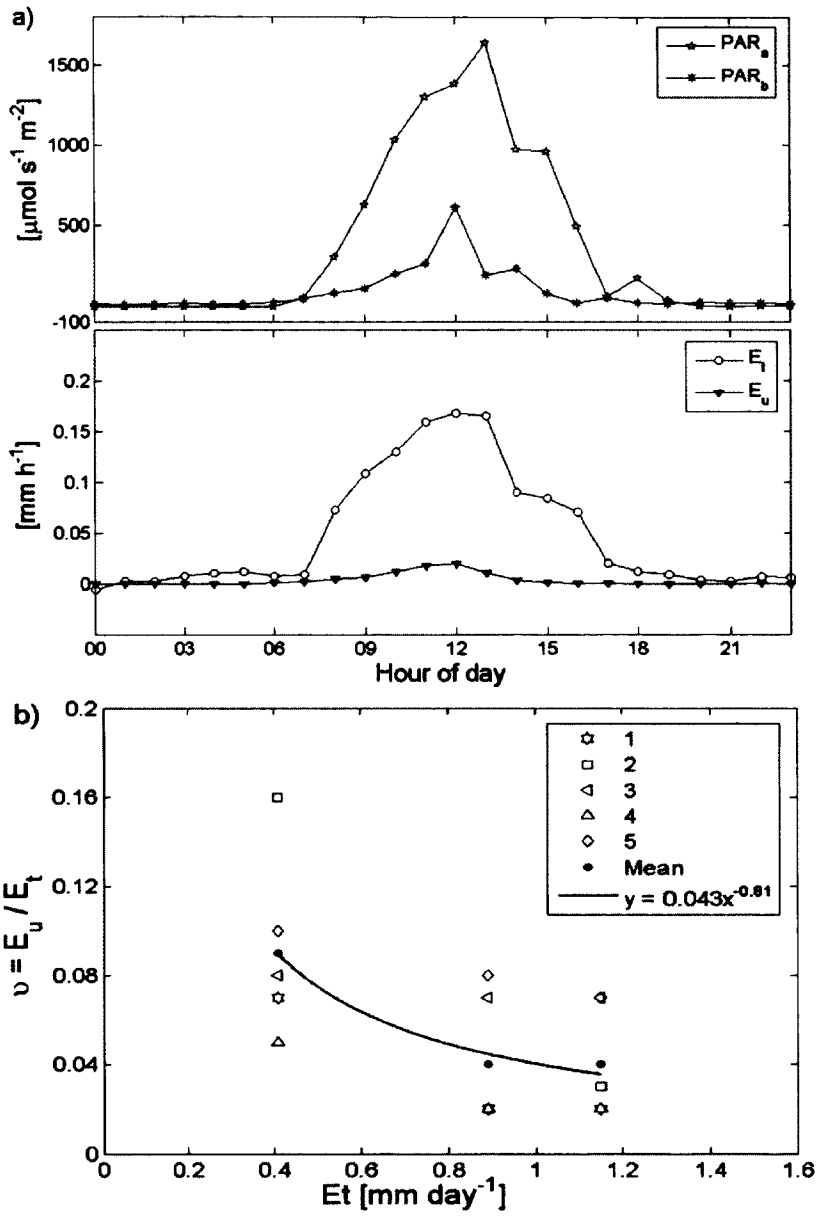

Figure 2.8. (a) Daily course of photosynthetically active radiation above (PAR_a) and below (PAR_b) the canopy and sapflow-derived stand-level understory (E_u) and tree (E_t) transpiration at a mature *Pinus patula* plantation (MREF) on April 3, 2010. (b) Variation of υ (the ratio E_u/E_t) with E_t for three days in late DS10 in which E_u data were available. Open symbols are data from five *Miconia glaberrima* shrubs, the closed circles depict their mean, and the solid line is the best nonlinear fit for the daily mean values ($r^2 = 0.97$; RMSE = 0.006).

3.3 Evapotranspiration (ET) across land cover types

Mean daily courses of R_n for clear-sky days show that there was more energy available on the surface covered by (young) *Pinus patula* than by pasture (Fig. 2.9). The mean daily measured albedo for clear-sky days was 0.14 ± 0.04 for YREF and 0.20 ± 0.05 for PAS.

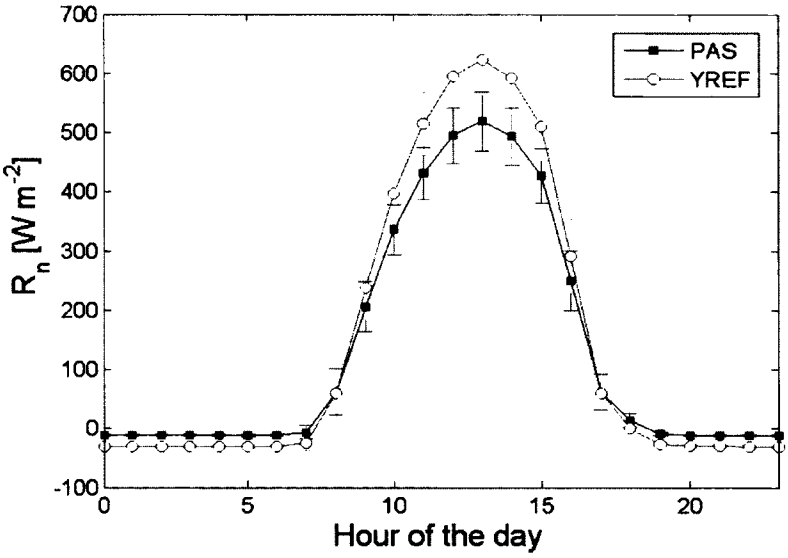

Figure 2.9. Mean daily course of net radiation (R_n [Wm^2]) for clear-sky days measured at PAS and YREF. Error bars are one standard deviation. Hourly R_n data for MREF was not available.

Annual ET estimated for PAS was 815 mm (DS09: 438 mm; WS09: 432 mm; DS10: 352). For YREF, annual ET was estimated in 779 mm, of which 134 mm was annual interception loss (E_i = 5.4% of annual P; F. Holwerda, unpubl. data). For MREF, annual ET was 541 mm, with annual E_i estimated at 167 mm (7.5% of P; F. Holwerda, unpubl. data) and annual E_s estimated at 100 mm. The ranking of land cover types by the proportion of available energy (R_n in water equivalent units) used for ET at an annual scale was: PAS (0.80) = YREF (0.80) > MREF (0.42) (Fig. 2.10).

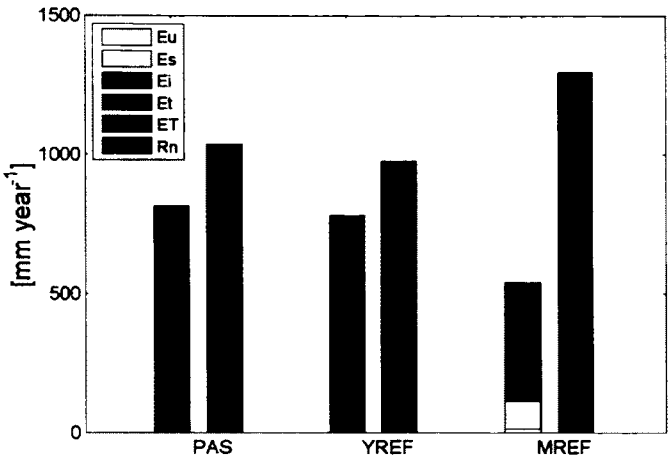

Figure 2.10. Annual evapotranspiration (ET) and available energy (R_n in water equivalent) for three land uses in the montane cloud belt of central Veracruz, Mexico: pasture (PAS), 10-year-old *Pinus patula* reforestation (YREF), and a mature conifer forest dominated by planted *P. patula* (MREF). ET for forested land uses is separated in its components: tree transpiration (E_t), rainfall interception loss (E_i), understory transpiration (E_u; only for MREF) and soil evaporation (E_s; only for MREF).

4. Discussion

Meteorological conditions during the study period were within the range of weather parameters reported previously for this site (Holwerda et al., 2010; Muñoz-Villers et al., 2011). The study included a period of La Niña during DS09, resulting in a more pronounced dry season (i.e. relatively less rainfall and fog occurrence compared to DS10 as discussed in more detail in Chapter 3). Nevertheless, relatively high soil moisture content was maintained even during the driest period across sites (Fig. 2.4.). Furthermore, E_T for both *P. patula* plantations was higher during DS09 compared DS10. These observations suggest that soil water availability may not have been a limiting factor for plant water use from *P. patula* plantations during the study period, similar to what has

been reported for forests from other montane cloud belts world-wide (e.g. Chu et al., 2012; McJannet et al., 2007; Schawe et al., 2007; cf. Bruijnzeel et al., 2011).

Similarly for PAS, cumulative ET was greater during DS09 than DS10. Although it is important to note that ET for PAS, as estimated here, is strictly speaking a potential amount (i.e. not different from ETo for this site). This is because surface conductance was a fixed value; that is, not constrained by limiting factors, such as using response functions as in the Jarvis-Stewart method for modeling surface conductance (Stewart, 1988). The assumption that PAS was 'well watered' made by using Allen et al.'s (1998) approach to estimate ET, may not have applied throughout the study period. In particular, this assumption was likely invalid during the rainless period at the end of DS09 (Fig 4a) given the observations of temporary and partial wilting of pasture vegetation combined with soil moisture values near permanent wilting point at -5 cm. Therefore, soil water availability may have limited transpiration; however, this limitation does not appear to have been sustained for prolonged periods of time. A step forward towards estimating actual ET for PAS is to develop a response function for surface conductance using soil moisture data.

Furthermore, the depths that were observed to have greater fluctuation in soil moisture content in YREF and MREF are within the range of inferred depth of plant soil water uptake determined for the dry season (or functional rooting depth; 20–50 cm) based on a previous study that analyzed xylem and soil water stable isotopes in the study area (Appendix D Table D1; Goldsmith et al., 2012b; G.R. Goldsmith and M.S. Alvarado-Barrientos, unpubl. data). Notably, there were no major differences in the inferred functional rooting depth between the two *P. patula* plantations (i.e. no effect of stand

development stage, or tree age and size; however, isotope analyses have revealed a positive relationship, albeit weak, between tree size and inferred depth of water uptake; G.R. Goldsmith and M.S. Alvarado-Barrientos, unpubl. data). The functional rooting depth of PAS was not examined, but field observations of root density (Table D1) suggest that its rooting is also relatively shallow. As discussed in Goldsmith et al. (2012b), consistent shallow rooting across land cover types likely reflects the patterns of water and nutrient availability in the area. Analyses of soil nutrient concentration revealed that available nitrogen and phosphorous decline sharply below ~40 cm across land cover types (D. Geissert, pers. comm.). These observations are similar to previous reports of nitrogen and phosphorous being concentrated mostly at shallow soil depths (< 20 cm) under forests in tropical montane regions (Cavelier, 1992; Silver et al., 1994). Moreover, it has been pointed out that high soil water content in cloud-affected ecosystems is the likely cause of reduced nitrogen cycling and consequently, of low nitrogen supply (cf. Benner et al., 2010).

The seemingly odd behavior of soil moisture dynamics at the deepest layer monitored in PAS (-100 cm), that is, showing lower values than expected and similar to what was observed at the shallowest layer (-5 cm), may be explained by differences in saturated hydraulic conductivity (*K*sat; Table D1). At the depth of 100 cm *K*sat was higher than at the topsoil. This difference was likely produced by compaction of the topsoil (0–20 cm deep) due to grazing. Macro-pores and old root channels were observed at the deeper layers in PAS allowing preferential water flow and increasing drainage (A. Gómez-Tagle, pers. comm.). Such physical soil characteristics are likely the result of land-cover legacy, that is, remains of root systems of the former lower montane cloud

forest. These observations suggest that the soils in the study area have relatively high resistance to degradation (Geissert et al., 2012; Gómez-Tagle et al., 2011).

Whole-tree E_t increased with tree age and size, as expected (Fig. 2.5). Similar relationships have been reported for a wide range of species and ecosystems (c.f. Meinzer et al., 2005). Research involving plantation chronosequences has shown that generally, whole-tree E_t normalized by the size of trees (i.e. by unit sapwood area, leaf area or basal area) is higher for smaller and younger trees compared to older and larger (Delzon and Loustau, 2005; Magnani et al., 2008; Ryan et al., 2000; Vertessy et al., 2001; Zimmermann et al., 2000). These differences have been attributed to reduced stomatal conductance and leaf area with increasing age and size (Ibid.). The present findings on E_t for *P. patula* are in line with these observations, in that at stand level, E_t for YREF was higher than at MREF (Fig. 2.6) due to higher LAI and stocking density (and higher sapwood per unit land area; not shown), and by having found a higher ratio of E_t to ETo regardless of the season (Fig. 2.7a). By comparing the ratio E_t/ETo between YREF and MREF, the meteorological drivers of transpiration are normalized across sites, and thus the resulting pattern should reflect differences in E_t due to structural variation and tree age and size affects without the confounding factor(s) arising from altitudinal differences among sites. On the other hand, after normalizing E_t by LAI, YREF presented only slightly higher E_t/ETo and therefore the difference with MREF was no longer significant (Fig. 2.7b). Moreover, ancillary data on leaf-level stomatal conductance under clear-sky conditions (Appendix E) suggest that mature pines have, on average, higher instantaneous rates than young pines. It is important to highlight, that higher leaf-level stomatal conductance for mature pines does not necessarily translate to higher E_t given

that other considerations come into play with the change of scale, such as boundary layer conductance and leaf area (Monteith and Unsworth, 2007) .

The ratio of daily E_u to E_t (υ) was found to change with the magnitude of E_t (Fig. 2.7b). This pattern may be explained by differences in light environment below the canopy compared to above the canopy, as illustrated by the daily course of PAR above and below the canopy (Fig. 2.7a). Clear-sky conditions produced higher daily E_t and highly variable PAR in the understory due to alternating shadows and sun flecks, with an overall result of low daily E_u, and consequently, low υ. In contrast, radiation under cloudy and foggy conditions reduced E_t, but the larger diffuse proportion of radiation allows more light to penetrate the canopy into the understory, resulting in relatively higher E_u (and higher υ) than under sunny conditions.

The proportional contribution of E_u (*Miconia glaberrima*) to E_T from the mature *Pinus patula* stand was unexpectedly small (5% of annual E_T), as an important turbulent transfer was expected between the understory and the overstory layers given the openness of the canopy and low tree density. Compared to many previous studies showing considerable contribution of E_u to E_T for stands with low tree density (e.g. Kagawa et al., 2009; Kelliher et al. ,1990; cf. Roberts, 1983; Spittlehouse and Black, 1982; Vertessey et al., 2001; Wedler et al., 1996), υ found for MREF appears very small. For instance, in a German *P. sylvestris* plantation (LAI: 2.8 m^2 m^{-2}), Wedler et al. (1996) found that the understory (grasses and sedges with LAI of 1.5 m^2 m^{-2}) transpired 13% of the pine's E_t. Spittlehouse and Black (1982) found that the understory (*Gaultheria shallon*; LAI: 3.0 m^2 m^{-2}) of a Douglas fir forest (LAI: 3.6 m^2 m^{-2}) transpired 35% of E_t. Also, Roberts et al. (1982) showed that although E_t for a *P. nigra* stand was higher than for a *P. sylvestris*

stand of similar age, the transpiration from vigorous understory (bracken) of the latter stand compensated for the differences in E_t. Given such reports and the suggestion that "understoreys can be regarded as effective buffers to the canopy differences" (Roberts 1983), it was expected that lower E_t for MREF compared to YREF would be compensated by considerable E_u such that E_T would not differ much between *P. patula* stands.

Due to technical difficulties it was not possible to obtain an independent assessment of E_u from *M. glaberrima* shrubs in order to evaluate the uncertainty of the heat balance sapflow method used, such as direct water uptake measurements with a cut-branch procedure analogous to that performed for the evaluation of HRM sapflow technique with young pines (see Chapter 1). Ancillary data of instantaneous rates of leaf-level stomatal conductance for *M. glaberrima* and mature pine trees (Appendix E) show higher and less variable rates for the former. These results, combined with the larger transpiration rates for the pines than for the understory shrubs, suggest that the leaf-atmosphere water vapour gradient in the understory of MREF was probably smaller than at the pine canopy height (Lambers et al., 2008), besides the differences in LAI. Another source of uncertainty with respect to E_u, is that other understory vegetation such as ferns and suppressed small trees were not taken into account due to logistical limitations. Nevertheless, given that these other understory species presented a relatively minor proportion of total area coverage and LAI relative to *M. glaberrima*, we consider that their contribution to E_T was likely small as well. Assuming that there was no important underestimation of E_u, the present results suggest that as *P. patula* plantations reach a

mature stage of stand development, tree LAI and E_T decreases, regardless of an increase in understory LAI.

The observed reduction of LAI at MREF may be related to productivity decline as a result of nutrient limitations because it is similar to the mid-rotation decline in LAI observed in loblolly pine (*P. taeda*) plantations in southern USA (Vose and Allen 1988). These observations suggest again, that the study area presents important nutrient limitations to primary productivity. Also, the decline in productivity may be due to maturity of the trees (Delzon and Loustau, 2005; Magnani et. al., 2008; Ryan et al., 2000; Vertessy et al., 2001).

In well-watered environments, ET has been shown to be similar (or even higher) in grasslands than in forests (Andre et al., 1989; Brauman et al., 2012; Kelliher et al., 1993; Wolf et al., 2011), which agrees with the findings for the pasture and pine plantations studied here. This contrasts with observations that, given similar atmospheric conditions, trees generally have deeper roots and higher LAI, resulting in greater transpiration and higher wet canopy evaporation rates, and in turn, with overall higher ET than shorter stature vegetation with shallow roots and lower LAI such as grasses (Calder, 1998; Zhang, 2001). Kelliher et al. (1993) reviewed surface parameters controlling ET of coniferous canopies and grasslands and found that regardless of structural differences, there were no important differences in maximum surface conductance, but rather, coniferous canopies presented light saturation reducing canopy conductance (and E_t) after having attained maximum values at lower light levels than for grasslands. On a daily basis, the result was significantly higher ET for grasslands than for coniferous stands (Ibid.). In the present case, although ET was slightly higher for PAS compared to YREF

and substantially higher compared to MREF, leaf-level stomatal conductance of the dominant grass species in PAS was on average lower than for both young and mature pines (Appendix E). It has been shown however, that for grasslands in humid climates (and under non-limiting soil water conditions), stomatal conductance explains a relatively small amount of the variation in ET (10-20%; Katerji and Rana, 2011), while aerodynamic conductance is very low for short-statured vegetation (Calder, 1998); even lower at sites with low wind speeds such as the present study site (Fig. 2.3f). Therefore, ET of a well-watered pasture is driven mainly by solar radiation (Jarvis and McNaughton, 1986; Katerji and Rana, 2011). The ratio of ET to available energy (ET/R_n) was consistent with the relative rates of ET across land uses: PAS $\geq$ YREF > MREF. This suggests that stomatal control appears to be limiting ET to some extent at the forested sites, which is consistent with findings that conifer canopies are well coupled to the atmosphere (Smith and Hinckley 1995). Furthermore, the low canopy interception loss (E_i) estimated for the pine plantations increased ET but not to the extent to be higher than for pasture, as has been reported for other forests in high rainfall areas (Calder, 1998). Despite the above, it is important to recall that ET for pasture as examined here (i.e. Allen et al., 1998) may be overestimating the evaporative losses for PAS, while for the pine plantations, the usage of sapflow techniques and rough estimations for soil evaporation may be underestimating ET. Eddy covariance measurements would have been a better approach perhaps (Wolf et al., 2011; Holwerda et al., 2013), but the mountainous terrain and patchy landscape present further important complications to the interpretation of data from such approach (Monteith and Unsworth, 2007).

ET from a combination of modeling and measurements for a nearby old-growth lower montane cloud forest (LMCF), 20-year-old regenerating LMCF, and shaded coffee plantation, has been reported recently (Holwerda et al., 2013; Muñoz-Villers et al., 2012). With an annual ET of 815 mm, the estimated total plant water use of PAS is lower than that of the old-growth and regenerating LMCFs (1350 mm and 1103 mm, respectively; Muñoz-Villers et al., 2012), as well as of shaded coffee (1066 mm; Holwerda et al., 2013). Total plant water use of both pine plantations rank lower than all of these land uses (779 mm and 541 mm for YREF and MREF, respectively). The present values should be taken with care, as discussed above due to unknown relevance of not fully accounting (or roughly estimating) some sources of evaporative losses.

5. Conclusions and Future Research

Similar to higher total plant water use per unit available energy by PAS compared to the two *P. patula* plantations at different stage of stand development, combined with relatively similar soil hydrological properties and functional rooting depth, suggest that differences in energy partitioning and in the relative importance of surface and aerodynamic conductance, were the drivers of ET variation across land cover types. Furthermore, the implications of the present results are important for land use management and policy. It appears that reforesting former pasture-lands with *P. patula* would not substantially increase ET after >10 years of planting, contrary to findings from other studies (cf. Scott et al., 2005). Therefore, reforesting pastures with native tree species, such as *P. patula*, seem to have a relatively low impact on the amount of evaporative losses in environments such as the study area. This is contrary to what has

been found in other environments where trees are planted in lands that do not naturally support forest ecosystems under current climate (e.g. afforestation of grasslands in Argentina and fynbos in South Africa; cf. Farley et al. 2005; cf. Scott et al. 2005). Significant hydrological impacts of land use change in environments such as the seasonally dry tropical montane area of central Veracruz, Mexico, may be more importantly driven by changes in hydrological properties of the soil (cf. Bruijnzeel 2004).

A modeling approach is recommended to assess ecohydrologic impacts of different land use change trajectories in the study area, and to test the response of ET to future climate scenarios. The approach used by Brauman et al. (2012) could be followed as a first step, to examine in more detail the drivers of potential ET for different land cover types. In such a way, the same methodological approach would be applied across land cover types, namely, the Penman-Montheith equation. Then, data as peresented here for the pine plantations, could be used as ground data to validate a model based on what is learned from analyzing potential ET. Furthermore, a hydrological modeling framework to sintethize data on other water balance components and hydrological processes in the study area (e.g. low cloud water interception across forest types, same functional rooting depth across land cover types, soils with high resistance to degradation, high infiltration rates, groundwater dominated flowpaths; Geissert et al., 2012; Gómez-Tagle, et al., 2011; Goldsmith et al., 2012b; Holwerda et al., 2010, 2013; Karlsen, 2010; Muñoz-Villers et al., 2012a, 2012b), is the logical next step to ultimately determine whether land use change affects ecohydrologic function strongly, expressed as catchment water yield, for example.

CHAPTER III

SUPPRESSION OF TRANSPIRATION DUE TO CLOUD IMMERSION IN A SEASONALLY DRY MEXICAN WEEPING PINE PLANTATION[1]

Abstract

Cloud immersion affects the water budget of fog-affected forests not only by introducing an additional source of water (via cloud water interception by plants), but also by suppressing plant transpiration. The latter effect is often overlooked and not routinely quantified, restricting a complete understanding of the net hydrological effect of cloud immersion and the possible consequences of projected reductions in cloud immersion under drier and warmer climates in tropical montane regions in the coming decades. This paper describes an approach to quantify the suppression of stand-level tree transpiration (E_t) due to cloud immersion using measurements of sapflow, fog occurrence (visibility), leaf wetness, and near-surface climate. Estimates of fog-induced E_t suppression in a 10-year-old *Pinus patula* plantation in the montane cloud belt of central Veracruz, Mexico, are presented for two contrasting dry seasons and a wet season. Fog occurred for 32% of total study period time, although showing pronounced seasonal variation (e.g. 44% during the second dry season). When fog occurred it was accompanied by rainfall during three quarters of the total time. Although the canopy was wet for almost a third of the time, fog-induced canopy wetness constituted only a very small portion of this total (2%).

[1] Manuscript prepared for submission to *Agricultural and Forest Meteorology*: Alvarado-Barrientos, M.S., Holwerda, F., Asbjornsen, H., Dawson, T.E., Bruijnzeel, L.A. Suppression of transpiration due to cloud immersion in a seasonally dry Mexican weeping pine plantation.

Relative to sunny conditions, E_t was suppressed by 90 ± 7% under conditions of dense fog versus 83 ± 7% under light fog and 78 ± 10% during overcast conditions. Quantification of the potential change in annual E_t associated with two scenarios for future cloud immersion at the study site revealed that: (i) when all fog occurrence is replaced by overcast conditions, mean annual E_t (645 ± 50 mm) is likely to increase by only 2 ± 1%; and, (ii) when sunny conditions replace all foggy conditions, the likely increase in annual E_t is 17 ± 3%. As the rise in the regional lifting condensation level is likely to be on the order of only a couple of hundred meters and will probably result in a shift to overcast rather than clear-sky conditions, the present results suggest that the corresponding impact on E_t may be relatively small. Consequently, climate change-related reduced dry-season precipitation, more than diminishing cloud immersion alone, presents a more worrisome prospect for plant-water relations and water yield from headwater catchments, due to the associated potential reductions in soil water reserves. The present results highlight the need for better projections of climate change-related alterations in cloud cover and immersion, as well as rainfall patterns for tropical montane regions.

1. Introduction

Frequent immersion in ground-level clouds, or fog, is the defining characteristic of cloud forests, which are widely regarded as biodiversity 'hot spots' and 'water towers', yet are among the most endangered terrestrial ecosystems in the world (Bruijnzeel et al., 2010; Viviroli et al., 2007). Projected future drier and warmer regional climate in many montane cloud belts world-wide is likely to cause an increase in the lifting condensation

level (LCL) (Barradas et al., 2010; Karmalkar et al., 2008; Lawton et al., 2001; Nair et al., 2003; Ray et al., 2006; Richardson et al., 2003; Still et al., 1999; Van der Molen et al., 2006; Williams et al., 2007). This would reduce the frequency of fog occurrence and/or its liquid water content, and might, in turn, impact such vital ecosystem services provided by tropical montane cloud forests, as the stable supply of dry-season baseflows from (Brown et al., 1996; Martinez et al., 2009; Ponce-Reyes et al., 2012; Zadroga, 1981). This rise in LCL has been suggested to be on the order of a few hundred meters. For instance, theoretical estimates suggest that an increase in the cloud base by up to 300 m for Costa Rica (Karmalkar et al., 2008), while observations of fog frequency in central Veracruz, Mexico, suggest an increase of 200–400 m (Barradas et al., 2010). Hence, it is likely that many montane cloud belt zones will experience a shift in prevailing conditions from frequent cloud immersion to mostly overcast. It must be noted, however, that there are no reliable projections to date for the trajectory of the LCL and the associated changes in cloud immersion occurrence and frequency under future climate (Bruijnzeel et al., 2011; Karmalkar et al., 2011; Williams et al., 2007).

Cloud immersion is known to affect the site water budget of a forest ecosystem directly via the capture of cloud water (i.e. fog) by the canopy, producing drip to the forest floor once the canopy's storage capacity is exceeded and increasing soil water availability above that maintained by rainfall alone (Bruijnzeel et al., 2011; Giambelluca and Gerold, 2011). The direct hydrometeorological effect of cloud immersion has attracted most attention (García-Santos and Bruijnzeel, 2011; Giambelluca et al., 2011; Gómez-Peralta et al., 2008; Haeger and Dohrenbusch, 2011; Holder, 2003; Hutley et al., 1997; Ingraham and Matthews, 1988; Juvik et al., 2011; Vogelmann, 1973), but the

indirect hydrological effects of foggy conditions produced by the reduction of evaporative demand (i.e. attenuation of incoming solar radiation and increased atmospheric humidity) and increased canopy wetness, have become acknowledged comparatively recently. These indirect effects include, firstly, the suppression of transpiration (Burgess and Dawson, 2004; Chu et al., 2012; Johnson and Smith, 2008; Reinhardt and Smith, 2008; Ritter et al., 2009), and, to a lesser extent, foliar absorption of cloud water accumulated on the canopy (Dawson, 1998; Goldsmith et al., 2012a; Limm et al., 2009; Simonin et al., 2009). Such indirect effects may be of greater importance for the water budget of fog-affected ecosystems in places where cloud-induced drip from the canopy contributes less to soil water reserves compared to rainfall (Dawson, 1998; García-Santos, 2007; Hildebrandt et al., 2007). Thus, a substantial reduction in soil water uptake due to cloud immersion may be highly relevant in producing the high streamflow volumes reported to emanate from catchments covered by tropical montane cloud forests (Brown et al., 1996; Bruijnzeel et al., 2011; Martinez et al., 2009; Muñoz-Villers et al., 2012; Zadroga, 1981). Indeed, a growing number of studies have demonstrated that the occurrence of fog in fog-affected forests, including TMCF, results in strong instantaneous reductions of transpiration rates compared to those under sunny conditions (Burgess and Dawson, 2004; Chu et al., 2012; García-Santos, 2012; Hildebrandt et al., 2007; Hutley et al., 1997; Johnson and Smith, 2008; Reinhardt and Smith, 2008; Ritter et al., 2009). However, the associated decreases in seasonal and annual transpiration totals have not been quantified. Moreover, whilst the effect of fog on transpiration is usually evaluated by comparing transpiration under foggy conditions with rates observed during clear-sky conditions (e.g. (Ritter et al., 2009), an arguably more realistic evaluation of the influence

of diminished cloud immersion would be to compare against overcast conditions, as these are more likely to replace foggy conditions in future (Barradas et al., 2010; Karmalkar et al., 2008).

The quantification of changes in seasonal/annual transpiration totals is especially relevant in seasonally dry regions experiencing not only changes in climate but also in land-use patterns, such as the expansion of planted forests observed in many fog-affected tropical headwater areas (Carabias et al., 2007; Evans, 1999; FAO, 2010) that supply water to lower-lying towns, agroecosystems and industries (Martinez et al., 2009; Muñoz-Piña et al., 2008). In the case of Mexico, the most widely used tree species in reforestation projects are conifers, and in the seasonal montane cloud belt of central Veracruz (eastern Mexico), this includes the Mexican weeping pine (*Pinus patula*) (Sánchez-Velásquez et al., 2009; Valtierra Pacheco et al., 2008).

This paper examines the effect of ground-level cloud occurrence, or fog, on stand-level tree transpiration (E_t) for a young *P. patula* plantation, as well as the implications of a projected rise in LCL within the seasonal montane cloud belt of central Veracruz, Mexico, by analyzing sapflow dynamics and concurring meteorological conditions over a 1.5-year period (November 2008–April 2010). Specific objectives were to:

- Characterize the local fog climatology and dynamics of leaf wetness in relation to fog occurrence and rainfall;
- Compare rates of E_t and the controlling meteorological variables for sunny versus overcast and foggy conditions; and,
- Quantify the seasonal and annual degree of suppression of E_t by fog relative to overcast and sunny conditions.

2. Material and Methods

2.1 Study site

The present study was carried out in a young *Pinus patula* plantation (see Table 3.1 for stand characteristics), located within the La Cortadura Forest Reserve owned by the municipality of Coatepec (19.4931° N, 97.0422° W; 2180 m a.s.l.). The plantation was established in the year 2000 and had not received any thinning treatments prior to the present study. The site was formerly covered with mature lower montane cloud forest, locally known as '*bosque mesófilo de montaña*' (García Franco et al., 2008). The seasonally dry montane cloud belt of central Veracruz, eastern Mexico ranges from ~1200 to ~3000 m elevation. As such, the investigated pine plantation is situated in the upper part of the cloud belt and near the level of the inversion layer marking the transition toward the (mostly coniferous) upper montane forest zone (Rzedowski, 1978). The climate between 2000 and 3000 m elevation in this region is 'temperate humid with abundant rains during the summer', with average annual temperatures between 12 and 18°C and mean annual precipitation totals (MAP) between 2000 and 3000 mm, respectively (García, 1973). The region has a seasonal rainfall and cloud immersion regime, with a wet season between May and October, during which approximately 80% of MAP falls, and a relatively dry season between November and April. Rainfall in the wet season is mostly of convective origin and brought by frequent showers and thunderstorms, while the dry season is characterized by an alternation of stable dry weather conditions and cloud immersion events, often accompanied by rain and/or drizzle (García-García and Zarraluqui, 2008; Holwerda et al., 2010; Muñoz-Villers et al., 2012).

Additional information on the site's climate, geology, topography, soil characteristics and hydrology is given by Holwerda et al. (2010), (Muñoz-Villers et al., 2012; Muñoz-Villers and McDonnell, 2012) and (Goldsmith et al., 2012b).

Table 3.1. Characteristics of the young *Pinus patula* plantation under study within the seasonally dry montane belt of central Veracruz, Mexico. HRM = Heat Ratio method for sapflow measurements; n = number of sample trees; DBH = diameter at breast height; LAI = leaf area index; DS09 and DS10 correspond to the two dry seasons under study (November 2008–April 2009 and November 2009–April 2010, respectively). Standard deviations are given after the ± symbol where available.

Elevation [m a.s.l.]		2180
Area [ha]		~1
Mean canopy height [m][a]		7 ± 1.5
LAI [m^2 m^{-2}]		DS09: 6.0 ± 0.6 [b]
		DS10: 6.5 ± 0.2 [b]; 5.2 ± 0.1[c]
Tree density [stems ha^{-1}][a]		3783 ± 652
Basal area [m^2 ha^{-1}][a]		34.3 ± 9.6
Trees with HRM probes:	n	8
	tree age [years][d]	10
	DBH range [cm][d]	9.6–11.8

[a] (Hernández Hernández, 2010) and Chapter 2.
[b] Estimated from photosynthetically active radiation measurements above and below the canopy for clear-sky conditions from 11:00-14:00 (Chapter 2) and the Beer-Lambert Law with an extinction coefficient of 0.52 (Pierce and Running, 1988).
[c] Measured with a LI-COR LAI-2000 canopy analyzer throughout DS10 and a correction factor of 1.6 (Chapter 2).
[d] As of 2010.

2.2 Meteorological and leaf wetness measurements

An automated weather station was installed in an open grassland area of south-easterly exposure at a distance of 350 m (2128 m a.s.l.) from the *P. patula* plantation. For the entire study period (November 2008–April 2010) meteorological data were available as 10-min averages from 30 s sampling intervals. Incoming solar radiation (R_s [W m^{-2}]) was measured with a Kipp & Zonen CMP3 pyranometer installed at a height of 3 m. Air

temperature (T [°C]) and relative humidity (RH [%]) were obtained from a shielded Vaisala HMP45C installed at 2 m above the ground. Vapor pressure (e [kPa]) was measured with custom made dry- and wet-bulb thermocouples (VU University, The Netherlands), also at 2 m. Vapor pressure deficit (D [kPa]) was computed as the difference between e and saturation vapor pressure (e_s; computed as in (Lowe, 1977) using T). D derived in this way was preferred over D as derived from the RH probe because of the faster response of the thermocouples. Gaps in the thermocouple-derived D data were filled using data from the RH probe. Dew temperature (T_d [°C]) was calculated with the following expression (Dingman, 2008): $T_{d\_c} = (\ln(e^*10) - 1.810)/(0.0805 - 0.00421^*\ln(e^*10))$. Wind speed ($u$ [m s^{-1}]) was measured with a Vector Instruments A100R cup anemometer at 2.5 m from the ground. Horizontal visibility (VIS [m]) data were collected with a Mini Optical Fog Sensor (Optical Sensors, Sweden) installed at a height of 3 m. Rainfall (P [mm]) was obtained from a tipping bucket rain gauge (ARG100, Environmental Measurements) installed 1.15 m above the ground.

Leaf wetness was measured with two Decagon LWL dielectric leaf wetness sensors installed at two heights within the canopy (4 and 6 m from the ground). The sensors were hung vertically to simulate the weeping orientation of *P. patula* needles. The canopy was considered to be wet when both sensors indicated that water was present on their surface (10-min readings > 300 mV).

2.3 Definition of rainfall and fog events and canopy wetness duration

Since the goal was to quantify the effect of cloud immersion on E_t, and given that cloud immersion in the study area was frequently accompanied by rainfall (see Section 3

below), the inclusion of periods during which the canopy was wetted by rainfall was minimized by defining fog events as either fog-only or fog-plus-rainfall, as described below.

First, the occurrence of fog was defined as VIS < 1000 m (Glickman, 2000; Tardif and Rasmussen, 2007). Since the size spectrum of the fog droplets was not measured, the above definition of fog occurrence includes "true" fog (i.e. cloud droplets < 200 μm; Glickman, 2000), as well as any reduction in VIS related to rainfall or drizzle. From the 10-min observations of VIS, hourly values of fog occurrence (in % of the time) were calculated. Next, fog events were defined as periods with fog occurrence separated by a fog-free period of at least three hours. Increasing the latter to six or nine hours resulted in a 12 to 21% decrease in the number of identified fog events, respectively, indicating a rather low sensitivity to the definition of the event separation period. The hourly median VIS observed during an event was taken as a measure of fog density. As can be seen in Fig. 3.1, the fog events can be divided roughly into two groups: a group with dense and persistent fog presence (median event VIS < 500 m), and a second group with light and/or intermittent fog presence (median event VIS ranging between 1000 and 4000 m). The events from the former group will be referred to hereafter as "dense fog events", and those from the latter as "light fog events".

Rainfall events were defined as periods with $P \geq 0.3$ mm, separated by a dry period of at least three hours (Gash, 1979; Holwerda et al., 2010). A fog event was then considered to be a fog-plus-rain event when a rainfall event occurred during or within the three hours preceding the onset of the fog event. Lastly, wet-canopy conditions were defined for all periods when the canopy was wet (as indicated by both leaf wetness

sensors). Fog events were merged when canopy wetness data indicated the canopy remained wet between such events. This proved to be particularly important for fog-only events that were preceded by a fog-plus-rain or rainfall-only event. In such situations, canopy wetness was often "carried over" from the previous event, making it impossible to determine whether canopy wetness during the fog-only event was due to rainfall or fog. The fog-only events for which this was the case were reclassified as fog-plus-rainfall events.

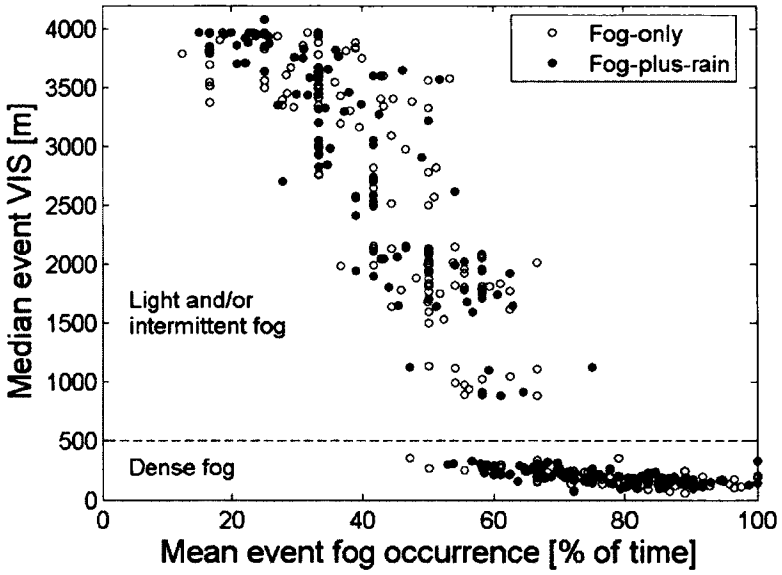

Figure 3.1. Relationship between median event horizontal visibility (VIS [m]) and mean event fog occurrence (expressed as % of time) as observed at 2180 m a.s.l. in central Veracruz, Mexico (19.4931° N, 97.0422° W). Open circles correspond to fog-only events, while closed circles denote fog-plus-rain events (see text for classification criteria). VIS threshold separating event-based fog density into two classes ("light" and "dense" fog) is represented by the dashed line.

2.4 Definition of sunny, overcast and foggy hours

In order to define daytime overcast conditions, an hourly cloudiness factor was computed as follows. First, daily values of theoretical clear-sky incident short-wave radiation (R_{clear}

[W m^{-2}]; cf. Dingman, 2008) and daily R_s were used to compute relative daily cloudiness using the following expression (Henderson-Sellers et al., 1987; Hildebrandt et al., 2007): $(R_{clear} - R_s) / R_{clear}$. Next, clear-sky days, hereafter referred to as 'golden days', were defined as days for which $R_s \geq R_{clear}$ (Appendix F1a). Finally, hourly values of R_s as observed during golden days at different times of the year were used to construct month-specific diurnal courses of R_s under clear-sky conditions (R_{s_golden}; Appendix F1b), thereby allowing the hourly relative cloudiness factor to be calculated as: $(R_{s\_golden} - R_s) / R_{s\_golden}$. No golden days occurred during the wet season, but given the sinusoidal seasonal trend of R_{clear} (Appendix F1a), golden days for the months of May, April and March were used to represent golden days for June–August, September and October, respectively.

Daytime ($R_s \geq 7$ W m^{-2}) overcast hours were then defined as fog-free hours with a cloudiness factor of ≥ 0.7 and dry canopy conditions. Sunny hours were defined in the same way, but with a cloudiness factor of < 0.7. Two classes of foggy daytime hours were defined: (i) dense fog with $\geq 60\%$ hourly fog occurrence, and (ii) light (and/or intermittent) fog with $< 60\%$ hourly fog occurrence. To minimize the influence of canopy wetness induced by rainfall in the analyses of E_t suppression, only those foggy hours were considered that pertained to a fog-only event or that preceded the first rainfall occurrence in a fog-plus-rainfall event. Table 3.2 summarizes the percentage of daytime hours corresponding to each of the above-defined conditions for the dry and wet seasons examined.

Table 3.2. Total daytime hours of different weather conditions per season (DS09: November 2008–April 2009; WS09: May–October 2009; DS10: November 2009–April 2010). Values expressed as % of total. Values between parentheses indicate the % of total hours during which the canopy was wet for each foggy condition. Daytime was defined as having solar radiation levels > 7 Wm^{-2}; see text for criteria to assign hours to a particular weather condition. NA = hours not taken into account in stand-level tree transpiration suppression analyses due to presence of a rainfall-induced wet canopy.

	DS09	**WS09**	**DS10**
Total daytime [hours]	2048	2280	2048
Dense fog (wet canopy)	8 (1)	5 (0)	11 (1)
Light fog (wet canopy)	6 (0.1)	7 (0)	6 (0.1)
Overcast	6	8	6
Sunny	65	56	49
NA*	15	24	28

2.5 Sapflow measurements and stand-level tree transpiration (E_t)

The Heat Ratio method (Burgess et al., 2001) was used to obtain point measurements of sap velocity within the sapwood at breast height (1.4 m above ground) in eight *P. patula* sample trees. The sample trees were growing within a circular plot (of 10 m radius) with similar aspect (South-East) and slope (20–26°). A detailed description of the collection of sap velocity data as well as the characterization of the radial profile of sap velocity for all sample trees is given by Alvarado-Barrientos et al. (2013). In short, the median radial profile shape for each sample tree (represented by a fixed value of the lumped shape parameter ρ) found in this previous study was used to derive maximum likelihood estimates of the time-variant component of the radial profile (i.e. the scaling parameter c_S [cm h^{-1}]) by fitting the Beta probability density function (Beta-PDF) to hourly radial profiles of sap velocity. These two parameters, together with measured sapwood depth

(L_s [cm]) of each tree were used to compute instantaneous hourly whole-tree sapflow, $F_s(t)$: $F_s(t) = 2\,\pi\,L_s^2\,\rho\,c_s(t)\,0.001$ [L h^{-1}] (Alvarado-Barrientos et al., 2013). The Beta-PDF did not provide a good fit for 24% of measured hourly radial profiles. These proved to be associated with conditions of very low evaporative demand producing either a relatively homogenous distribution of sap velocity across the sapwood or radial patterns not conforming to the Beta-PDF (Alvarado-Barrientos et al., 2013). Thus, an area-weighted average point sap velocity (v_{wa}) was computed after Hatton et al., (1990) such that $F_s = A_s\,v_{wa}$, where A_s is measured sapwood area [cm^2] for each tree.

F_s was assumed to be equal to transpiration at the whole-tree level, i.e. any time lags due to stem capacitance were ignored. This is a reasonable assumption because time lags between F_s and R_s after sunrise were never larger than 1 h (the finest time scale involved in the present study) and there were many instances when F_s increased in the dark after having declined at sunset and maintained steadily low for the first hours of the night (cf. Dawson et al., 2007). Consequently, sapflow-derived stand-level tree transpiration (E_t [mm h^{-1}]) was computed simply by averaging hourly F_s across all sample trees and multiplying times stand density (3783 pine trees ha^{-1}), as the stand was even-aged and tree spacing was fairly homogeneous (cf. Čermák et al., 2004).

The time series of hourly E_t was not complete for the entire study period due to equipment malfunction; 26% of total hours were missing. To produce a complete time series of E_t, days with complete hourly values of E_t (36% of the total number of days in the study period) were used to derive daily totals of E_t [mm day^{-1}]. Next, these were regressed against daily reference evapotranspiration (ET_o; computed with measured

meteorological variables following (Allen et al., 1998)). The resulting regression was: E_t = -6.04exp$^{-0.25ETo}$ + 5.3 (r^2 = 0.88; RMSE = 0.43 mm day^{-1}; see Chapter 2).

Uncertainty bounds for seasonal and annual E_t totals were computed by propagating errors from: (i) up-scaling F_s as measured in individual trees to the stand level; and (ii) modeling daily totals of E_t to fill gaps in the time series of sapflow-derived daily E_t. Errors stemming from (i) included the error in average F_s due to variability amongst trees (i.e. SE of the mean) and uncertainty in the scaling factor (i.e. SE of tree density in this case) (cf. Kostner et al., 1998). Thus, the total scaling error was estimated as the propagation of errors in a simple product. The modeling error in turn, was the RMSE of the relationship between modeled and observed daily E_t. Total errors in seasonal and annual E_t totals were computed as the quadratic sum of total scaling and modeling errors (Muñoz-Villers et al., 2012).

2.6 Quantification of the E_t suppression effect of fog

To quantify how much water was prevented from being transpired due to the occurrence of fog, subsets of hourly E_t data corresponding to each of the above-defined weather conditions (Section 2.4) were first grouped by season and then summarized by the hour of day. Next, mean daytime courses of E_t [mm h^{-1}] were calculated for each weather condition and season; corresponding daytime totals of E_t [mm] were computed by integrating the mean daytime courses. Average hour-specific E_t suppression rates for dense and light fog relative to overcast and sunny conditions were then calculated as the difference between the respective mean daytime courses. For example, the average suppression of E_t for light fog relative to overcast conditions was calculated as: $\bar{E}_{t\_overcast,j}$

$- \bar{E}_{t\_light\ fog,\,j}$ [mm h^{-1}], where the index j denotes the hour of day. Finally, seasonal totals of E_t suppression were computed by summing the average hour-specific E_t suppression rates multiplied times the corresponding total number of hours with dense or light fog. For example, the total E_t suppression for light fog relative to overcast conditions was calculated as: $\sum (\bar{E}_{t\_overcast,\,j} - \bar{E}_{t\_light\ fog,\,j}) * n_{light\ fog,\,j}$ [mm], where n is the total number of hours in a particular season. Uncertainty bounds for estimates of fog-induced E_t suppression were computed by propagating errors from up-scaling F_s to the stand level (see Section 2.5) and from the standard error (SE) of $\bar{E}_t$ of a specific hour of day and season.

2.7 Statistical analyses

Due to non-normal data distributions and the need to reduce the weight of long tails, meteorological data were characterized by their median values. The median absolute deviation (MAD) was used as the variability estimator (Sachs, 1984), and the data spread around the median was quantified by the standard error of the median (SE_M). The latter was estimated with a non-parametric bootstrapping method (Efron, 1981). Significant differences between frequency distributions (e.g. time of day when fog-only hours occurred) were tested with the Kruskal-Wallis one-way analysis of variance on ranks, and post-hoc pair-wise multiple comparisons were carried out with Dunn's method (Dunn, 1964).

The strength of the relationship between meteorological variables and E_t was examined by computing correlation coefficients. Only variables with the highest correlation coefficients were considered as meteorological controls of E_t ($r > 0.50$).

Furthermore, analyses of covariance and post-hoc Tukey-Kramer tests (Hochberg and Tamhane, 1987) were conducted to compare each meteorological control of E_t as observed during contrasting non-sunny weather conditions (i.e. subsets for dense fog, light fog, and overcast) relative to sunny conditions, thereby allowing an examination of the differences in the degree of reduction of these variables under the respective non-sunny conditions (i.e. test for significant differences between slopes and intercepts of individual linear regressions). The same approach was used to test for significant differences in E_t between the respective non-sunny conditions relative to sunny conditions. In addition, the effect of weather condition on the relationship between E_t and its main meteorological controls was examined using an analysis of covariance. The E_t and meteorological data used in these analyses pertained to daytime conditions only. Moreover, data were summarized by the hour of day for each subset (i.e. weather condition and season) before computation of coefficients of correlation and hypothesis testing, to avoid any bias introduced by the diurnal variation in these variables, as well as to deal to some extent with the autocorrelation inherent to such data-sets. The significance level used throughout was 0.05. All statistical analyses were implemented with the Statistics Toolbox of Matlab R2012a (The Mathworks, Inc.).

3. Results

3.1 General meteorological conditions

The study period included two contrasting dry seasons (November 2008–April 2009 and November 2009–April 2010, hereafter referred to as DS09 and DS10, respectively) and a wet season (May 2009–October 2009, hereafter WS09). DS10 was relatively wetter and

foggier than DS09, as *P* and fog event occurrence (in % of time) were almost twice as large (Fig. 3.2). Cumulative *P* was 430 mm and 752 mm for DS09 and DS10, respectively. In contrast, cumulative *P* during WS09 was 2545 mm (Fig. 3.2a). Further details of the meteorological setting of the study period are presented in Chapter 2.

3.2 Fog climatology

A total of 404 fog events were recorded throughout the 18-month study period. About half of the total number of fog events (53%) were classified as light fog. Then, 54% of the dense fog events and 45% of the light fog events were accompanied by rain. Furthermore, there was a clear seasonal pattern with respect to fog occurrence (Figs. 2b–d). A larger number of fog events occurred during WS09 (about one per day) compared to the two dry seasons. However, wet-season fog events consisted mostly of light fog, while dense fog events were generally more common during the dry season (Fig. 3.2b).

Although much variability was observed in the duration of fog events (Fig. 3.2c), fog-plus-rain events were generally of longer duration than fog-only events (median ± MAD: 11 ± 7 h versus 4 ± 2 h, respectively). Similarly, dense fog-plus-rain events were of longer duration than light fog-plus-rain events (median ± MAD: 13 ± 8 h versus 7 ± 5 h, respectively), while dense fog-only events lasted longer than light fog-only events (median ± MAD: 6 ± 2 h versus 3 ± 1 h, respectively). Furthermore, dry-season fog events were generally of longer duration compared to wet-season events (Fig. 3.2c). The median duration of all fog events was also greater in DS10 relative to DS09, mostly due to the occurrence of longer dense fog-plus-rain events in the former (Fig. 3.2c). For

instance, the longest fog event recorded during the entire study period lasted 128 h (8–13 January 2010) with fog occurring for 76% of this time, a median event VIS of only 214 m, and a total of 38 mm of concurring rainfall. Nevertheless, fog events lasting ≥ 24 h were generally infrequent and totaled <10% of all fog events during DS09, 3% in WS09, and 22% in DS10.

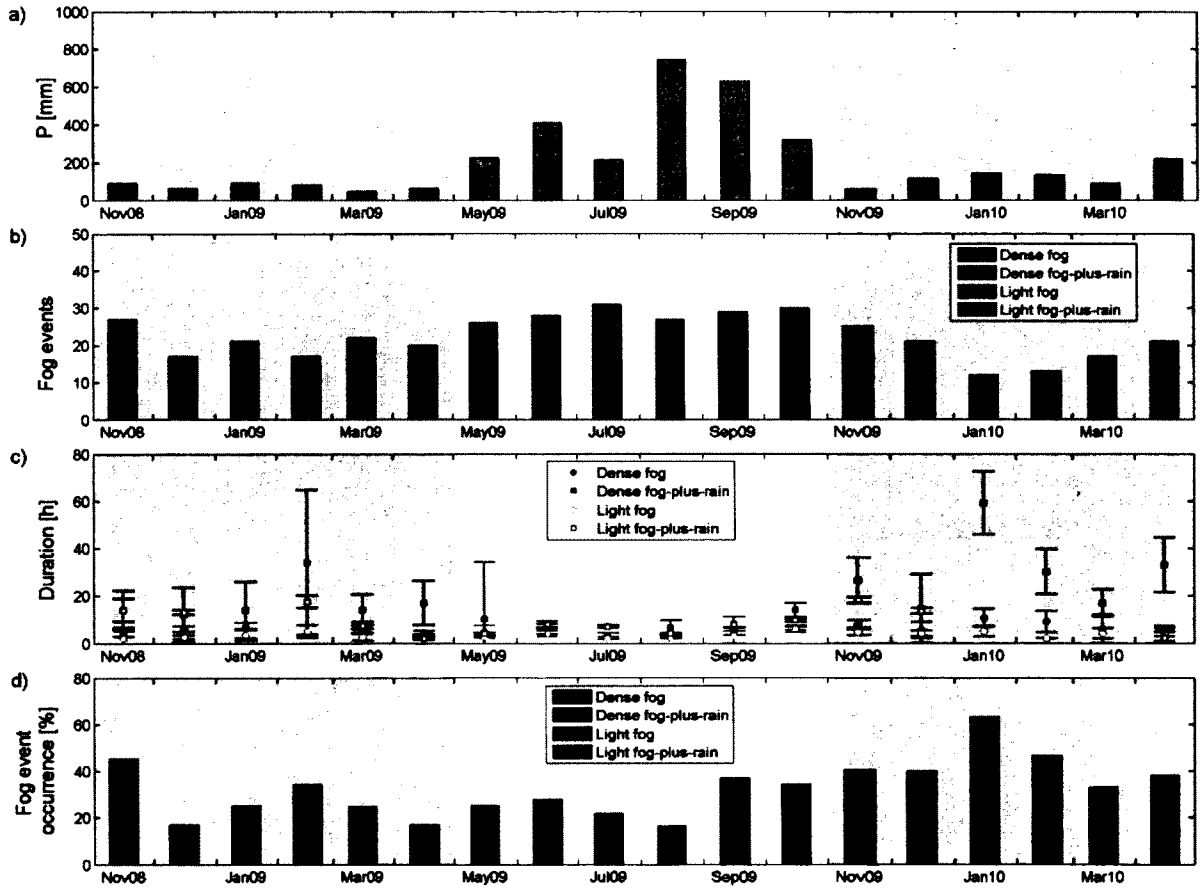

Figure 3.2. (a) Monthly total rainfall and (b–d) event-based fog climatology as observed at 2180 m a.s.l. in central Veracruz, Mexico (19.4931° N, 97.0422° W). (b) Total number of fog events. (c) Median fog event duration with standard error of the median (SE_M) indicated by error bars. (d) Percentage of total hours per month with fog events. See text for criteria to classify fog events as dense or light, or as fog-plus-rain. Light-gray shaded areas indicate two dry seasons under study while the white area corresponds to the wet season.

Fog occurred for 32% of the total study period, although it exhibited important seasonal variation. While the percentage of time during which the canopy was immersed in fog during DS09 and WS09 was the same (27%), fog occurrence in DS10 was much higher (44%). The increase in fogginess occurred mostly in December, January and April, representing a two-fold difference relative to DS09 (Fig. 3.2d). Notably, the increase in fog occurrence during DS10 reflected the greater frequency of longer dense fog-plus-rain events referred to earlier (Fig. 3.2d). Moreover, for the entire study period, conditions with fog-only occurred for only 8% of the time, whereas conditions with fog-plus-rain occurred for 24% of the time.

On a diurnal basis, both fog density classes showed higher frequency of occurrence during the late afternoon and early evening hours of the day (Fig. 3.3a). However, this higher frequency was much more pronounced for dense fog than for light fog, such that the distributions for the two fog classes were significantly different (Fig 3a). Furthermore, there were only significant seasonal differences for dense fog (Fig 3a).

3.3 Canopy wetness

Overall, the canopy was wet for almost a third of the total time. Not surprisingly, all fog-plus-rain events produced a wetted canopy. The onset of rainfall during fog-plus-rain events typically occurred within 0–4 h after the onset of fog, whereas canopy wetness almost always concurred with the onset of rainfall or shortly thereafter (see thick lines along upper horizontal axis in Fig. 3.4). Only in a few fog-plus-rain events (2% of dense and 15% of light fog-plus-rain events) did rainfall start before the onset of fog, and consequently, in these cases the canopy was already wet before the fog started. Rainfall

generally ended between 5 h before and 1 h after the end of fog occurrence in all fog-plus-rain events; however, variability was very large (range: 30 h before – 10 h after; Fig. 3.4). After the end of rainfall in fog-plus-rain events, the canopy typically remained wet for 3–10 h, whereas after the termination of fog during these mixed events the canopy remained wet most frequently for 2–7 h (Fig. 3.4).

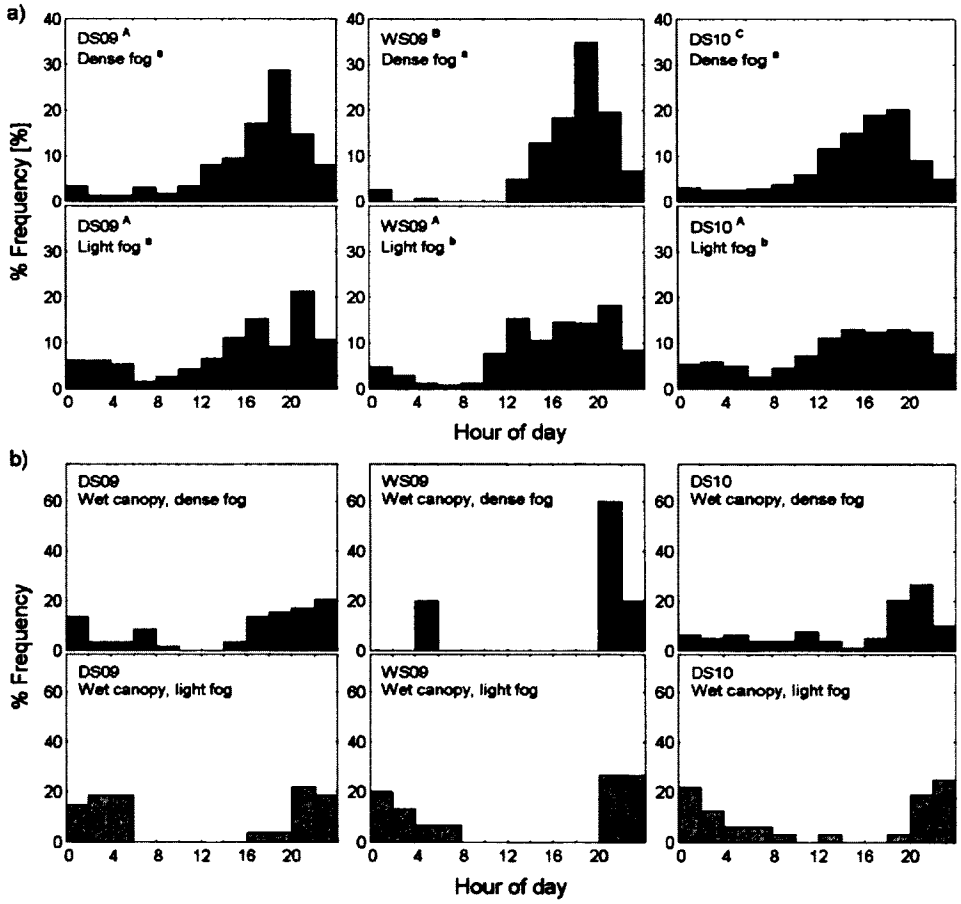

Figure 3. (a) Frequency distribution of fog-only conditions as a function of the time of day and separated by season. Different superscript upper-case letters indicate significant seasonal differences for each fog density class (i.e. between panels in the same line), while different superscript lower-case letters indicate significant differences between light and dense fog distributions for each season (i.e. between panels in the same column). (b) Idem for canopy wetness occurrence due to fog-only conditions. Differences among seasons and between dense and light fog were not large enough to discard the possibility of random variability.

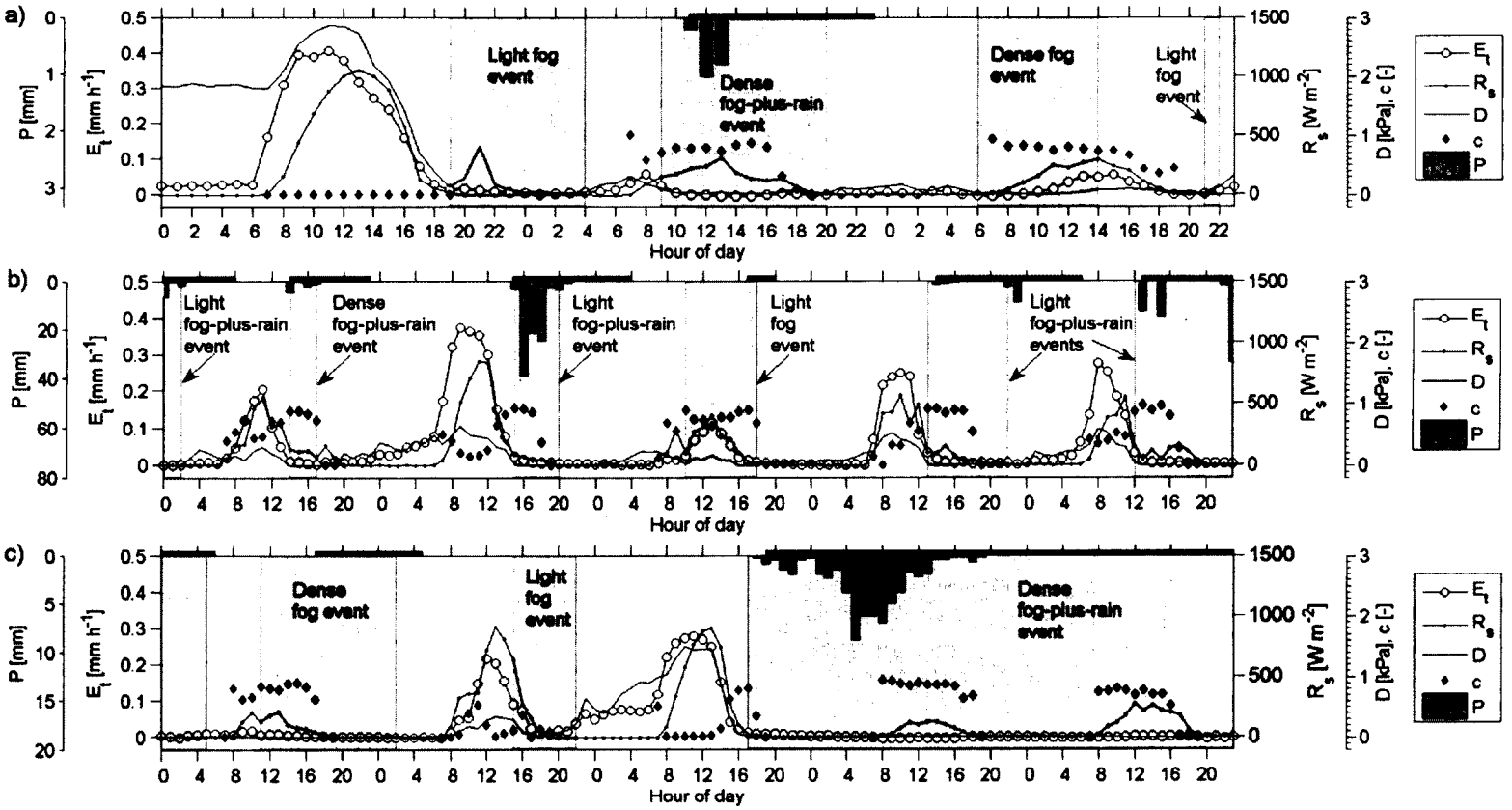

Figure 3.4. Examples of hourly dynamics of stand-level tree transpiration (E_t [mm h^{-1}]) from the young *Pinus patula* plantation under study, and concurring micrometeorological conditions (incoming solar radiation (R_s [W m^{-2}]), vapor pressure deficit (D [kPa]), daytime cloudiness factor (c [-]) and rainfall (P [mm])). These types of responses were observed throughout the investigation. (a) Three typical dry-season days in 2009 (February 28–March 2) starting with a 'golden day' followed by various fog events. (b) Passing of typical wet-season fog events (June 21–25, 2009). (c) Fog events during the dry season of 2010 (January 13–17). Fog events are represented by the light-gray shaded area whereas canopy wetness occurrence is represented by the thick black lines along the upper x-axis.

Furthermore, canopy wetness associated with fog-only events occurred during 36% of the events with dense fog, and only in 4% of the ones with light fog. Besides having mostly dense fog (median VIS ± MAD: 198 ± 50 m), fog events that produced wet canopy conditions occurred almost exclusively during the dry season (mostly DS10) and were of long duration (median ± MAD: 8 ± 3 h). Moreover, the onset of canopy wetness in these fog-only events generally occurred 3–7 h after the start of the fog, and the canopy remained wet generally between 1–5 h after fog occurrence had ended (Fig. 3.4).

On an hourly basis, very little daytime canopy wetness occurred during either dense or light fog-only conditions. During the two dry seasons studied, fog-induced canopy wetness duration totalized only 1.1% of daytime hours (Table 3.2 and Fig. 3.3b) whereas during the wet season fog-induced canopy wetness this did not occur (Table 3.2 and Fig. 3.3b). Regardless of season, there were almost no daytime hours during which the canopy was wet after a fog-only event (0.1% of all daytime hours). The only instances observed concerned the first hour of the day following a nocturnal fog event (Fig. 3.4).

3.4 E_t and its meteorological controls under different weather conditions

Under clear-sky and dry-canopy conditions, hourly E_t increased sharply after sunrise (Fig. 3.4). Maximum hourly E_t occurred typically between 10:00 and 12:00, i.e. a few hours before maximum hourly R_s, after which E_t started to decrease until sunset (Fig. 3.4 and 7a). There was no indication of E_t lagging behind R_s once it had reached steady state after sunset. However, on many occasions and regardless of the season, E_t started well

before sunrise; significant E_t was recorded during 15% of the total nighttime hours, at an average rate of 0.04 mm h^{-1} and with maximum values of up to 0.2 mm h^{-1} (see Chapter 4 for more details).

The strongest correlation between daytime E_t and the respective meteorological variables was found with R_s (r = 0.85), followed closely by D (r = 0.82). E_t was also positively correlated with T, albeit less strongly (r = 0.56). Hence, R_s and D were considered to be the main meteorological controls of E_t.

During conditions of dense fog, daytime R_s was only 21 ± 5% of that common for sunny conditions at a given hour of day (based on the difference in slope ± 95% CI for the relationships between R_s under conditions of dense fog *versus* during sunny conditions; Fig 3.5a). Light fog and overcast conditions, in turn, presented a very similar degree of attenuation of R_s (24 ± 6% and 25 ± 4%, respectively; the difference in the slopes of the respective regression equations were not significant: $F = 0.82$, $p = 0.44$; Fig. 3.5a). However, the intercepts of the respective regressions differed significantly (F = 7.71, $p < 0.01$); specifically, the intercept of the regression for radiation under conditions of light fog was larger compared to values for either dense fog or overcast conditions (Fig. 3.5a). Also, there were no seasonal effects in terms of differences between the various non-sunny conditions (dense fog: F = 2.09, p = 0.15; light fog: F = 2.94, p = 0.07; overcast: F = 2.64, p = 0.09). There was, however, a marked seasonality in amounts of R_s under sunny conditions, such that during the wet season, values were (on average) 74 ± 12% of dry-season values.

Not surprisingly, for the entire study period daytime D was the lowest (near-zero) during conditions of dense fog (median ± MAD: 0.005 ± 0.004 kPa), slightly higher

during light fog (median ± MAD: 0.06 ± 0.02 kPa), higher during overcast conditions (median ± MAD: 0.14 ± 0.03 kPa), and highest under sunny conditions (median ± MAD: 0.65 ± 0.12 kPa). The diurnal variation of D under sunny conditions was larger than under either type of non-sunny conditions; regardless of the time of day, D under non-sunny conditions remained within a rather narrow range (i.e. the slopes of the regressions in the ANCOVA contrasting D-values for non-sunny conditions with those for sunny conditions were not significantly different from zero; Fig. 3.5b). The range in D-values differed significantly between overcast and foggy conditions ($F = 131.82$, $p = 0$; Fig 5b). The season did not affect daytime D for non-sunny conditions; however, D-values observed under sunny conditions were lower during the wet season compared to the dry season (Fig. 3.5b).

Daytime T observed during non-sunny conditions was not affected as strongly as found earlier for D and R_S. T was generally lower during dense fog than during light fog, which in turn decreased T to a greater extent relative to overcast conditions (Fig. 3.5c). However, during the course of the day for a given season, T under non-sunny conditions nearly converged with T for sunny conditions (not shown). Furthermore, there was no strong evidence to suggest significantly different slopes among the respective regressions for non-sunny conditions ($F = 0.49$, $p = 0.61$), all of which were close to unity. The intercept of the regression for overcast conditions, however, was significantly different from those for either type of foggy conditions ($F = 7.49$, $p < 0.01$; Fig. 3.5c). There was a more pronounced reduction of T relative to sunny conditions during the dry seasons, mostly because T did not vary much between weather conditions during the wet season

(Fig. 3.5c). Moreover, minimum daytime T was higher (by 2–5°C) during the wet season compared to the two dry seasons for all weather conditions.

There was a fairly good relationship between daytime hourly E_t and R_s considering all weather conditions and seasons (r^2 = 0.72; RSME = 0.04). Weather conditions did have a significant effect, however (Fig. 3.6a). Although the slopes of the individual regressions did not differ significantly (F = 0.93; p = 0.43), the intercept of the regression for sunny conditions was significantly different from the ones associated with the respective non-sunny conditions (F = 33.19, p < 0.01). No seasonal effects were significant for given weather conditions (dense fog: F = 0.97, p = 0.39; light fog: F = 0.78, p = 0.47; overcast: F = 0.39; p = 0.68; sunny: F = 0.74; p = 0.48). Moreover, considerable scatter was present in most of the individual regressions, particularly for sunny conditions, which was related to hysteresis in the relationship between E_t and R_s arising from the diurnal variation in the two variables (see clockwise loop for DS09 in Fig. 3.6a).

In contrast, weather conditions had no significant effect on the linear regression between daytime hourly E_t and D (test for equal slopes: F = 0.09, p = 0.96; test for equal intercepts: F = 0.39; p = 0.76; Fig. 3.6b). The linear regression for all weather conditions and seasons had a reasonably good fit (y = 28x + 0.016; r^2 = 0.75; RMSE = 0.04). However, while the intercept did not differ between seasons, the slope was significantly affected by season (F = 14.81, p = 0; slope for DS09: 0.31; slope for WS09: 0.43; slope for DS10: 0.22). Again, an important source of variation in the regressions was the hysteresis of the relationship (Fig. 3.6b).

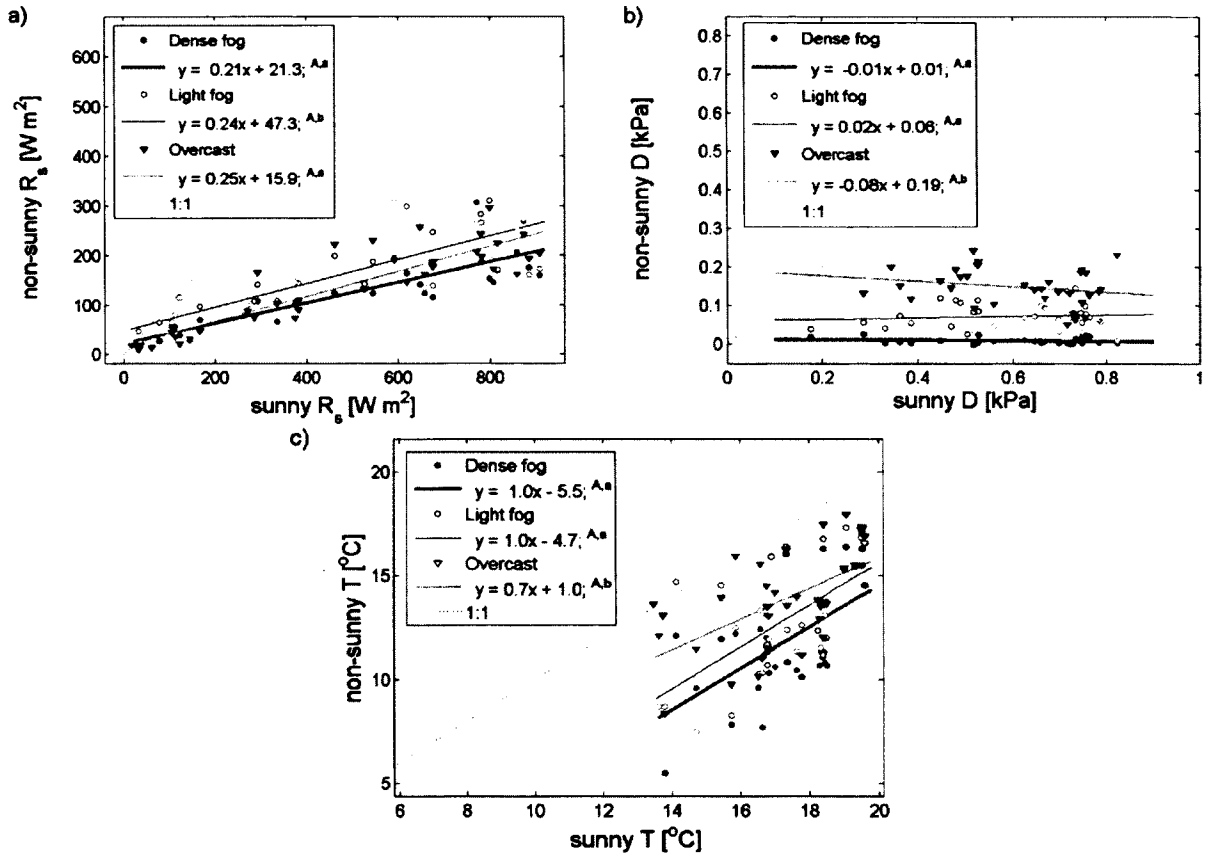

Figure 3.5. Comparison of meteorological controls of stand-level tree transpiration of a young *Pinus patula* plantation, during sunny and various types of non-sunny conditions: (a) incoming solar radiation (R_s), (b) vapor pressure deficit (D), and (c) air temperature (T). Symbols represent hourly medians aggregated by the hour of day and grouped by season. Different colors represent a particular season (red: DS09; blue: WS09; green: DS10). Best linear fits for each non-sunny condition considering all seasons together are presented as solid lines and described in the legend. Different upper-case superscript letters indicate significantly different slopes among the linear regressions, while significantly different intercepts are shown by different lower-case superscript letters.

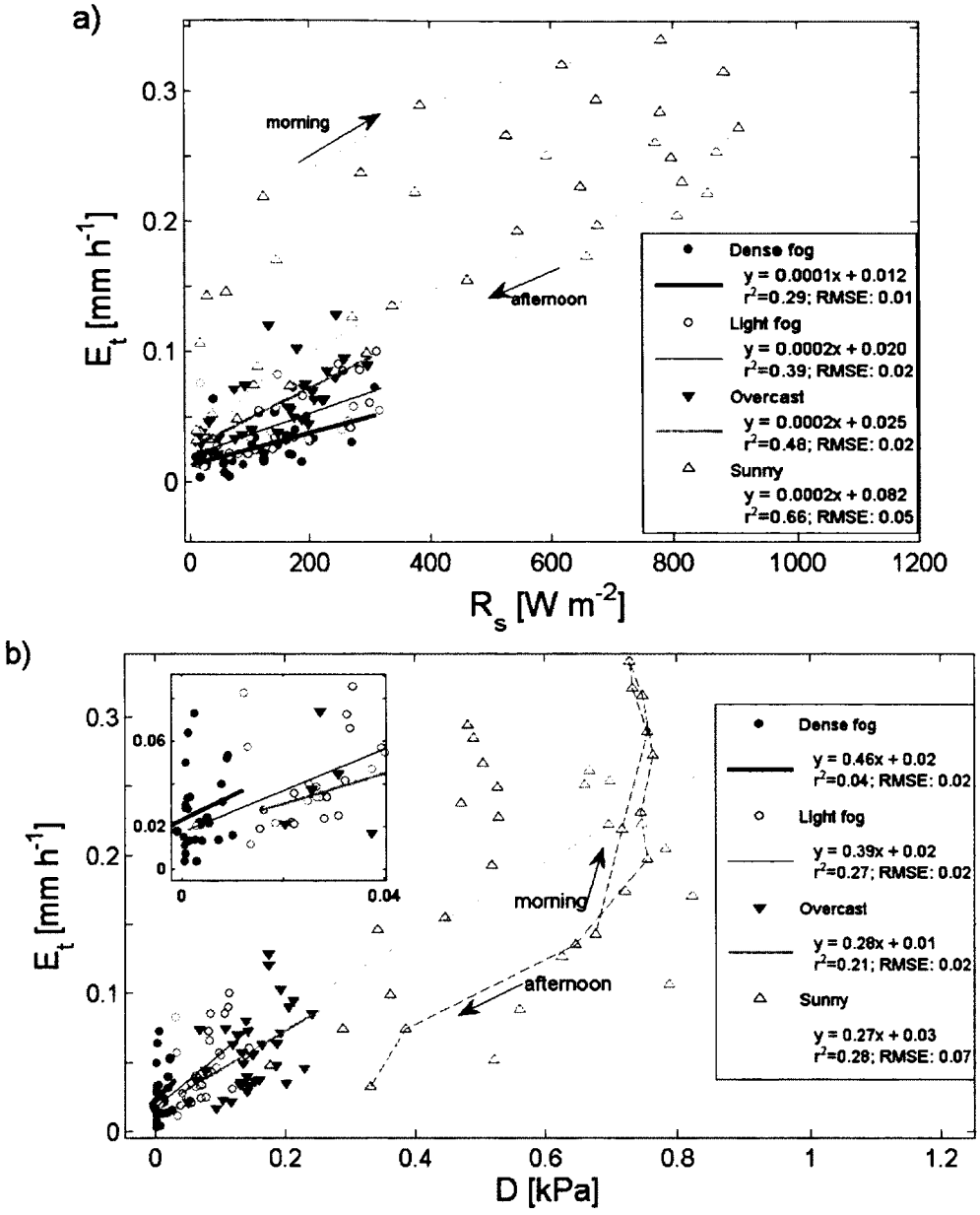

Figure 3.6. Relationship between stand-level tree transpiration (E_t) in a young *Pinus patula* plantation and its main meteorological controls: (a) incoming solar radiation (R_s), and (b) vapor pressure deficit (D). Symbols are daytime values aggregated (mean) by the hour of day, separated by weather condition (dense fog, light fog, overcast and sunny) and season (red: DS09; blue: WS09; green: DS10). Solid lines depict linear regressions fitted to data for each weather condition considering all seasons, and are described in the legend. Dotted lines and arrows show an example (sunny condition during DS09) of the hysteresis found in the relationships. Inset in (b) shows data for dense and light fog more clearly.

3.5 Suppression of E_t during non-sunny conditions

Hourly dynamics of E_t with concurrent meteorological variables during non-sunny weather conditions (Fig. 3.4), as well as the relationship between E_t and its chief meteorological controls (Fig. 3.6), demonstrate that E_t is suppressed considerably under non-sunny conditions compared to sunny conditions, particularly during fog. However, fog tends to be more frequent at certain times of the day (Fig. 3.3a) whereas the meteorological controls of E_t also vary during the day. Therefore, in order to properly quantify the suppression effect of fog, the mean daytime course of E_t was analyzed, grouped by weather condition class and season (Fig. 3.7a). Notably, E_t under non-sunny conditions presented a damped diurnal course, to the extent that under dense fog E_t almost did not vary with the hour of day; however, during the wet season the diurnal course of E_t for the various non-sunny conditions were less damped compared to dry-season conditions (Fig. 3.7a).

At 2.6 ± 0.2 mm, total daytime E_t under sunny conditions was larger during DS09 than during the 2009 wet season (2.3 ± 0.3 mm) or DS10 (2.1 ± 0.3 mm; Fig. 3.7b). For non-sunny conditions, a similar seasonal pattern was observed for total daytime E_t: the two dry seasons had relatively similar daytime total E_t-values, both of which were lower than the ones observed during the wet season (Fig. 3.7b). Interestingly, total daytime E_t during overcast conditions was only slightly higher than that during light fog conditions throughout the study period (Fig. 3.7b). The lowest daytime E_t totals were associated with dense fog conditions during either dry season (0.3 ± 0.1 mm: Fig. 3.7b).

Overall, hourly rates of E_t under conditions of dense fog were suppressed by 90 ± 7% relative to sunny conditions whereas light fog suppressed E_t by 83 ± 7%, and overcast conditions by 78 ± 10% (based on the slope ± 95% confidence interval for the respective regressions in Fig. 3.7c). Interestingly, differences in slope between the regressions comparing non-sunny and sunny conditions were not significant (F = 1.92; p = 0.15). Neither were seasonal effects within the regression for conditions of dense fog (F = 0.67, p = 0.52). However, for conditions of light fog the slope of the regression for wet-season data was significantly steeper than the ones for dry–season data (F = 5.37, p = 0.01). By contrast, seasonal effects within the regression for overcast conditions only affected the intercept (F = 10.33, $p < 0.01$).

3.6 To what extent is E_t suppressed by fog?

Relative to overcast conditions, the presence of dense fog suppressed E_t by a mere seasonal total of 3.4 ± 1.2 mm for DS09 versus 3.9 ± 1.6 mm for DS10 and only 2.8 ± 1.1 mm for WS09. Even smaller amounts of E_t were suppressed by light fog relative to overcast conditions (DS09: 1.2 ± 1.0 mm; WS09: 2.6 ± 1.6 mm; DS10: 1.1 ± 1.4 mm). Taking all foggy conditions together, total suppressed E_t relative to overcast conditions represented only about 2 ± 1% of seasonal E_t with little seasonal variation (Fig. 3.8a). Thus, for a scenario in which all fog occurrence is replaced by overcast conditions as a result of a rise in the LCL, annual E_t (645 ± 50 mm on average) is likely to increase by only 2 ± 1%.

In contrast, taking sunny conditions as the reference, dense fog prevented a total of 21.2 ± 1.6 mm and 28.6 ± 1.9 mm from being transpired during DS09 and DS10,

respectively, while the corresponding amount during WS09 was only 9.7 ± 1.6 mm. Furthermore, light fog suppressed E_t by a total of 17.8 ± 1.5 mm during DS09 and by a similar amount during the other two seasons (WS09: 18.8 ± 2.0 mm; DS10: 16.6 ± 1.7 mm). Taking dense and light fog occurrence together, the combined suppression effect ranged from 9 ± 2% mm (WS09) to 15 ± 1% (DS10) of seasonal E_t (Fig. 3.8b). Hence, a likely increase of 17 ± 3% of annual E_t may be expected from an extreme scenario in which all fog occurrence would be replaced by sunny conditions.

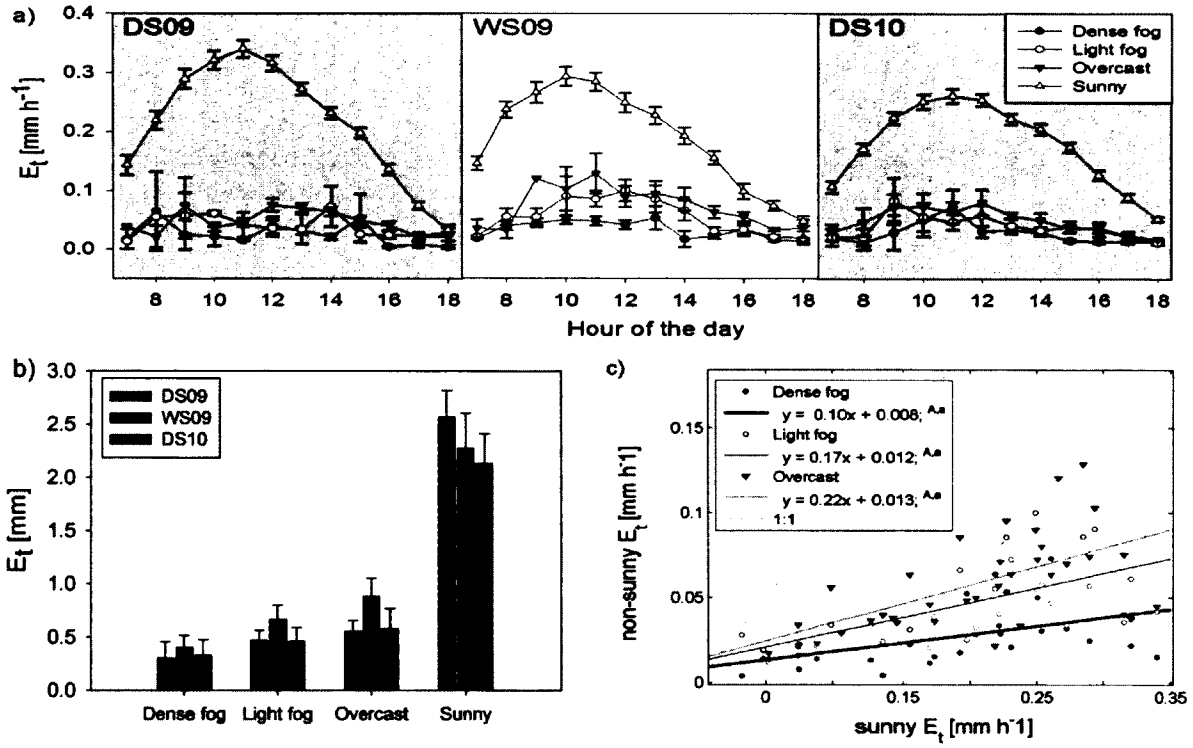

Figure 3.7. (a) Mean daytime courses of stand-level tree transpiration (E_t [mm h^{-1}]) for a young *Pinus patula* plantation. Error bars represent standard error of the mean. (b) Daytime total E_t [mm] for different weather conditions and separated by season (DS09: November 2008–April 2009; WS09: May–October 2009; DS10: November 2009–April 2010). (c) Comparison of mean hourly E_t under various types of non-sunny conditions with E_t during sunny conditions. Seasons are indicated with different colors (red: DS09; blue: WS09; green: DS10). For each non-sunny condition the best linear fits are presented as solid lines and described in the legend, where different superscript upper-case letters indicate significantly different slopes and lower-case letters indicate differences among intercepts.

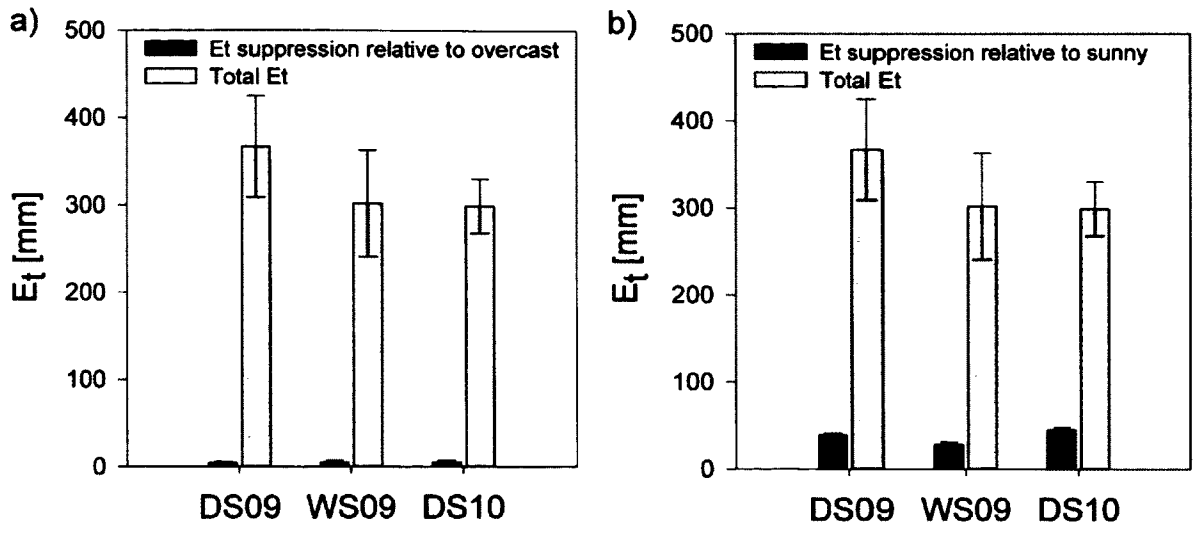

Figure 3.8. Total seasonal stand level tree transpiration (E_t [mm]) for a young *Pinus patula* plantation, plus derived estimates of the amounts of suppressed E_t due to both dense and light fog combined, relative to (a) overcast or (b) sunny conditions. Three seasons under study are shown (DS09: November 2008–April 2009; WS09: May–October 2009; and DS10: November 2009–April 2010).

4. Discussion

4.1 Variability in fog occurrence

By observing sapflow dynamics and micrometeorological conditions during 1.5 years it was possible to examine not only seasonal variability in weather conditions (and E_t responses), but also, to some extent, interannual variability. Seasonal characteristics observed in fog occurrence, fog event duration, and fog event density, reflect the seasonality in weather systems producing cloud immersion in central Veracruz (García-García and Zarraluqui, 2008; Holwerda et al., 2010). During the wet season, daily short-duration fog events composed mainly of light fog are due to the typical diurnal pattern of orographic-convective cloud development over the mountain. Conversely, during the dry season, there is an alternation of high pressure systems (i.e. no or very little fog occurrence) and cold front intrusions (i.e. long-duration fog events composed mostly of

dense fog). Also, rainfall accompanying fog occurrence is typical of the foggy conditions produced by orographic clouds, as reflected by similar patterns documented for the montane cloud belt of Hawaii (Giambelluca et al., 2011), Canary Islands (García-Santos and Bruijnzeel, 2011) and Puerto Rico (Eugster et al., 2006), for example.

The difference with respect to rainfall totals and fog occurrence between the two dry seasons studied here may have been related to the El Niño/La Niña–Southern Oscillation phenomenon (Ponette-Gonzalez et al., 2010). La Niña conditions prevailed during DS09, enhancing the dry season at the study site (i.e. relatively less rainfall and fog occurrence). The average monthly Southern Oscillation Index for DS09 was 10.6 versus -3.4 for DS10 (http://www.bom.gov.au/climate/current/soihtm1.shtml). It is unclear whether more frequent La Niña or El Niño conditions will be the norm under future climatic conditions for central Veracruz, although modeling studies have predicted reductions in dry-season precipitation and greater variability for Central America and Mexico (Karmalkar et al., 2011).

4.2 E_t in seasonally dry fog-affected forests

Trees growing in environments subject to frequent cloud immersion face strong (and often rapid) changes in solar radiation, air humidity and canopy wetness produced by alternating sunny, cloudy and foggy conditions (Cavelier, 1996). Therefore, E_t rates can be expected to vary widely under different weather conditions as shown for the 10-year-old *Pinus patula* plantation studied here, as well as reported for many other fog-affected forests (Burgess and Dawson, 2004; Chu et al., 2012; García-Santos, 2012; Goldsmith et al., 2012a; Hildebrandt et al., 2007; Hutley et al., 1997; Johnson and Smith, 2008;

Reinhardt and Smith, 2008; Ritter et al., 2009). Also, in seasonal environments there may be periods when soil moisture limits E_t, thus producing additional seasonal variation in E_t. Average daily E_t for the *P. patula* plantation (1.7 ± 1.24 mm day^{-1}) was high compared to values reported for other seasonal fog-affected forests such as ridge-top *fayal-brezal* forest (1.2 ± 0.12 mm day^{-1}; García-Santos, 2012) and *Pinus canariensis*-dominated forest (0.82 mm day^{-1}; Luis et al., 2005) in the Canary Islands, or *Anogeissus dhofarica*-dominated forest in Dhofar, Oman (range of modeled E_t: 0.55–0.96 mm day^{-1}; Hildebrandt and Eltahir, 2007). The latter sites all have a very pronounced dry season (i.e. Mediterranean to semi-arid climates) causing periodic soil moisture limitation to E_t, in contrast to the present study site, which maintained high levels of soil moisture even during the driest period (> 0.4 m^3 m^{-3} at a depth of 20 cm; Fig. 3.4 in Chapter 2). Moreover, there was a lower seasonal E_t total for DS10, which had both higher rainfall and more frequent fog occurrence, compared to DS09 (Fig. 3.8). Therefore, soil water availability was not a limiting factor for E_t, similar to what has been reported for other montane cloud forests (e.g. Chu et al., 2012; McJannet et al., 2007; Schawe et al., 2007; cf. Bruijnzeel et al., 2011). Consequently, the results suggest that the observed variability in E_t rates is largely due to variable atmospheric conditions.

Average daytime E_t for *P. patula* under clear-sky conditions (Fig. 3.7b) showed a distinctive seasonal pattern, which may be explained largely by the corresponding seasonal variation in R_s and D (Fig. 3.6). However, the two dry seasons presented similar radiation inputs (and average D-values), but different average daytime E_t under sunny conditions (Fig. 3.7b). Therefore, other factors must have contributed to the reduction in daytime E_t under sunny conditions during DS10. Visual observations of a more closed

canopy during DS10 relative to DS09, confirmed by a slightly higher measured LAI in DS10 (Table 3.1), suggest that perhaps a lower proportion of the canopy was sun-exposed. On the other hand, the two dry seasons showed very similar average daytime E_t values under non-sunny conditions, with higher rates during the wet season (Fig 7b). This may be explained by the higher temperatures prevailing during the wet season (Fig. 3.6c). The similarity in non-sunny daytime E_t for the two dry seasons suggests that the higher proportion of diffuse light under these conditions overrides any effect of an increase in canopy closure and self-shadowing, in contrast to the situation under sunny conditions.

With a mean annual E_t of 645 ± 50 mm, the water lost via transpiration from the young *P. patula* plantation was less compared to that for nearby mature and 20-year-old regenerating cloud forest (787 ± 126 mm $year^{-1}$ and 788 ± 166 mm $year^{-1}$, respectively; Muñoz-Villers et al., 2012). However, annual E_t for the present study is very similar to the average value reported for lower montane cloud forests throughout the world (average ± SD: 646 ± 123 mm; n = 10; (Bruijnzeel et al., 2011).

4.3 On the processes causing E_t to be suppressed under foggy conditions

Reports of the suppression of E_t by foggy conditions relative to sunny conditions in fog-affected forests are variable. For instance, daily E_t was suppressed by 40% for an emergent *Sloanea woollsii* tree in a subtropical rain forest in Queensland, Australia (Hutley et al., 1997), and by 43% for mature *Abies fraseri* forest (and up to 95% for seedlings) in the southern Appalachians (Johnson and Smith, 2008; Reinhardt and Smith, 2008), whereas hourly E_t was reduced by 10–90% for evergreen ridge-top heath-laurel cloud forest in the Canary Islands (García-Santos, 2007; García-Santos, 2012; Ritter et

al., 2009). The high range reported for the latter site was probably because the comparison was made "with preceding hours without fog or rain" (García-Santos, 2007), which could have been either sunny or overcast. Reductions in E_t for *P. patula* ranged from 83 ± 7% up to 90 ± 7%, under conditions of light and dense fog, respectively. The large variation in earlier reported values for the suppression of E_t may be explained largely by the different characteristics of fog occurrence (e.g. fog density, leaf wetness patterns due to fog occurrence), site exposure and wind speeds across sites, physiological and structural differences between the species and forests studied, as well as methodological differences (e.g. daily versus hourly analyses, not taking into account the hour of day, or including both sunny and overcast hours in the comparison).

It has been argued that the suppression of E_t due to fog may be explained mainly by strong reductions in meteorological variables such as R_s, D and T, as these alter the leaf energy balance and reduce evaporative demand (Ritter et al., 2009). On the other hand, gas exchange reductions via stomatal blockage due to water deposited on leaf surfaces has also been pointed out as a process through which E_t is suppressed under foggy conditions (Ishibashi and Terashima, 1995; Smith and McClean, 1989). The relative importance of these factors in explaining E_t suppression depends on the site's fog climatology and on the degree of leaf hydrophobicity (cf. Rosado and Holder, 2012). For instance, the duration of cloud immersion events, fog density and the type and amount of accompanying precipitation (i.e. 'true' fog, drizzle, or rainfall), combined with the canopy's structure and degree of hydrophobicity of the leaf surfaces will dictate whether or not the canopy will be fully wetted, for how long it is kept wet after the termination of cloud immersion, and consequently, the extent to which canopy wetness suppresses E_t.

For the seasonally dry montane cloud belt studied here, fog was usually accompanied by rainfall, but during the occasional fog-only conditions, daytime canopy wetness was a rare phenomenon (1.1% of all dry-season daytime hours; Table 3.2). Moreover, *P. patula* is native to the cloud belt of the eastern Sierra Madre, Mexico (Dvorak et al., 2000; Vela, 1990) and thus the surface of its needles may have some degree of hydrophobicity as an adaptation to the wet and fog-affected environment (cf. Smith and McClean, 1989). Irrespectively, the needles of *P. patula* are clustered in fascicles hanging in a characteristic weeping fashion, such that intercepted water is easily shed. In combination, these results and observations suggest that in the seasonally dry fog-affected montane zone of central Veracruz, the reduction of evaporative potential (due to reduced available energy and high humidity) is relatively more important in suppressing E_t by *P. patula* trees during fog-only conditions than the wetting of leaf surfaces by fog. The E_t suppressing effect of fog in the present pine stand was therefore associated mainly with a reduction in R_s ranging from ~70% under light fog up to ~80% under dense fog, and near-zero *D*. Similar conclusions were reached in earlier investigations on the E_t suppression effect of fog at other sites, including the Canary Islands (Ritter et al., 2009) and Taiwan (Chu et al., 2012).

Furthermore, there was a low frequency of early-morning fog occurrence (Fig. 3.3a) as well as very few instances when nighttime fog-induced canopy wetness continued for more than one hour after sunrise. Therefore, fog-only conditions did not postpone the morning initiation of E_t to a large extent. On the contrary, it is possible that stomatal conductance was enhanced in the early morning as a consequence of conditions

stemming from late-afternoon/nighttime fog occurrence, similarly to what was observed for yellow cypress in Taiwan (Chu et al., 2012).

Significant hourly E_t, albeit low, occurred both during dense and light fog-only conditions, instances in which canopy wetness data indicated that leaf surfaces were largely dry (Figs. 2 and 7). In contrast, non-significant (i.e. near-zero) rates of E_t were generally recorded during rainy conditions when the canopy could be considered wet (Fig. 3.2). Therefore, it is concluded that only the water deposited on the needle surfaces by rain was usually sufficient to produce stomatal gas exchange blockage. This agrees well with visual observations that canopy wetness due to rainfall caused the needles of various fascicles to clump together with a visible coat of water, while during conditions of fog-only the needles tended to feel humid to the touch but did not clump together. It is important to note, however, that the assumption that the canopy wetness sensor data closely resemble the actual wetting (and drying) of the *P. patula* canopy was not experimentally verified. And, the uncertainty in canopy wetness data remains unknown (cf. Klemm et al., 2002), therefore, instances of a 'dry canopy' recorded during many foggy conditions may actually have included periods when the canopy was partially wet. Nevertheless, the canopy wetness data are considered to satisfactorily reflect the general wetness status of the pine needles based on the various observations mentioned above. Also, in order to be as unambiguous as possible, and given the limitations posed by leaf wetness sensors (Klemm et al., 2002), a conservative designation of canopy wetness was achieved by considering it 'wet' only when both sensors indicated wet conditions.

4.4 Implications of the rise in the lifting condensation level for E_t

Based on several climate change modeling studies and some observational data discussed earlier (Barradas et al., 2010; Karmalkar et al., 2008; Lawton et al., 2001; Nair et al., 2003; Ray et al., 2006; Richardson et al., 2003; Still et al., 1999; Van der Molen et al., 2006), it is suggested that a rise in the LCL in tropical montane regions is likely to result in a shift from frequent cloud immersion to overcast, rather than to clear-sky conditions. However, there are no detailed projections of how changes in regional and global climate may affect the degree of cloud immersion frequency, fog density, or the potential increase in overcast conditions. Consequently, the effect on E_t suppression was examined for two classes of fog density and overcast conditions (relative to sunny conditions) to determine whether this effect varied among the respective non-sunny conditions. To the best of our knowledge, only Reinhardt and Smith (2008) compared the suppression of E_t for overcast conditions to that under foggy conditions (20% versus 43% for *A. fraseri* in the Apalachians). Consistent with these findings, results from the present study also indicate that E_t was suppressed to a lesser degree for overcast conditions than for either light or dense fog, while adding a new finding: the reduction associated with overcast conditions did not differ greatly from that for light fog (78 ± 10% versus 83 ± 7%, respectively). This may be explained by the very similar reduction in solar radiation recorded during all types of non-sunny conditions examined here, even though vapor pressure deficit and temperature were generally higher under overcast conditions (Fig. 3.5).

Given the inherent diurnal variation in E_t and its meteorological controls, the timing of fog occurrence (from time of day to season of the year) is an important

determinant of the magnitude of the E_t suppression effect of fog (or its impact on seasonal and annual amounts of E_t). For instance, if foggy conditions occur more frequently during the late afternoon and night, i.e. when the available energy for evaporation is very low (even under clear-sky conditions), the net effect of fog on monthly, seasonal and annual amounts of E_t would be expected to be small. For the case reported here, fog occurrence in the late afternoon and early evening was the norm (Fig. 3.3), as is typical for many fog-affected forests due to the diurnal pattern of orographic-convective cloud development over mountains, as mentioned earlier. Therefore, even if strong reductions in E_t are found when comparing foggy with sunny (or overcast) conditions, the total amount of water prevented from being transpired seasonally and annually may be low, depending on the timing of fog immersion. As such, reports of strong instantaneous reductions in E_t due to cloud immersion without the proper context may present an exaggerated picture of the impact of the E_t suppressing effect of fog (e.g. Ritter et al., 2009).

The total amount of water prevented from being transpired annually from the *P. patula* plantation due to foggy (relative to sunny) conditions was 17 ± 3% of mean annual E_t (i.e. 113 ± 19 mm). This is considerably higher than the amount of cloud water interception estimated for this stand (~35 mm year^{-1}; F. Holwerda, unpublished data), or for the nearby mature and regenerating lower montane cloud forests (50 ± 51 mm and 38 ± 46 mm, respectively; Muñoz-Villers et al., 2012). However, since a shift to overcast (rather than clear-sky) conditions would seem a more realistic consequence of a climate change-related rise in the average regional cloud base, the present results suggest the impact of a rise in the LCL on annual E_t may actually be much lower (2 ± 1% of annual

E_t). In this case, the amount of annual fog-induced suppression of E_t (13 ± 6 mm) would be comparable to the estimated additional water inputs from cloud water interception.

A related aspect concerns the uptake of water deposited on leaf surfaces by wetting events, or foliar water uptake, which has been highlighted recently as being a prevalent phenomenon across fog-affected sites and species (cf. Goldsmith et al., 2012a), including *P. patula* and other species at the present study site (S.G. Gotsch et al., unpubl. data; G.R. Goldsmith and M.S. Alvarado-Barrientos, unpubl. data). Moreover, it has been argued that a potential consequence of diminished cloud immersion and associated reduction in leaf wetting would be increased plant water stress (especially during the dry season), since foliar water uptake has been demonstrated to improve plant water status in fog-affected ecosystems (cf. Goldsmith et al., 2012a). Although foliar water uptake was not considered directly in the present study, it was possible to detect small sap velocities as well as the direction of the flow by using the Heat Ratio method (Burgess et al., 2001), such that significant reverse sapflow would suggest hydraulic redistribution within the stem, possibly due to foliar water uptake (Nadezhdina et al., 2010). However, hourly rates of reverse flow detected in the stem at breast height were mostly insignificant (<0.02 mm h^{-1}) and typically associated with instances when the canopy was wetted by rain. Thus, the effects of foliar uptake for *P. patula* at the study site and under current climate conditions are not likely to extend beyond the leaf level, and are associated more with rain- than fog-induced canopy wetness.

More importantly, the present results suggest that dry-season precipitation, combined with suppressed E_t due to cloudy and foggy conditions, as well as the favorable hydraulic properties of volcanic soils (Geissert et al., 2012), maintain high levels of soil

water content during the dry season. Therefore, it may be argued that diminished dry-season precipitation, which has been projected to decrease by 14% in general for Central America and Mexico (Karmalkar et al., 2011), presents a more worrisome prospect for plant-water relations and soil water availability, beyond diminishing fog occurrence alone. As both dry-season precipitation and fog concur in central Veracruz, a considerable decrease in both may have a synergistic effect of increased water losses via transpiration and potentially reduced soil water storage with associated ecohydrological consequences (e.g. soil water deficit and reduced catchment water yield). This is particularly important in view of increases in tree planting in tropical montane headwater catchments, combined with the seemingly prolific water use by young stands of fast-growing species used in the reforestation such as *P. patula*.

5. Conclusions

The potential increase in the lifting condensation level is likely to be in the order of a couple of hundred meters and will probably result in a shift to overcast rather than clear-sky conditions. As such, the present results suggest that the impact on seasonal and annual E_t may be relatively small. Moreover, reduced dry-season precipitation as a consequence of projected climate change for regions such as central Veracruz, more than diminishing cloud immersion alone, presents a worrisome prospect for plant-water relations and water yield from headwater catchments, due to the associated potential reductions in soil water reserves. Given the importance of examining these postulates for water management planning, the need for better projections of climate change-related alterations in rainfall patterns, as well as cloud cover and immersion, in tropical montane regions is highlighted.

CHAPTER IV

IS NIGHTTIME TRANSPIRATION ENHANCED AFTER FOG EVENTS?[1]

Abstract

Fog occurrence has been shown to suppress transpiration (E_t). On the other hand foggy conditions during which leaf wetness does not block stomatal gas exchange may enhance stomatal conductance, and so E_t immediately after fog. Furthermore, although nighttime E_t has been found to be prevalent for a wide range of species from cloud-affected forests, its magnitude relative to daytime E_t has been reported to be generally small. Here, we report considerable variability in nighttime E_t rates of *Pinus patula* trees associated to rapidly changing meteorological conditions typical for the dry season in the tropical montane cloud belt of the Eastern Sierra Madre, Mexico. Stand level tree E_t was derived from sapflow measurements with the Heat Ratio Method in the stem of *P. patula* trees growing in contrasting stands and at different elevations within the cloud belt: 10-year-old reforestation at 2180 m a.s.l. and mature forest at 2470 m a.s.l. The dry-season range of nighttime E_t for the young and mature forest was 0-0.08 and 0-0.06 mm h^{-1}, respectively. Expressed as a proportion of dry-season daily totals, nighttime E_t was high and variable (42 ± 28% and 19 ± 23% for the young and mature stand, respectively). This large variation was related to the wide range of air humidity, caused by the alternation of cold front intrusions bringing about fog events and high pressure weather characterized

[1] Article in press: Alvarado-Barrientos, M.S., Holwerda, F., Asbjornsen. Is nighttime transpiration enhanced after fog events? Proceedings of the 9th International Workshop on Sap Flow, *Acta Horticulturae*

by dry nights with vapor pressure deficits up to 2 kPa. Shortly after the end of fog events without concurring rainfall, nighttime E_t for the young stand was higher (although not significantly) and more variable than for fog-free nights. Climate change-related alterations in lifting condensation level that have been projected for tropical montane regions will also affect the dynamics of the inversion layer, and as shown here, nighttime E_t may increase/decrease considerably depending on a lowering/rise of the cloud ceiling.

1. Introduction

Projected future drier and warmer regional climate in tropical montane regions worldwide is likely to cause a rise in the lifting condensation level, thereby reducing the frequency of fog occurrence in many cloud forests (Still et al., 1999). The reduction in cloud immersion may considerably affect the hydrological cycle in these environments, as well as many ecological functions. Frequent cloud immersion not only can introduce an additional source of water (via cloud water interception), but also can suppress transpiration (Ritter et al., 2009; Chapter 3). On the other hand, foggy conditions may enhance stomatal conductance (Reinhardt and Smith, 2008), and so transpiration (E_t). E_t may be enhanced as long as stomatal gas exchange is not blocked by a film of water formed by fog deposition, as in light and/or intermitted fog with relatively low liquid water content and/or because of hydrophobic leaf surfaces (Rosado and Holder, 2012).

In many tropical montane regions, fog events occur more frequently during the late afternoon and nighttime due to the diurnal pattern of orographic-convective cloud development over the mountains. Furthermore, although nighttime E_t has been found to be prevalent for a wide range of species from cloud-affected forests, its magnitude

relative to daytime E_t has been reported to be relatively small (Dawson et al., 2007). In order to better understand the net effect of fog on E_t, we formulated the following research question: is nighttime E_t enhanced immediately after fog (as compared to nights without fog)?

Additional objectives were to determine the amount E_t that occurs at night as a proportion of daily E_t, and to examine the strength of the relationship between vapor pressure deficit and nighttime E_t under different weather conditions. We investigated this for *Pinus patula*, a widely used tree species for reforestation projects in the tropical uplands of Mexico, as it is of public interest that the water use patterns of this increasing land use are well understood (particularly in the face of climate change-related alterations in cloud immersion frequency). We focused our analysis on the dry season, as this is when fog occurrence is more frequent in our study region (see below). We used observations from the dry seasons of 2008/09 and 2009/10. The present is a report of the first findings, and as such, this is a work in progress.

2. Material and Methods

The study sites are within the seasonally dry tropical montane cloud belt of central Veracruz, Mexico. Two *Pinus patula* stands were under study: a 10-year-old reforestation located at 2180 m a.s.l. (19.4931° N, 97.0422° W) and a mature forest located at 2470 m a.s.l. (19.5054° N, 97.0559° W). Table 1 summarizes their structural characteristics. More details on the study sites are given in Alvarado-Barrientos et al. (2013). The climate between 2000 and 3000 m a.s.l. in the study region is temperate humid, with an average temperature between 12 and 18°C and a mean annual precipitation (MAP) between 2000

and 3000 mm. The region has a seasonal rainfall and cloud immersion regime, with a wet season between May and October, in which approximately 80% of MAP falls. The dry season (November–April) is characterized by an alternation of stable dry weather conditions and cloud immersion events, often accompanied by rain and/or drizzle (Holwerda et al., 2010).

Table 1. Characteristics of the two *Pinus patula* stands under study. HRM = Heat Ratio Method for sap flow measurements; n = number of sample trees; DBH = diameter at breast height; LAI = leaf area index. Standard deviations are given between parentheses where available.

	Young plantation	**Mature forest**
Elevation [m a.s.l.]	2180	2470
Area [ha]	~1	~20
Mean canopy height [m][a]	7 (1.5)	23 (2.80)
LAI [m^2 m^{-2}][b]	5.21 (0.10)	3.23 (0.32)
Tree density [stems ha^{-1}][a]	3,783 (652)	662 (92)
Basal area [m^2 ha^{-1}][a]	34.3 (9.6)	46.7 (15.3)
Trees with HRM probes: n	8	10
tree ages [years][c]	10	17–34
DBH range [cm]	9.6–11.8	20.4–61

[a] Hernandez-Hernandez (2010) and M.S. Alvarado-Barrientos, unpublished data.
[b] Measured with a LICOR LAI-2000 canopy analyzer throughout the dry season of 2010 (M.S. Alvarado-Barrientos, unpublished data).
[c] as of 2010

Automated weather stations were installed in open areas with SE exposure at a distance of 350 m (2128 m a.s.l.) and 450 m (2400 m a.s.l.) from the young and mature stands, respectively. Meteorological data were available as 10-min averages from 30 s sampling intervals. Variables measured included: incoming solar radiation (R_s [W m^{-2}]), air temperature (T [°C]), vapor pressure (e [kPa]), wind speed (u [m s^{-1}]), rainfall (P [mm]), and horizontal visibility (VIS [m]). Vapor pressure deficit (D [kPa]) was

computed as the difference between e and saturation vapor pressure (e_s; computed as in (Lowe, 1977) using T). Further details on meteorological data collection are also given in Alvarado-Barrientos et al. (2013). The occurrence of fog was defined as VIS < 1000 m (Glickman, 2000). From 10-min observations of VIS, hourly values of fog occurrence (in % of the time) were calculated and used to identify fog events, which were defined as periods with fog occurrence separated by a fog-free period of at least three hours.

Leaf wetness was measured with two Decagon LWL dielectric leaf wetness sensors installed hanging vertically to simulate the weeping orientation of *P. patula* needles at 4 and 6 m from the ground within the canopy of the young plantation. The canopy was considered to be wet when both sensors indicated that water was present on their surface (10-min reading > 300 mV). Visual inspection of sensors and needles confirmed that this best reflected the wetting and drying of the needles. At the mature forest, no leaf wetness measurements were performed because of logistical reasons.

The Heat Ratio method (Burgess et al., 2001) was used to obtain point measurements of sap velocity within the sapwood at breast height (1.4 m above ground) for 8 sample *P. patula* trees in each stand. A detailed description of sap velocity data collection as well as the characterization of the radial profile of sap velocity for all sample trees is given in Alvarado-Barrientos et al. (2013). The median radial profile shape for each sample tree (i.e. fixed value of the lumped shape parameter ρ) found in this previous study was used to derive maximum likelihood estimates of the time-variant component of radial profile by fitting the Beta probability density function (Beta-PDF) to hourly radial profiles of sap velocity (Alvarado-Barrientos et al. 2013). These two parameters together with measured sapwood depth of each tree (L_s [cm]) were used to

compute hourly whole-tree sapflow: $F_s(t) = 2\ \pi\ L_s^2\ \rho\ c_s(t)\ 0.001$ [L h^{-1}]. The Beta-PDF was not a good fit for 24% of the hourly radial profiles, which were associated with low evaporative demand conditions producing either a relatively homogenous distribution of sap velocity across the sapwood or radial patterns not conforming to the Beta-PDF (Alvarado-Barrientos et al., 2013). Thus an area-weighted average of point sap velocity (v_{wa}) was computed such that $F_s = A_s\ v_{wa}$, where A_s is measured sapwood area [cm^2] for each tree.

F_s was assumed equal to transpiration at the whole-tree level, that is, we ignored any time lag due to stem capacitance (see also further below). Stand level tree transpiration (E_t [mm h^{-1}]) for the young stand was derived simply by averaging hourly F_s across all sample trees and multiplying by stand density (Table 1), as the stand was even-aged and trees were spaced fairly homogeneous (cf. Čermák et al., 2004). Given the more complex structure of the mature stand, the method of scaling up based on sap flow distribution in DBH classes was followed (cf. Čermák et al., 2004): sample mature trees were assigned to one of four discrete DBH classes of *P. patula* derived from a survey at this site to derive mean F_s values for each class, and subsequently, these were multiplied by the number of trees ha^{-1} in each DBH class and summed (see Chapter 2).

Nighttime was defined as between 19:00 and 5:00 local standard time ($R_s < 7$ Wm^{-2}). The ratio of nighttime E_t to total daily E_t (i.e. night and daytime hours of the same calendar day) was computed using only those days for which all 24 hourly values of E_t were available; 36% and 42% of the total number of days were used for the young plantation and mature forest, respectively. To examine our driving research question, only data from the young stand were considered, as leaf wetness data were not available

for the mature stand. Furthermore, even though we considered that capacitance-induced lags can be safely ignored at time scales larger than an hour in this study, to be conservative and minimize any flow related to recharge of internal water storage, we considered only hours belonging to the second half of the night (i.e. from midnight to 5:00) for hypothesis testing. These hours were classified as: (i) 'clear', when the entire night was fog free and the preceding day was had a (near) clear sky; (ii) 'foggy'. when fog occurred, with the event starting at the latest at 19:00; and, (iii) 'clear-after-fog', for those hours after the occurrence of a fog-only event (i.e. no concurring rainfall) that ended not earlier than at 19:00. With these criteria, we selected the data to test the hypothesis that mean nighttime E_t is higher after the occurrence of fog as compared to that in nights not preceded by fog. Significant differences among frequency distributions of E_t [mm h^{-1}] for each of the three classes were tested with the Kruskal-Wallis one-way analysis of variance on ranks, and post-hoc pair-wise multiple comparisons were carried out with the Dunn's method. Also, to take into account the differences in D among the night categories defined, a general linear model (lm, R version 2.15.0) was fitted to the data with nighttime E_t as the response variable, while D, night category and their interaction were the explanatory variables.

3. Results and Discussion

Under clear sky and dry canopy conditions for the young stand, hourly E_t increased sharply at sunrise, reached a maximum typically around 11:00 (i.e. few hours before maximum hourly R_s), started to decrease shortly after, and reached near-zero values almost immediately after sunset (Fig. 1a and 1c). However, in many occasions E_t had

actually already started well before sunrise; significant E_t was recorded in 30% of total nighttime (dry-season) hours at this site, with hourly rates ranging from 0 to 0.08 mm h^{-1}. At the mature stand, we observed similar patterns; however, hourly E_t rates were considerably lower compared to the young stand, regardless of the time of day (Fig. 1b). Moreover, significant E_t was recorded only in 2.5% of the total number of dry-season nighttime hours, and hourly rates reached up to 0.06 mm h^{-1}. Differences in E_t between stands may be explained by differences in tree density and leaf area index; however, age/size effects can also not be excluded (Table 1; Chapter 2).

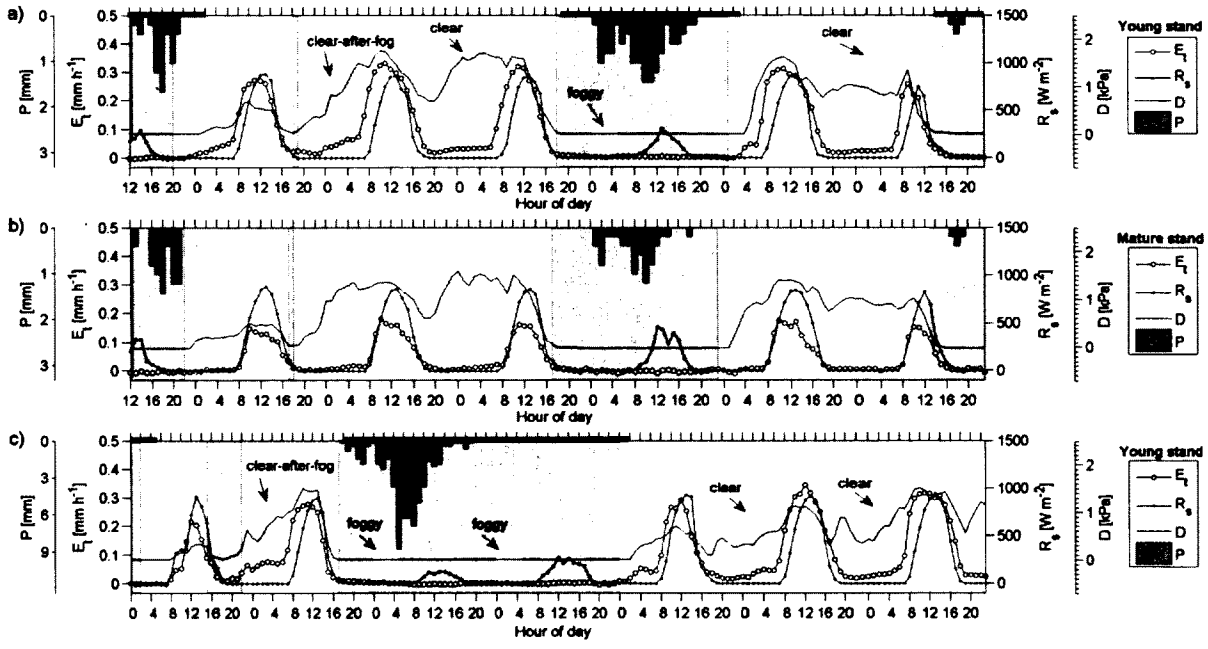

Fig. 4.1. Examples of stand level tree transpiration (E_t) for *Pinus patula* and concurring incoming solar radiation (R_s), vapor pressure deficit (D), precipitation (P), fog events, and canopy wetness. These types of responses were observed throughout the investigation. Dark gray areas depict fog events, black bars on top x-axis show leaf wetness duration, and light gray boxes indicate nighttime hours used for hypothesis testing. (a) and (b) show December 21 (from noon) to 27, 2009, for the young and mature stand, respectively. (c) Shows January 14 to 20, 2010, for the young stand.

We consider that sapflow activity during the night did not represent xylem storage tissue recharge for *P. patula* trees of any size sampled, because there was no indication of E_t lagging after R_s after sunset, even following clear-sky conditions (Fig. 1; cf. Fisher et al., 2007). Moreover, there were many instances when E_t increased in the dark, coinciding with relatively high D (sometimes >1 kPa), after having declined at sunset and maintained steadily low for the first hours of the night (Fig. 1; cf. Dawson et al., 2007). The observed nighttime E_t in both stands under study is not unexpected, given the increasing evidence of nighttime E_t, and stomatal conductance, in a wide range of woody species from many ecosystems, including tropical montane and cloud-affected regions (Dawson et al., 2007; Fetene and Beck, 2004; Garcia-Santos, 2012; Motzer et al., 2005). There was a high day-to-day variation in the total amount of E_t observed during the night. For the young stand, the range of the ratio of total nighttime E_t to total daily E_t was 0.01 – 1.28. A similar wide range was found for the mature stand (0 – 1.42). The average ratio we found for the young stand (0.42 ± 0.28) by far exceeded previously reported average or maximum ratios for other montane tree species, whereas the average ratio observed for the mature stand (0.19 ± 0.23) was at the high end of the range for these species. For instance, an average ratio of 0.05 was reported for *Myrica faya* and *Erica arborea* in the cloud belt of the Canary Islands (Garcia-Santos, 2012), a maximum of 0.18 for *Metrosideros polymorpha* in a tropical montane forest of Hawaii (Dawson et al., 2007), and an average of 0.20 for *P. ponderosa* in the Sierra Nevada Mountains (Fisher et al., 2007). At our study site, nights with high D were relatively common during the dry season and occurred primarily during conditions of high pressure following cold front passage. The often sharp increases in D and temperature (not shown) observed during

such nights suggest that an inversion layer descended below our study sites (Hubbart et al., 2007).

Interestingly, nighttime E_t was occasionally higher following fog-only events compared to fog-free nights, and this was more pronounced for the young stand (Fig. 1). On average, rates of nighttime E_t observed during hours classified as clear-after-fog were slightly higher and much more variable than for clear conditions; the difference was, however, not significant at the 0.05 level (Fig. 2a). D increased dramatically from near-zero values up to >1 kPa after the passage of fog events at night (Fig. 1). Furthermore, nighttime E_t was strongly correlated to D for clear nights as well as for clear-after-fog conditions (Fig. 2b). The general linear model revealed that the variability in nighttime E_t can be explained by D ($F = 292.7$ $p < 0.001$), and that the interaction between D and night category (i.e. clear, clear-after-fog, and foggy) is significant ($F = 4.2$; $p = 0.02$).

Our data suggest that stomatal conductance might have been enhanced under the humid conditions associated with fog events. Consequently, the very dry air following immediately after fog may have resulted in higher E_t as compared to similar dry nights not preceded by fog. Increased stomatal conductance under foggy conditions has been reported previously for other conifer species in cloud-affected environments (Chu et al., 2012; Johnson and Smith, 2008; Reinhardt and Smith, 2008). Canopy wetness data at the young stand indicated that the canopy remained dry during the majority of fog-only events. It can not entirely be excluded that even though the sensors indicated dry canopy conditions the canopy was in reality, partially wet. We believe however, that is unlikely that stomatal gas exchange was blocked by water deposited on the surface of the needles after the passage of fog-only events. The fact that the canopy could have been partially

wet keeps open the possibility for some foliar water uptake (Burgess and Dawson, 2004; Goldsmith et al., 2012a; Nadezdhina et al., 2010) although probably very small quantities (near-zero and slightly negative rates shown in Fig. 2b), thus enhancing E_t as soon as the canopy dried out, which we believe is very quick under the very dry conditions following fog occurrence. Importantly, a 'wet-enhanced/dry-reduced' water use strategy as postulated for yellow cypress (Chu et al., 2012) may also be the case for *P. patula*, indicating that it is prone to profligate transpiration to some extent, and young stands relatively more than mature stands.

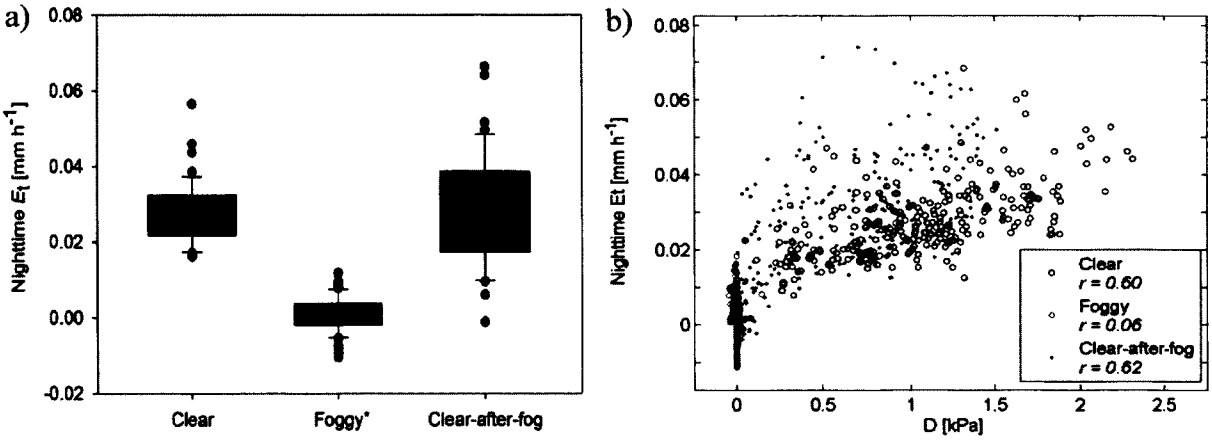

Fig. 4.2. (a) Comparison of mean nighttime E_t under three classes of weather conditions for the young *Pinus patula* stand. See text for classification criteria. * = significantly different at the 0.05 level. (b) Nighttime E_t against vapour pressure deficit (D) for the young *Pinus patula* stand and the three classes of weather conditions. Correlation coefficients (r) are given in the legend.

4. Conclusions

Nighttime E_t was much more pronounced for the young than for the mature stand. Improvements to be addressed in a forthcoming article are analyses at the whole-tree

level to determine the relative importance of hydraulic differences between trees of different size (e.g. tree nighttime conductance) and microclimatic heterogeneity inside the stands. Under similar conditions of high atmospheric evaporative demand, rates of nighttime E_t were occasionally higher immediately after the passage of fog compared to fog-free nights; the difference was not significant, however. Climate change-related alterations in the lifting condensation level that have been projected for tropical montane regions may affect both fog occurrence and the occurrence of nights with high atmospheric demand. This, in turn, may affect patterns of nighttime E_t in this environment. Given the considerable amount of nighttime E_t from young *P. patula* reforestations, our results highlight the need for better projections of alterations in cloud immersion frequency and the occurrence of nights with high atmospheric demand in order to better predict ecohydrological impacts of expanding pine plantations in tropical uplands.

LIST OF REFERENCES

Aide, T.M., Ruiz-Jaen, M.C., Grau, H.R., 2010. What is the state of tropical montane cloud forest restoration? In: Bruijnzeel, L.A., Scatena, F.N.,Hamilton, L.S. (Eds.), Tropical montane cloud forests. Cambridge University Press, Cambridge, pp. 101-109.

Allen, R.G., Pereira, L.S., Raes, D., Smith, M., 1998. Crop evapotranspiration – Guidelines for computing crop water requirements. FAO, Rome.

Alvarado-Barrientos, M.S., Hernández-Santana, V., Asbjornsen, H., 2013. Variability of the radial profile of sap velocity in *Pinus patula* from contrasting stands within the seasonal cloud forest zone of Veracruz, Mexico. Agricultural and Forest Meteorology 168: 108-119.

Andre, J.C., Bougeault, P., Mahfouf, J.F., Mascart, P., Noilhan, J., Pinty, J.P., 1989. Impact of forests on mesoscale meteorology. Philosophical Transactions of the Royal Society of London Series B-Biological Sciences 324(1223): 407-422.

Anfodillo, T., Sigalotti, G.B., Tomasi, M., Semenzato, P., Valentini, R., 1993. Applications of a thermal imaging technique in the study of the ascent of sap in woody species. Plant Cell and Environment 16(8): 997-1001.

Asbjornsen, H., Goldsmith, G.R., Alvarado-Barrientos, M.S., Rebel, K., Van Osch, F.P., Rietkerk, M., Chen, J., Gotsch, S., Tobon, C., Geissert, D.R., Gómez-Tagle, A., Vache, K., Dawson, T.E., 2010. Ecohydrological advances and applications in plant-water relations research: a review. Journal of Plant Ecology 4(1-2): 3-22.

Barradas, V.L., Cervantes-Pérez, J., Ramos-Palacios, R., Puchet-Anyul, C., Vásquez-Rodríguez, P., Granados-Ramirez, R., 2010. Meso-scale climate change in the central mountain región of Veracruz State, Mexico. In: Bruijnzeel, L.A., Scatena, F.N.,Hamilton, L.S. (Eds.), Tropical Montane Cloud Forests: Science for Conservation and Management. Cambridge University Press, Cambridge, pp. 549-556.

Benner, J., Vitousek, P.M., Ostertag, R., 2010. Nutrient cycling and nutrient limitation in tropical montane cloud forests. In: Bruijnzeel, L.A., Scatena, F.N.,Hamilton, L.S. (Eds.), Tropical montane cloud forests. Cambridge University Press, Cambridge, pp. 90-100.

Bleby, T.M., Burgess, S.S.O., Adams, M.A., 2004. A validation, comparison and error analysis of two heat-pulse methods for measuring sap flow in *Eucalyptus marginata* saplings. Functional Plant Biology 31(6): 645-658.

Booker, R.E., Kininmonth, J.A., 1978. Variation in longitudinal permeability of green Radiata pine wood. New Zealand Journal of Forestry Science 8(2): 295-308.

Bosch, J.M., Hewlett, J.D., 1982. A review of catchment experiments to determine the effect of vegetation changes on water yield and evapotranspiration. Journal of Hydrology 55(1-4): 3-23.

Brauman, K.A., Freyberg, D.L., Daily, G.C., 2012. Potential evapotranspiration from forest and pasture in the tropics: A case study in Kona, Hawai ' i. Journal of Hydrology 440: 52-61.

Brown, M.B., de la Roca, I., Vallejo, A., Ford, G., Casey, J., Aguilar, B., Haacker, R., 1996. A valuation analysis of the role of cloud forests in watershed protection: Sierra de las Minas Biosphere Reserve, Guatemala and Cusuco N.P. Honduras, RARE Center for Tropical Conservation, Philadelphia.

Bruijnzeel, L.A., 2004. Hydrological functions of tropical forests: not seeing the soil for the trees? Agriculture Ecosystems & Environment 104(1): 185-228.

Bruijnzeel, L.A., Mulligan, M., Scatena, F.N., 2011. Hydrometeorology of tropical montane cloud forests: emerging patterns. Hydrological Processes 25(3): 465-498.

Bruijnzeel, L.A., Scatena, F.N., Hamilton, L.S. (Eds.), 2010. Tropical montane cloud forests: Science for conservation and management. Cambridge University Press, Cambridge.

Burgess, S.S.O., Adams, M., Turner, N.C., Beverly, C.R., Ong, C.K., Khan, A.A.H., Bleby, T.M., 2001. An improved heat pulse method to measure low and reverse rates of sap flow in woody plants. Tree Physiology 21(15): 1157-1157.

Burgess, S.S.O., Dawson, T.E., 2004. The contribution of fog to the water relations of *Sequoia sempervirens* (D. Don): Foliar uptake and prevention of dehydration. Plant Cell and Environment 27(8): 1023-1034.

Calder, I.R., 1998. Water use by forests, limits and controls. Tree Physiology 18(8-9): 625-631.

Carabias, J., Arriaga, V., Cervantes Guitiérrez, V., 2007. Las políticas públicas de la restauración ambiental en México: limitantes, avances, rezagos y retos. Boletín de la Sociedad Botánica de México 80: 85-100.

Cavelier, J., 1992. Fine-root biomass and soil properties in a semideciduous and lower montane rain-forest in Panama. Plant and Soil 142(2): 187-201.

Cavelier, J., 1996. Environmental factors and ecophysiological processes along altitudinal gradients in wet tropical mountains. In: Mulkey, S., Chazdon, R.,Smith, A. (Eds.), Tropical forest plant ecophysiology. Springer, New York, pp. 399-439.

Caylor, K.K., Dragoni, D., 2009. Decoupling structural and environmental determinants of sap velocity: Part I. Methodological development. Agricultural and Forest Meteorology 149(3-4): 559-569.

Čermák, J., Cienciala, E., Kučera, J., Hallgren, J.E., 1992. Radial-velocity profiles of water-flow in trunks of Norway spruce and oak and the response of spruce to severing. Tree Physiology 10(4): 367-380.

Čermák, J., Kučera, J., Nadezhdina, N., 2004. Sap flow measurements with some thermodynamic methods, flow integration within trees and scaling up from sample trees to entire forest stands. Trees-Structructure and Function 18(5): 529-546.

Čermák, J., Nadezhdina, N., 1998. Sapwood as the scaling parameter defining according to xylem water content or radial pattern of sap flow? Annales des Sciences Forestieres 55(5): 509-521.

Čermák, J., Nadezhdina, N., Meiresonne, L., Ceulemans, R., 2008. Scots pine root distribution derived from radial sap flow patterns in stems of large leaning trees. Plant and Soil 305(1-2): 61-75.

Chu, H.-S., Chang, S.-C., Klemm, O., Lai, C.-W., Lin, Y.-Z., Wu, C.-C., Lin, J.-Y., Jiang, J.-Y., Chen, J., Gottgens, J.F., Hsia, Y.-J., 2012. Does canopy wetness matter? Evapotranspiration from a subtropical montane cloud forest in Taiwan. Hydrological Processes: DOI: 10.1002/hyp.9662.

Cohen, Y., Cohen, S., Cantuarias-Aviles, T., Schiller, G., 2008. Variations in the radial gradient of sap velocity in trunks of forest and fruit trees. Plant Soil 305(1-2): 49-59.

Dawson, T.E., 1998. Fog in the California redwood forest: Ecosystem inputs and use by plants. Oecologia 117(4): 476-485.

Dawson, T.E., Burgess, S.S.O., Tu, K.P., Oliveira, R.S., Santiago, L.S., Fisher, J.B., Simonin, K.A., Ambrose, A.R., 2007. Nighttime transpiration in woody plants from contrasting ecosystems. Tree Physiology 27(4): 561-575.

Delzon, S., Loustau, D., 2005. Age-related decline in stand water use: Sap flow and transpiration in a pine forest chronosequence. Agricultural and Forest Meteorology 129(3-4): 105-119.

Delzon, S., Sartore, M., Granier, A., Loustau, D., 2004. Radial profiles of sap flow with increasing tree size in maritime pine. Tree Physiology 24(11): 1285-1293.

Denmead, O.T., 1984. Plant physiological methods for studying evapotranspiration: Problems of telling the forest from the trees. Agricultural Water Management 8(1-3): 167-189.

Dingman, S.L., 2008. Physical hydrology. Prentice-Hall, Englewood Cliffs, NJ, 646 pp.

Domec, J.C., Meinzer, F.C., Gartner, B.L., Woodruff, D., 2006. Transpiration-induced axial and radial tension gradients in trunks of Douglas-fir trees. Tree Physiology 26(3): 275-284.

Dragoni, D., Caylor, K.K., Schmid, H.P., 2009. Decoupling structural and environmental determinants of sap velocity Part II. Observational application. Agricultural and Forest Meteorology 149(3-4): 570-581.

Dunn, G.M., Connor, D.J., 1993. An analysis of sap flow in Mountain Ash (*Eucalyptus regnans*) forests of different age. Tree Physiology 13(4): 321-336.

Dunn, O.J., 1964. Multiple comparisons using rank sums. Technometrics 6(3): 241-252.

Dvorak, W.S., Hodge, G.R., Kietzka, J.E., Malan, F., Osorio, L.F., Stanger, T.K., 2000. *Pinus patula*, Conservation & testing of tropical & subtropical forest tree species. College of Natural Resources, North Carolina State University, Raleigh.

Dye, P.J., Olbrich, B.W., Poulter, A.G., 1991. The influence of growth rings in *Pinus patula* on heat pulse velocity and sap flow measurement. Journal of Experimental Botany 42(240): 867-870.

Dye, P.J., Soko, S., Poulter, A.G., 1996. Evaluation of the heat pulse velocity method for measuring sap flow in *Pinus patula*. Journal of Experimental Botany 47(300): 975-981.

Edwards, W.R.N., Warwick, N.W.M., 1984. Transpiration from a kiwifruit vine as estimated by the heat pulse technique and the Penman-Monteith equation. New Zealand Journal of Agricultural Research 27(4): 537-543.

Efron, B., 1981. Nonparametric estimates of standard error - the jackknife, the bootstrap and other methods. Biometrika 68(3): 589-599.

Eugster, W., Burkard, R., Holwerda, F., Scatena, F.N., Bruijnzeel, L.A., 2006. Characteristics of fog and fogwater fluxes in a Puerto Rican elfin cloud forest. Agricultural and Forest Meteorology 139(3-4): 288-306.

Evans, J., 1999. Planted forests of the wet and dry tropics: their variety, nature, and significance. New Forests 17(1-3): 25-36.

FAO, 2010. Global forest resources assessment 2010: Main report. Food and Agriculture Organization of the United Nations, Rome.

Farley, K.A., Jobbagy, E.G., Jackson, R.B., 2005. Effects of afforestation on water yield: a global synthesis with implications for policy. Global Change Biology 11(10): 1565-1576.

Fetene, M., Beck, E.H., 2004. Water relations of indigenous versus exotic tree species, growing at the same site in a tropical montane forest in southern Ethiopia. Trees-Structure and Function 18(4): 428-435.

Fiora, A., Cescatti, A., 2008. Vertical foliage distribution determines the radial pattern of sap flux density in *Picea abies*. Tree Physiology 28(9): 1317-1323.

Fisher, J.B., Baldocchi, D.D., Misson, L., Dawson, T.E., Goldstein, A.H., 2007. What the towers don't see at night: nocturnal sap flow in trees and shrubs at two AmeriFlux sites in California. Tree Physiology 27(4): 597-610.

Fisher, J.B., Malhi, Y., Bonal, D., Da Rocha, H.R., De Araujo, A.C., Gamo, M., Goulden, M.L., Hirano, T., Huete, A.R., Kondo, H., Kumagai, T., Loescher, H.W., Miller, S., Nobre, A.D., Nouvellon, Y., Oberbauer, S.F., Panuthai, S., Roupsard, O., Saleska, S., Tanaka, K., Tanaka, N., Tu, K.P., Von Randow, C., 2009. The land-atmosphere water flux in the tropics. Global Change Biology 15(11): 2694-2714.

Ford, C.R., Goranson, C.E., Mitchell, R.J., Will, R.E., Teskey, R.O., 2004a. Diurnal and seasonal variability in the radial distribution of sap flow: Predicting total stem flow in *Pinus taeda* trees. Tree Physiology 24(9): 941-950.

Ford, C.R., Hubbard, R.M., Vose, J.M., 2011. Quantifying structural and physiological controls on variation in canopy transpiration among planted pine and hardwood species in the southern Appalachians. Ecohydrology 4(2): 183-195.

Ford, C.R., McGuire, M.A., Mitchell, R.J., Teskey, R.O., 2004b. Assessing variation in the radial profile of sap flux density in Pinus species and its effect on daily water use. Tree Physiol 24(3): 241-249.

Frumau, A., Bruijnzeel, L.A., Tobón, C., 2006. Final technical report DFID-FRP Project R7991, Annex 2: Hydrological measurement protocol for montane cloud forest, Vrije Universiteit, Amsterdam, and Forestry Research Programme of the U.K. Department for International Development.

García-García, F.G., Zarraluqui, V., 2008. A fog climatology for Mexico. Erde 139(1-2): 45-60.

García-Santos, G., 2007. An ecohydrological and soils study in a montane cloud forest in the National Park of Garajonay, La Gomera (Canary Islands, Spain). PhD Dissertation Thesis, VU University.

García-Santos, G., 2012. Transpiration in a sub-tropical ridge-top cloud forest. Journal of Hydrology 462: 42-52.

García-Santos, G., Bruijnzeel, L.A., Dolman, A.J., 2009. Modelling canopy conductance under wet and dry conditions in a subtropical cloud forest. Agricultural and Forest Meteorology 149(10): 1565-1572.

García-Santos, G., Bruijnzeel, L.A., 2011. Rainfall, fog and throughfall dynamics in a subtropical ridge top cloud forest, National Park of Garajonay (La Gomera, Canary Islands, Spain). Hydrological Processes 25(3): 411-417.

García, E., 1973. Modificaciones al sistema de clasificación climática de Köppen. Instituto de Geografía, Mexico D.F., 246 pp.

García Franco, J.G., Castillo-Campos, G., Mehltreter, K., Martínez, M.L., Vázquez, G., 2008. Composición florística de un bosque mesófilo del centro de Veracruz, México. Boletín de la Sociedad Botánica de México 83: 37-52.

Gash, J.H.C., 1979. Analytical model of rainfall interception by forests. Quarterly Journal of the Royal Meteorological Society 105(443): 43-55.

Gebauer, T., Horna, V., Leuschner, C., 2008. Variability in radial sap flux density patterns and sapwood area among seven co-occurring temperate broad-leaved tree species. Tree Physiology 28(12): 1821-1830.

Geissert, D., Gómez-Tagle, A., Marín, B., Castro, A., Karlsen, R., Holwerda, F., Tobón, C., 2012. Soil water dynamics of andosol soils in tropical montane cloud forest in eastern Mexico, 2nd International Conference on Hydropedology, Leipzig, Germany.

Giambelluca, T., Gerold, G., 2011. Hydrology and biogeochemistry of tropical montane cloud forests. In: Levia, D.F., Carlyle-Moses, D.,Tanaka, T. (Eds.), Forest Hydrology and Biogeochemistry. Ecological Studies. Springer Netherlands, Dordrecht, pp. 221-259.

Giambelluca, T.W., Delay, J.K., Nullet, M.A., Scholl, M.A., Gingerich, S.B., 2011. Canopy water balance of windward and leeward Hawaiian cloud forests on Haleakala, Maui, Hawai'i. Hydrological Processes 25(3): 438-447.

Glickman, T.S. (Ed.), 2000. Glossary of Meteorology. American Meteorological Society, Boston, 855 pp.

Goldsmith, G.R., Matzke, N.J., Dawson, T.E., 2012a. The incidence and implications of clouds for cloud forest plant water relations. Ecology Letters: doi:10.1111/ele.12039.

Goldsmith, G.R., Muñoz-Villers, L.E., Holwerda, F., McDonnell, J.J., Asbjornsen, H., Dawson, T.E., 2012b. Stable isotopes reveal linkages among ecohydrological processes in a seasonally dry tropical montane cloud forest. Ecohydrology 5: 779–790.

Gómez-Peralta, D., Oberbauer, S.F., McClain, M.E., Philippi, T.E., 2008. Rainfall and cloud-water interception in tropical montane forests in the eastern Andes of Central Peru. Forest Ecology and Management 255(3-4): 1315-1325.

Gómez-Tagle, A.J., Geissert, D., Perez-Maqueo, O., Marin-Castro, B., Rendon-Lopez, B., 2011. Saturated hydraulic conductivity and land use change, new insights to the payments for ecosystem services programs: a case study from a tropical montane cloud forest watershed in eastern central Mexico. In: Dikinya, O. (Ed.), Developments in Hydraulic Conductivity Research. InTech, pp. 225-247.

Haeger, A., Dohrenbusch, A., 2011. Hydrometeorology and structure of tropical montane cloud forests under contrasting biophysical conditions in north-western Costa Rica. Hydrological Processes 25(3): 392-401.

Hatton, T.J., Catchpole, E.A., Vertessy, R.A., 1990. Integration of sapflow velocity to estimate plant water-use. Tree Physiology 6(2): 201-209.

Hatton, T.J., Moore, S.J., Reece, P.H., 1995. Estimating stand transpiration in a *Eucalyptus-Populnea* woodland with the heat pulse method - Measurement errors and sampling strategies. Tree Physiology 15(4): 219-227.

Henderson-Sellers, A., Drake, F., McGuffie, K., Fattori, A.P., Marques, A.d.O., Lloyd, C.R., Shuttleworth, W.J., 1987. Observations of day-time cloudiness over the Amazon forest using an all-sky camera. Weather 42: 209-218.

Hernández-Santana, V., Asbjornsen, H., Sauer, T., Isenhart, T., Schilling, K., Schultz, R., 2010. Enhanced transpiration by riparian buffer trees in response to advection in a humid temperate agricultural landscape. Forest Ecology and Management 261(8): 1415-1427.

Hernandez-Santana, V., David, T.S., Martinez-Fernandez, J., 2008. Environmental and plant-based controls of water use in a Mediterranean oak stand. Forest Ecology and Management 255(11): 3707-3715.

Hildebrandt, A., Al Aufi, M., Amerjeed, M., Shammas, M., Eltahir, E.A.B., 2007. Ecohydrology of a seasonal cloud forest in Dhofar: 1. Field experiment. Water Resources Research 43(10).

Hildebrandt, A., Eltahir, E.A.B., 2007. Ecohydrology of a seasonal cloud forest in Dhofar: 2. Role of clouds, soil type, and rooting depth in tree-grass competition. Water Resources Research 43(11).

Hochberg, Y., Tamhane, A.C., 1987. Multiple comparison procedures. John Wiley & Sons, Hoboken, NJ.

Holder, C.D., 2003. Fog precipitation in the Sierra de las Minas Biosphere Reserve, Guatemala. Hydrological Processes 17(10): 2001-2010.

Holwerda, F., Bruijnzeel, L.A., Barradas, V.L., Cervantes, J., 2013. The water and energy exchange of a shaded coffee plantation in the lower montane cloud forest zone of central Veracruz, Mexico. Agricultural and Forest Meteorology 173(0): 1-13.

Holwerda, F., Bruijnzeel, L.A., Munoz-Villers, L.E., Equihua, M., Asbjornsen, H., 2010. Rainfall and cloud water interception in mature and secondary lower montane cloud forests of central Veracruz, Mexico. Journal of Hydrology 384(1-2): 84-96.

Hubbart, J.A., Kavanagh, K.L., Pangle, R., Link, T., Schotzko, A., 2007. Cold air drainage and modeled nocturnal leaf water potential in complex forested terrain. Tree Physiology 27(4): 631-639.

Huber, B., Schmidt, E., 1937. Eine Kompensationsmethode zur thermoelektrischen Messung langsamer Saftströme. Ber. Dtsch. Bot. Ges. 55: 514-529.

Hutley, L.B., Doley, D., Yates, D.J., Boonsaner, A., 1997. Water balance of an Australian subtropical rainforest at altitude: The ecological and physiological significance of intercepted cloud and fog. Australian Journal of Botany 45(2): 311-329.

Ingraham, N.L., Matthews, R.A., 1988. Fog-drip as a source of groundwater recharge in Northern Kenya. Water Resources Research 24(8): 1406-1410.

IPCC, 2007. The Intergovernmental Panel on Climate Change, World Meteorological Organization, Geneva, Switzerland.

Ishibashi, M., Terashima, I., 1995. Effects of continuous leaf wetness on photosynthesis - adverse aspects of rainfall. Plant Cell and Environment 18(4): 431-438.

Jackson, R.B., Carpenter, S.R., Dahm, C.N., McKnight, D.M., Naiman, R.J., Postel, S.L., Running, S.W., 2001. Water in a changing world. Ecological Applications 11(4): 1027-1045.

James, S.A., Clearwater, M.J., Meinzer, F.C., Goldstein, G., 2002. Heat dissipation sensors of variable length for the measurement of sap flow in trees with deep sapwood. Tree Physiology 22(4): 277-283.

Jarvis, P.G., McNaughton, K.G., 1986. Stomatal control of transpiration: Scaling up from leaf to region. Advances in Ecological Research 15: 1-49.

Jimenez, M.S., Nadezhdina, N., Čermák, J., Morales, D., 2000. Radial variation in sap flow in five laurel forest tree species in Tenerife, Canary Islands. Tree Physiology 20(17): 1149-1156.

Johnson, D.M., Smith, W.K., 2008. Cloud immersion alters microclimate, photosynthesis and water relations in *Rhododendron catawbiense* and *Abies fraseri* seedlings in the southern Appalachian Mountains, USA. Tree Physiology 28(3): 385-392.

Juvik, J.O., Delay, J.K., Kinney, K.M., Hansen, E.W., 2011. A 50th anniversary reassessment of the seminal 'Lana'i fog drip study' in Hawai'i. Hydrological Processes 25(3): 402-410.

Kagawa, A., Sack, L., Duarte, K.e., James, S., 2009. Hawaiian native forest conserves water relative to timber plantation: Species and stand traits influence water use. Ecological Applications 19(6): 1429-1443.

Kaimowitz, D., 2005. Useful myths and intractable truths: The politics of the link between forests and water in Central America. In: Bonell, M.,Bruijnzeel, L.A. (Eds.), Forests, water and people in the humid tropics. Cambridge University Press, Cambridge, pp. 86-98.

Karlsen, R., 2010. Stormflow processes in a mature tropical montane cloud forest catchment, Coatepec, Veracruz, Mexico, Vrije Universiteit Amsterdam, 127 pp.

Karmalkar, A.V., Bradley, R.S., Diaz, H.F., 2008. Climate change scenario for Costa Rican montane forests. Geophysical Research Letters 35(11).

Karmalkar, A.V., Bradley, R.S., Diaz, H.F., 2011. Climate change in Central America and Mexico: regional climate model validation and climate change projections. Climate Dynamics 37(3-4): 605-629.

Katerji, N., Rana, G., 2011. Crop reference evapotranspiration: A discussion of the concept, analysis of the process and validation. Water Resources Management 25(6): 1581-1600.

Kelliher, F.M., Whitehead, D., McAneney, K.J., Judd, M.J., 1990. Partitioning evapotranspiration into tree and understory components in 2 young *Pinus radiata* D. Don stands Agricultural and Forest Meteorology 50(3): 211-227.

Kelliher, F.M., Leuning, R., Schulze, E.D., 1993. Evaporation and canopy characteristics of coniferous forests and grasslands. Oecologia 95(2): 153-163.

Klemm, O., Milford, C., Sutton, M.A., Spindler, G., van Putten, E., 2002. A climatology of leaf surface wetness. Theoretical and Applied Climatology 71(1-2): 107-117.

Kostner, B., Granier, A., Čermák, J., 1998. Sapflow measurements in forest stands: Methods and uncertainties. Annales des Sciences Forestieres 55(1-2): 13-27.

Kozlowski, T.T., Pallardy, S.G., 1997. Physiology of woody plants. Academic Press, New York, 412 pp.

Kravka, M., Krejzar, T., Čermák, J., 1999. Water content in stem wood of large pine and spruce trees in natural forests in central Sweden. Agricultural and Forest Meteorology 98(9): 555-562.

Kubota, M., Tenhunen, J., Zimmermann, R., Schmidt, M., Kakubari, Y., 2005. Influence of environmental conditions on radial patterns of sap flux density of a 70-year *Fagus crenata* trees in the Naeba Mountains, Japan. Annals of Forest Science 62(4): 289-296.

Lambers, H., Chapin, F.S., Pons, T.L., 2008. Plant physiological ecology. Springer Science, New York.

Lawton, R.O., Nair, U.S., Pielke, R.A., Welch, R.M., 2001. Climatic impact of tropical lowland deforestation on nearby montane cloud forests. Science 294(5542): 584-587.

Limm, E.B., Simonin, K.A., Bothman, A.G., Dawson, T.E., 2009. Foliar water uptake: A common water acquisition strategy for plants of the redwood forest. Oecologia 161(3): 449-459.

Lowe, P.R., 1977. An approximating polynomial for the computation of saturation vapor pressure. Journal of Applied Meteorology 16(1): 100-103.

Luis, V.C., Jiménez, M.S., Morales, D., Kucera, J., Wieser, G., 2005. Canopy transpiration of a Canary Islands pine forest. Agricultural and Forest Meteorology 135(1–4): 117-123.

Luttschwager, D., Remus, R., 2007. Radial distribution of sap flux density in trunks of a mature beech stand. Annals of Forest Science 64(4): 431-438.

Magnani, F., Bensada, A., Cinnirella, S., Ripullone, F., Borghetti, M., 2008. Hydraulic limitations and water-use efficiency in *Pinus pinaster* along a chronosequence. Canadian Journal of Forest Research-Revue Canadienne De Recherche Forestiere 38(1): 73-81.

Manley, R.E., Askew, A.J., 1993. Operational hydrology problems in the humid tropics. In: Bonell, M., Hufschmidt, M.M.,Gladwell, J.S. (Eds.), Hydrology and water management in the humid tropics. Cambridge University Press, Cambridge, pp. 34-44.

Mark, W.R., Crews, D.L., 1973. Heat-pulse velocity and bordered pit condition in living Engelmann spruce and Lodgepole pine prees. Forest Science 19(4): 291-296.

Marshall, D.C., 1958. Measurement of sap flow in conifers by heat transport. Plant Physiology 33(6): 385-396.

Martinez, M.L., Perez-Maqueo, O., Vazquez, G., Castillo-Campos, G., Garcia-Franco, J., Mehltreter, K., Equihua, M., Landgrave, R., 2009. Effects of land use change on biodiversity and ecosystem services in tropical montane cloud forests of Mexico. Forest Ecology and Management 258(9): 1856-1863.

Mata-Gonzalez, R., McLendon, T., Martin, D.W., 2005. The inappropriate use of crop transpiration coefficients (K-c) to estimate evapotranspiration in arid ecosystems: A review. Arid Land Research and Management 19(3): 285-295.

McJannet, D., Fitch, P., Disher, M., Wallace, J., 2007. Measurements of transpiration in four tropical rainforest types of north Queensland, Australia. Hydrological Processes 21(26): 3549-3564.

Medhurst, J.L., Battaglia, M., Beadle, C.L., 2002. Measured and predicted changes in tree and stand water use following high-intensity thinning of an 8-year-old *Eucalyptus nitens* plantation. Tree Physiology 22(11): 775-784.

Meinzer, F.C., Bond, B.J., Warren, J.M., Woodruff, D.R., 2005. Does water transport scale universally with tree size? Functional Ecology 19(4): 558-565.

Monteith, J.L., 1965. Evaporation and environment. Symposia of the Society for Experimental Biology 19: 205-34.

Monteith, J.L., Unsworth, M.H., 2007. Principles of environmental physics. Edward Arnold, London.

Moore, G.W., Heilman, J.L., 2011. Proposed principles governing how vegetation changes affect transpiration. Ecohydrology 4(3): 351-358.

Motzer, T., Munz, N., Kuppers, M., Schmitt, D., Anhuf, D., 2005. Stomatal conductance, transpiration and sap flow of tropical montane rain forest trees in the southern Ecuadorian Andes. Tree Physiology 25(10): 1283-1293.

Muñoz-Piña, C., Guevara, A., Torres, J.M., Brana, J., 2008. Paying for the hydrological services of Mexico's forests: Analysis, negotiations and results. Ecological Economics 65(4): 725-736.

Muñoz-Villers, L.E., 2008. Efecto del cambio en el uso del suelo sobre la dinámica hidrológica y calidad de agua en el trópico húmedo del centro de Veracruz, México, Universidad Autónoma Metropolitana, México D.F., 93 pp.

Muñoz-Villers, L.E., Holwerda, F., Gómez-Cárdenas, M., Equihua, M., Asbjornsen, H., Bruijnzeel, L.A., Marín-Castro, B.E., Tobón, C., 2012. Water balances of old-growth and regenerating montane cloud forests in central Veracruz, Mexico. Journal of Hydrology 462-463: 53-66.

Muñoz-Villers, L.E., Lopez-Blanco, J., 2008. Land use/cover changes using Landsat TM/ETM images in a tropical and biodiverse mountainous area of central-eastern Mexico. International Journal of Remote Sensing 29: 71-93.

Muñoz-Villers, L.E., McDonnell, J.J., 2012. Runoff generation in a steep, tropical montane cloud forest catchment on permeable volcanic substrate. Water Resources Research 48(9): W09528.

Nadezhdina, N., Čermák, J., Ceulemans, R., 2002. Radial patterns of sap flow in woody stems of dominant and understory species: Scaling errors associated with positioning of sensors. Tree Physiology 22(13): 907-918.

Nadezhdina, N., Čermák, J., Meiresonne, L., Ceulemans, R., 2007a. Transpiration of Scots pine in Flanders growing on soil with irregular substratum. Forest Ecology and Management 243(1): 1-9.

Nadezhdina, N., David, T.S., David, J.S., Ferreira, M.I., Dohnal, M., Tesar, M., Gartner, K., Leitgeb, E., Nadezhdin, V., Čermák, J., Jimenez, M.S., Morales, D., 2010. Trees never rest: The multiple facets of hydraulic redistribution. Ecohydrology 3(4): 431-444.

Nadezhdina, N., Nadezhdin, V., Ferreira, M.I., Pitacco, A., 2007b. Variability with xylem depth in sap flow in trunks and branches of mature olive trees. Tree Physiology 27(1): 105-113.

Nair, U.S., Lawton, R.O., Welch, R.M., Pielke, R.A., 2003. Impact of land use on Costa Rican tropical montane cloud forests: Sensitivity of cumulus cloud field characteristics to lowland deforestation. Journal of Geophysical Research-Atmospheres 108(D7).

Niyogi, D., Mahmood, R., Adegoke, J.O., 2009. Land-use/land-cover change and Its impacts on weather and climate. Boundary Layer Meteorology 133(3): 297-298.

Pausch, R.C., Grote, E.E., Dawson, T.E., 2000. Estimating water use by sugar maple trees: considerations when using heat-pulse methods in trees with deep functional sapwood. Tree Physiology 20(4): 217-227.

Pérez-Maqueo, O., Delfin, C., Fregoso, A., Cotler, H., Equihua, M., 2005. Modelos de simulación para la elaboración y evaluación de los programas de servicios ambientales hídricos. Gaceta Ine. 78: 47-66.

Phillips, N., Oren, R., Zimmermann, R., 1996. Radial patterns of xylem sap flow in non-, diffuse- and ring-porous tree species. Plant Cell and Environment 19(8): 983-990.

Pielke, R.A., Avissar, R., Raupach, M., Dolman, A.J., Zeng, X.B., Denning, A.S., 1998. Interactions between the atmosphere and terrestrial ecosystems: Influence on weather and climate. Global Change Biology 4(5): 461-475.

Pielke, R.A., Pitman, A., Niyogi, D., Mahmood, R., McAlpine, C., Hossain, F., Goldewijk, K.K., Nair, U., Betts, R., Fall, S., Reichstein, M., Kabat, P., de Noblet, N., 2011. Land use/land cover changes and climate: modeling analysis and observational evidence. Wiley Interdisciplinary Reviews-Climate Change 2(6): 828-850.

Pinheiro, J., Bates, D., DebRoy, S., Sarkar, D., Team, R.D.C., 2011. nlme: Linear and nonlinear mixed effects models.

Pitman, A.J., 2003. The evolution of, and revolution in, land surface schemes designed for climate models. International Journal of Climatology 23(5): 479-510.

Ponce-Reyes, R., Reynoso-Rosales, V.-H., Watson, J.E.M., VanDerWal, J., Fuller, R.A., Pressey, R.L., Possingham, H.P., 2012. Vulnerability of cloud forest reserves in Mexico to climate change. Nature Climate Change 2(6): 448-452.

Ponette-Gonzalez, A.G., Weathers, K.C., Curran, L.M., 2010. Water inputs across a tropical montane landscape in Veracruz, Mexico: Synergistic effects of land cover, rain and fog seasonality, and interannual precipitation variability. Global Change Biology 16(3): 946-963.

Poyatos, R., Čermák, J., Llorens, P., 2007. Variation in the radial patterns of sap flux density in pubescent oak (*Quercus pubescens*) and its implications for tree and stand transpiration measurements. Tree Physiology 27(4): 537-548.

Ray, D.K., Nair, U.S., Lawton, R.O., Welch, R.M., Pielke, R.A., 2006. Impact of land use on Costa Rican tropical montane cloud forests: Sensitivity of orographic cloud formation to deforestation in the plains. Journal of Geophysical Research-Atmospheres 111(D2).

Reinhardt, K., Smith, W.K., 2008. Impacts of cloud immersion on microclimate, photosynthesis and water relations of *Abies fraseri* (Pursh.) Poiret in a temperate mountain cloud forest. Oecologia 158(2): 229-238.

Richardson, A.D., Denny, E.G., Siccama, T.G., Lee, X., 2003. Evidence for a rising cloud ceiling in eastern North America. Journal of Climate 16(12): 2093-2098.

Ritter, A., Regalado, C.M., Aschan, G., 2009. Fog reduces transpiration in tree species of the Canarian relict heath-laurel cloud forest (Garajonay National Park, Spain). Tree Physiology 29(4): 517-528.

Roberts, J., Pitman, R.M., Wallace, J.S., 1982. A comparison of evaporation from stands of Scots pine and Corsican pine in Thetford Chase, East Anglia. Journal of Applied Ecology 19(3): 859-872.

Roberts, J., 1983. Forest transpiration: A conservative hydrological process? Journal of Hydrology 66(1–4): 133-141.

Rosado, B.H.P., Holder, C.D., 2012. The significance of leaf water repellency in ecohydrological research: A review. Ecohydrology 6(1): 150-161.

Ryan, M.G., Bond, B.J., Law, B.E., Hubbard, R.M., Woodruff, D., Cienciala, E., Kucera, J., 2000. Transpiration and whole-tree conductance in ponderosa pine trees of different heights. Oecologia 124(4): 553-560.

Rzedowski, J., 1978. Vegetación de México. Limusa, Mexico D.F.

Sachs, L., 1984. Applied statistics: A handbook of techniques. Springer-Verlag, New York, 707 pp.

Sakuratani, T., 1981. A heat balance method for measuring water flux in the stem of intact plants. Journal of Agricultural Meteorology 37: 9-17.

Sánchez-Velásquez, L.R., Pineda-López, M.R., Galindo-González, J., Díaz-Fleischer, F., Zúñiga González, J.L., 2009. Opportunity for the study of critical successional processes for the restoration and conservation of mountain forest: The case of mexican pine plantations. Interciencia 34(7): 518-522.

Saveyn, A., Steppe, K., Lemeur, R., 2008. Spatial variability of xylem sap flow in mature beech (*Fagus sylvatica*) and its diurnal dynamics in relation to microclimate. Botany-Botanique 86(12): 1440-1448.

Schawe, M., Glatzel, S., Gerold, G., 2007. Soil development along an altitudinal transect in a Bolivian tropical montane rainforest: Podzolization vs. hydromorphy. Catena 69(2): 83-90.

Scott, D.F., Bruijnzeel, L.A., Mackensen, J., 2005. The hydrological and soil impacts of forestation in the tropics. In: Bonell, M.,Bruijnzeel, L.A. (Eds.), Forests, water and people in the humid tropics. Cambridge University Press, Cambridge.

Scullion, J., Thomas, C.W., Vogt, K.A., Perez-Maqueo, O., Logsdon, M.G., 2011. Evaluating the environmental impact of payments for ecosystem services in Coatepec (Mexico) using remote sensing and on-site interviews. Environmental Conservation 38(4): 426-434.

Senock, R.S., Ham, J.M., 1995. Measurements of water-use by prairie grasses with heat-balance sap flow gauges. Journal of Range Management 48: 150-158.

Shuttleworth, W.J., 2012. Terrestrial hydrometeorology. Wiley-Blackwell, Oxford.

Silver, W.L., Scatena, F.N., Johnson, A.H., Siccama, T.G., Sanchez, M.J., 1994. Nutrient availability in a montane wet tropical forest - Spatial patterns and methodological considerations. Plant and Soil 164(1): 129-145.

Simonin, K.A., Santiago, L.S., Dawson, T.E., 2009. Fog interception by *Sequoia sempervirens* (D. Don) crowns decouples physiology from soil water deficit. Plant Cell and Environment 32(7): 882-892.

Smith, W.K., Hinckley, T.M. (Eds.), 1995. Resource physiology of conifers. Academic Press, San Diego. 396 pp.

Smith, W.K., McClean, T.M., 1989. Adaptive relationship between leaf water repellency, stomatal distribution, and gas-exchange. American Journal of Botany 76(3): 465-469.

Spittlehouse, D.L., Black, T.A., 1981. A growing season water balance model applied to 2 Douglas fir stands. Water Resources Research 17(6): 1651-1656.

Steppe, K., De Pauw, D.J.W., Doody, T.M., Teskey, R.O., 2010. A comparison of sap flux density using thermal dissipation, heat pulse velocity and heat field deformation methods. Agricultural and Forest Meteorology 150(7-8): 1046-1056.

Stewart, J.B., 1988. Modeling surface conductance of pine forest. Agricultural and Forest Meteorology 43(1): 19-35.

Still, C.J., Foster, P.N., Schneider, S.H., 1999. Simulating the effects of climate change on tropical montane cloud forests. Nature 398(6728): 608-610.

Still, C.J., Riley, W.J., Biraud, S.C., Noone, D.C., Buenning, N.H., Randerson, J.T., Torn, M.S., Welker, J., White, J.W.C., Vachon, R., Farquhar, G.D., Berry, J.A., 2009. Influence of clouds and diffuse radiation on ecosystem-atmosphere CO_2 and $CO^{18}O$ exchanges. Journal of Geophysical Research-Biogeosciences 114.

Swanson, R.H., 1994. Significant historical developments in thermal methods for measuring sap flow in trees. Agricultural and Forest Meteorology 72(1-2): 113-132.

Tallis, H., Kareiva, P., Marvier, M., Chang, A., 2008. An ecosystem services framework to support both practical conservation and economic development. Proceedings of the National Academy of Sciences of the United States of America 105(28): 9457-9464.

Tardif, R., Rasmussen, R.M., 2007. Event-based climatology and typology of fog in the New York City region. Journal of Applied Meteorology and Climatology 46(8): 1141-1168.

Thom, A.S., 1975. Momentum, mass and heat exchange of plant communities. In: Press, A. (Ed.), Vegetation and the Atmosphere, London, pp. 55-109.

Valtierra Pacheco, E., Magana Torres, O.S., Vanegas López, M., Lozano Contreras, M.d.P., Hernández González, C.M., Fierro Pérez, L.H., 2008. Evaluación externa de los apoyos de reforestación 2007, Colegio de Posgraduados, Mexico.

Van der Molen, M.K., Dolman, A.J., Waterloo, M.J., Bruijnzeel, L.A., 2006. Climate is affected more by maritime than by continental land use change: A multiple scale analysis. Global and Planetary Change 54(1-2): 128-149.

Vela, L., 1990. Contribución a la ecología de *Pinus patula*, Subsecretaría Forestal y Recursos Hidráulicos, Instituto Nacional de Investigación Forestales, Mexico D.F.

Vertessy, R.A., Watson, F.G.R., O'Sullivan, S.K., 2001. Factors determining relations between stand age and catchment water balance in mountain ash forests. Forest Ecology and Management 143(1-3): 13-26.

Viviroli, D., Durr, H.H., Messerli, B., Meybeck, M., Weingartner, R., 2007. Mountains of the world, water towers for humanity: Typology, mapping, and global significance. Water Resources Research 43(7).

Vogelmann, H., 1973. Fog precipitation in the cloud forests of eastern Mexico. Bioscience 23: 96-100.

Vose, J. M. and H. L. Allen. 1988. Leaf area, stemwood growth, and nutrition relationships in loblolly pine. Forest Science 34: 547-563.

Waring, R.H., Roberts, J.M., 1979. Estimating water flux through stems of Scots pine with tritiated water and P-32. Journal of Experimental Botany 30(116): 459-471.

Waterloo, M.J., Bruijnzeel, L.A., Vugts, H.F., Rawaqa, T.T., 1999. Evaporation from *Pinus caribaea* plantations on former grassland soils under maritime tropical conditions. Water Resources Research 35(7): 2133-2144.

Wedler, M., Heindl, B., Hahn, S., Kostner, B., Bernhofer, C., Tenhunen, J.D., 1996. Model-based estimates of water loss from "patches" of the understory mosaic of the Hartheim Scots pine plantation. Theoretical and Applied Climatology 53(1-3): 135-144.

Williams, J.W., Jackson, S.T., Kutzbacht, J.E., 2007. Projected distributions of novel and disappearing climates by 2100 AD. Proceedings of the National Academy of Sciences of the United States of America 104(14): 5738-5742.

Wolf, S., Eugster, W., Majorek, S., Buchmann, N., 2011. Afforestation of tropical pasture only marginally affects ecosystem-scale evapotranspiration. Ecosystems 14(8): 1264-1275.

Wullschleger, S.D., King, A.W., 2000. Radial variation in sap velocity as a function of stem diameter and sapwood thickness in yellow-poplar trees. Tree Physiology 20(8): 511-518.

Zadroga, F., 1981. The hydrological importance of a montane cloud forest area of Costa Rica. In: Lal, R.,Russel, E.W. (Eds.), Tropical Agriculatural Hydrology. John Wiley, New York, pp. 59-73.

Zeppel, M.J.B., Murray, B.R., Barton, C., Eamus, D., 2004. Seasonal responses of xylem sap velocity to VPD and solar radiation during drought in a stand of native trees in temperate Australia. Functional Plant Biology 31(5): 461-470.

Zhang, K., Kimball, J.S., Nemani, R.R., Running, S.W., 2010. A continuous satellite-derived global record of land surface evapotranspiration from 1983 to 2006. Water Resources Research 46.

Zhang, L., Dawes, W.R., Walker, G.R., 2001. Response of mean annual evapotranspiration to vegetation changes at catchment scale. Water Resources Research 37(3): 701-708.

Zimmermann, R., Schulze, E.D., Wirth, C., Schulze, E.E., McDonald, K.C., Vygodskaya, N.N., Ziegler, W., 2000. Canopy transpiration in a chronosequence of Central Siberian pine forests. Global Change Biology 6(1): 25-37.

Zuur, A.F., Ieno, E.N., Walker, N.J., Saveliev, A.A., Smith, G.M., 2009. Mixed effects models and extensions in ecology with R. Springer, New York, 574 pp.

APPENDICES

APPENDIX A

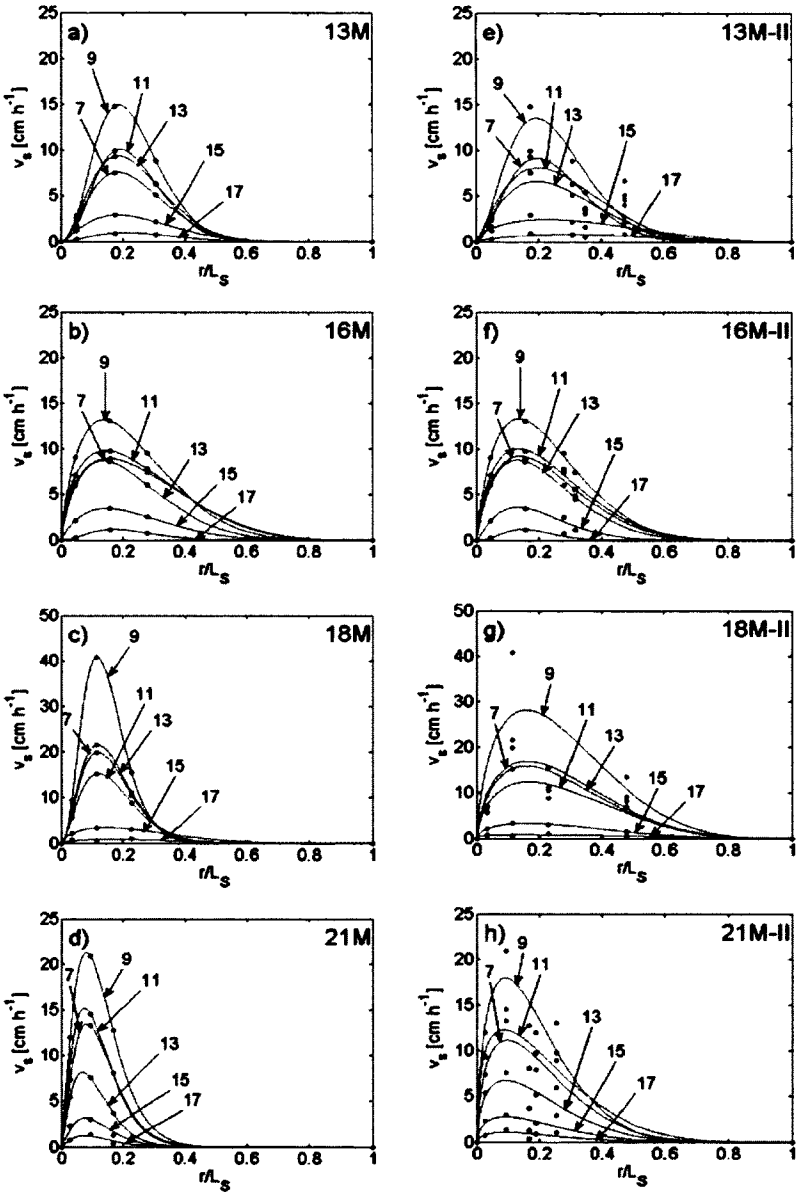

Figure A1. Additional examples of radial profiles of sap velocity (v_S) of mature *Pinus patula* trees during a sunny day. Panels a-d show profiles characterized with only three v_S data points (Dataset I), and e-h show the same trees and during the same day, only with additional points deeper into their sapwood (Dataset I+II). Tree ID's are shown in each panel. Numbers with arrows indicate the hour of day and dots depict v_S data points and added zero velocity points at the cambium-sapwood (r/L_S=0) and sapwood-heartwood (r/L_S =1) interfaces. Lines show the fitted Beta-pdf to data points where $r^2 \geq 0.90$.

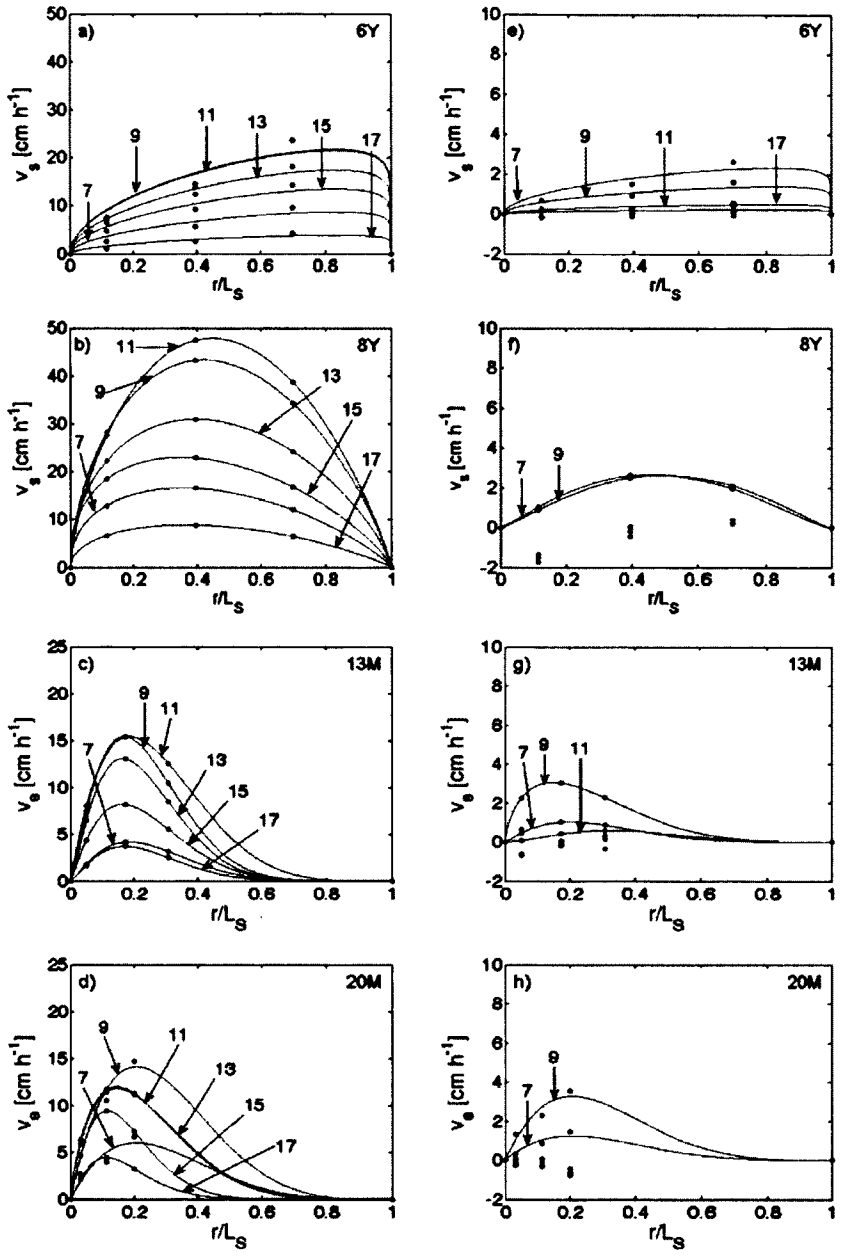

Figure A2. Additional examples of the hourly dynamics of the radial profile of sap velocity (v_s) of *Pinus patula* trees during typical dry season conditions in the cloud forest zone of central Veracruz, Mexico. Panels a-d show a sunny day (28 Feb 2009), while e-h show the following day in which a cloud immersion event occurred from 9 am. Tree ID's are shown in each panel. Trees selected represent the tree-to-tree variation in lumped shape parameter (ρ) characterizing radial profiles (Figure 5) as well as different % of sapwood depth sampled (Fig. 1). Numbers with arrows indicate the hour of day and dots depict v_S data points (Dataset I) and added zero velocity points at the cambium-sapwood ($r/L_S = 0$) and sapwood-heartwood ($r/L_S = 1$) interfaces. Lines show the fitted Beta-pdf to data points where $r^2 \geq 0.90$.

APPENDIX B

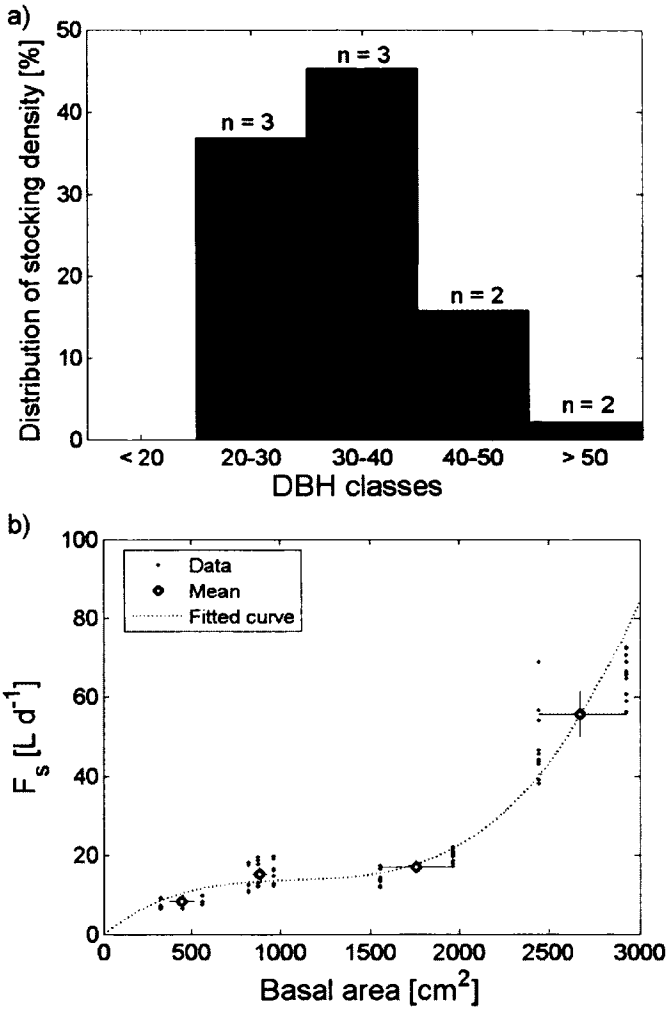

Figure B1. (a) Frequency distribution of stocking density by DBH classes for the mature *Pinus patula* plantation (MREF). n = number of sample trees instrumented with Heat Ratio Method sapflow probes. (b) Relationship between basal area and daily totals of whole-tree sapflow (F_s [L day^{-1} $tree^{-1}$]) of mature *P. patula* trees for days with near clear-sky. Open circles show mean F_s for each DBH class and the continuous line depict the best non-linear fit for the means, bounded at the origin.

APPENDIX C

1. LAI from destructive measurements of pasture and MREF's understory

Estimates of leaf area index (LAI) for PAS and the understory of MREF were obtained by destructively sampling the dominant vegetation. Briefly, in several randomly selected sampling points at each site, all the foliage within a frame of known area was collected, projected leaf area (LA) of fresh subsamples was determined with a LI-3100C leaf area meter (LI-COR), and lastly, subsamples and all foliage collected were oven-dried and weighted. The ratio of LA to leaf dry mass (or specific leaf area –SLA [m^2 kg^{-1}]) was determined for each subsample and LAI [m^2 m^{-2}] was computed as: SLA * total dry mass / area of the frame.

The frame used in PAS was a ring with an inner area of 53.5 cm^2 and a total of 10 samples were taken only once during late DS10. The subsamples consisted of about 10 green leaves and the resulting SLA ± SD was 13.1 ± 2.2 m^2 kg^{-1}. And on average ± SD, LAI was 1.2 ± 0.4 m^2 m^{-2}.

At MREF, only *Miconia glaberrima*'s LAI was estimated and a square frame with an inner area of 0.25 m^2 was used. The frame had strings and weights attached to each corner such that it could be elevated above the shrubs projecting the frame's area and delimiting the foliage to be collected. The frame was positioned at random by throwing the frame at 10 different shrub conglomerates and it was leveled above the foliage using a hand level. The SLA ± SD was 14.1 ± 1.5 m^2 kg^{-1} and LAI was 2.8 ± 1.4 m^2 m^{-2}.

2. LAI from PAR attenuation and LAI-2000 measurements at YREF and MREF

Continuous measurements of photosynthetically active radiation (PAR [μmol s^{-1} m^{-2}]) were obtained above (PAR_a) and below the canopy (PAR_b) at YREF throughout the study period. Above-the-canopy data were obtained with a LI-190SL quantum point sensor (LI-COR) installed on a metallic tower, while below-the-canopy data were collected with a LI-191SL quantum line sensor (LI-COR) installed on a leveled wooden bench at ~30cm from the ground and with a NS orientation. Due to logistical constraints, only PAR_b measurements were possible at MREF (starting in late Feb 2009), and the LI-191SL sensor was installed as in YREF. PAR_a at MREF was therefore obtained from R_s measured at the nearby weather station using an empirical linear model relating R_s and PAR_a derived with YREF data: $PAR_a = 1.64R_s$ (fixed bound at the origin; $r^2 = 0.90$; RSME = 192). This relationship was also used to fill gaps in PAR_a data from YREF (15% of the study period).

Mean canopy transmittance (τ) for YREF and MREF was calculated by dividing PARb by PARa using the average of hourly values between 11:00 and 14:00 under near-clear sky conditions (i.e. near-zero cloudiness factor; Appendix E), and subsequently converted to LAI using the Beer-Lambert Law and an extinction coefficient (k) of 0.52 (midpoint in the range k reported for conifer canopies; cf. (Pierce and Running, 1988)): $LAI = -\ln(\tau)/k$. Only early dry-season values (Nov–Feb) were used because PAR_b data became noisier from March on (Fig. C1 and C2; this was noted also in Pierce and Running, 1988). An average LAI value for each dry season was then derived with this approach as reported in Chapter 2 (Table 1).

A LAI-2000 plant canopy analyzer (LI-COR) was also available during DS10 and used to derive LAI based on diffuse light attenuation. Two grids of 10 m x 10 m per site were set up, and ten randomly selected points within the grids were measured during 3 different days (under overcast conditions or after sunset) following the manufacturer's instructions for one sensor mode. A correction factor of 1.6 for as recommended to account for clumpiness of conifer canopies (Gower and Norman, 1991).

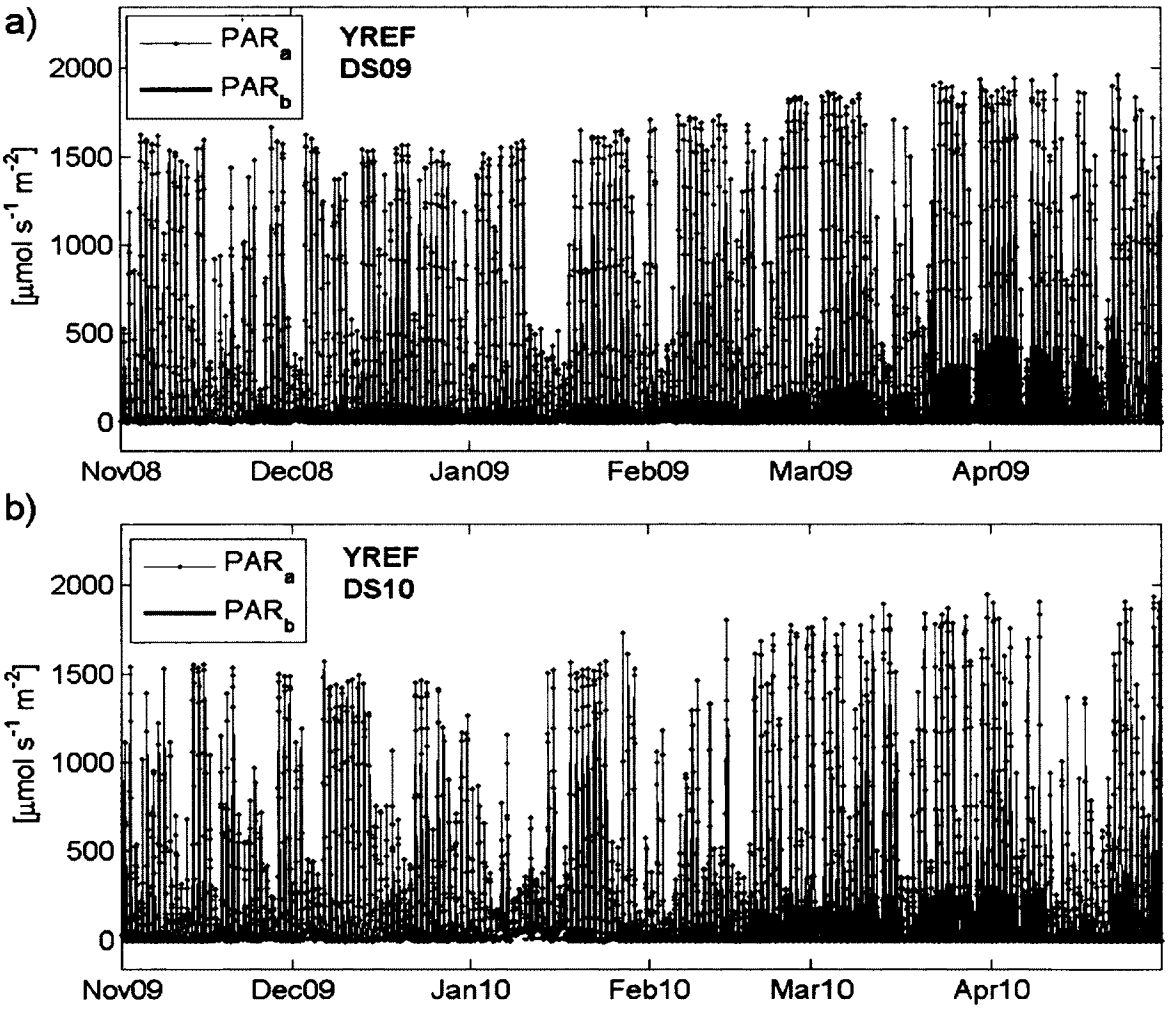

Figure C1. Hourly values of photosynthetically active radiation above (PAR_a) and below the canopy (PAR_b) measured at YREF during the dry seasons of 2008/09 (DS09) and 2009/2010 (DS10).

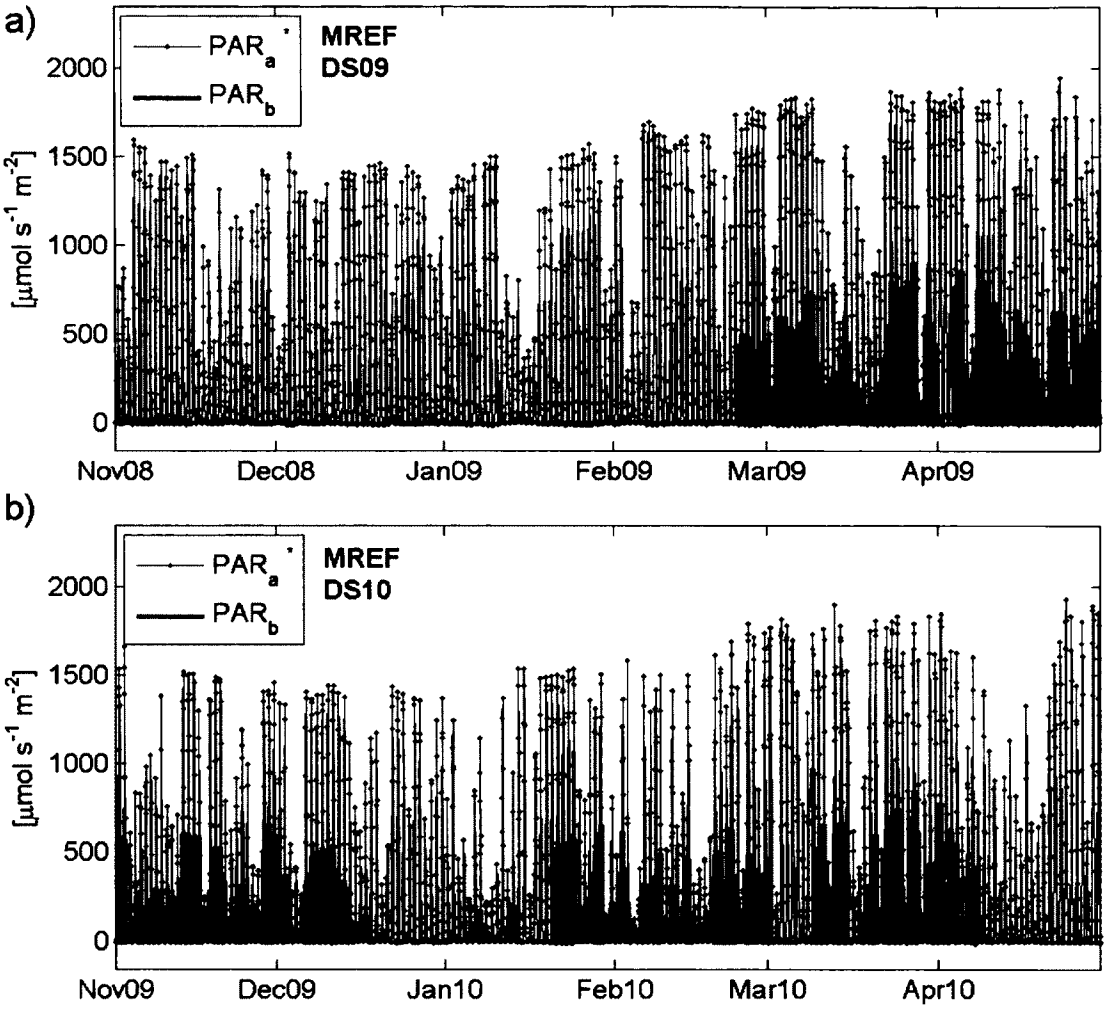

Figure C2. Hourly values of photosynthetically active radiation above (PAR_a*) and below the canopy (PAR_b) measured at MREF during the dry seasons of 2008/09 (DS09) and 2009/2010 (DS10). * PAR_a was modeled using R_s from the Tierra Grande weather station and using the regression developed for analogous measurements at YREF: $PAR_a = 1.64R_s$.

APPENDIX D

Soil characterization and (calibrated) soil moisture dynamics

Pits for soil characterization, soil sample collection and installation of soil moisture probes were dug down to ~1.5 m deep next to the sapflow monitoring plots in YREF (1 pit) and MREF (2 pits, ca. 100 m apart), and next to the mast with meteorological equipment in PAS (Fig. D1a-b). Soil characterization and determination of soil hydraulic properties were conducted by Dr. Daniel Geissert and Dr. Alberto Gómez-Tagle (Soil Laboratory, Instituto de Ecologia A.C., Xalapa, Veracruz); selected data is provided Table D1. After the completion of the study period, the pits were reopened and soil moisture probes were extracted together with the surrounding volume of soil (~$3x10^{-3}$ m^3) using PVC cylinders (Fig. D1c). This was done to calibrate raw readings from soil moisture probes (Campbel Scientific S616 and Decagon EC5) as recommended for volcanic soils (Frumau et al., 2006). Simultaneous probe readings and gravimetric determination of soil moisture were conducted by Dr. Geissert and Edgar Hincapié at the Soil Laboratory, Instituto de Ecología A.C. (Fig. D1d) to develop site- and depth-specific calibration equations following the protocol described in (Frumau et al., 2006). Table D2 and D3 provide the resulting equations for all probes used in this study.

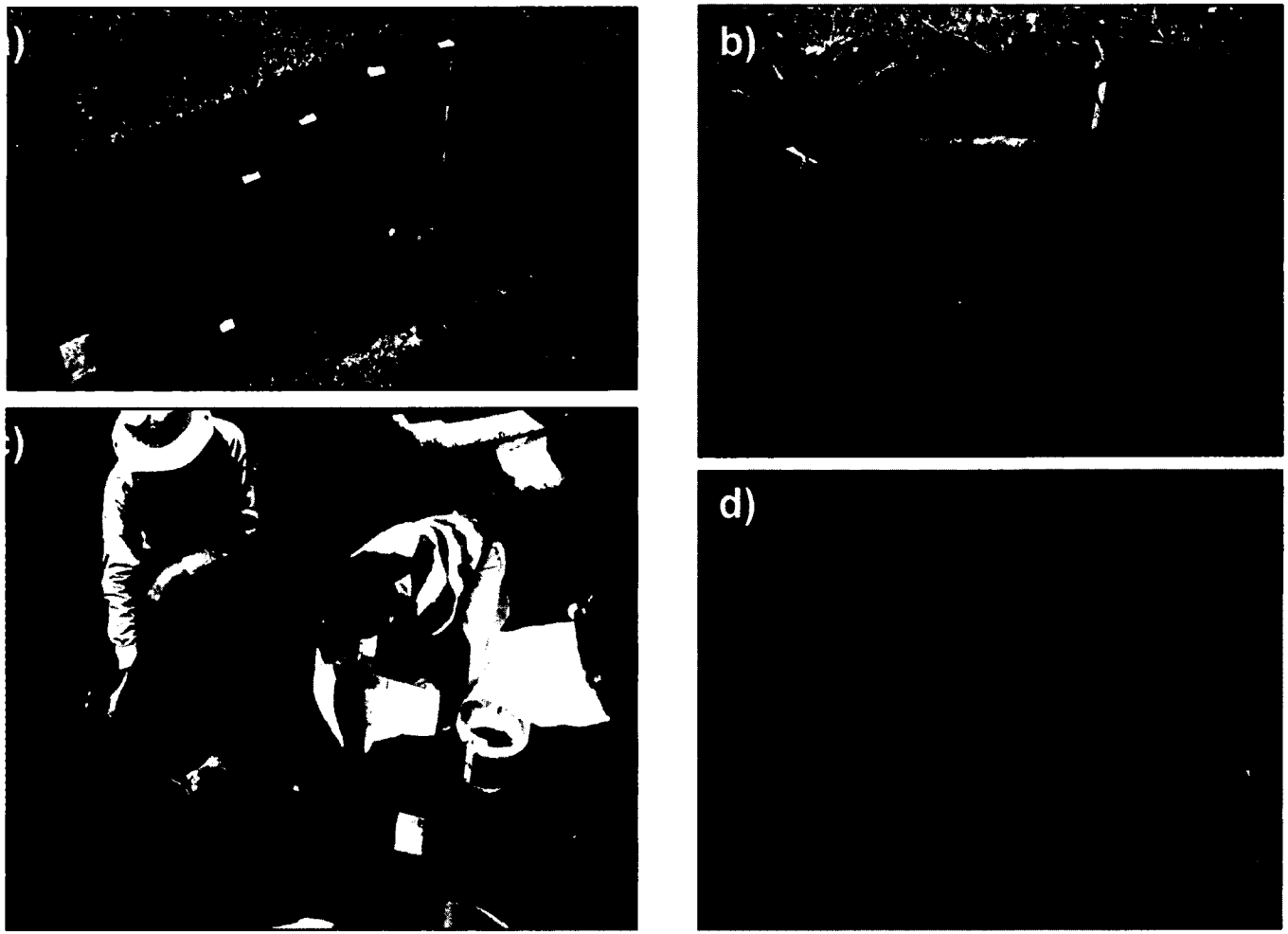

Figure D1. Examples of soil moisture probes installation and calibration procedure. (a) S616 probes installed at PAS. (b) EC5 probes installed in MREF2 (c) Extraction of soil moisture probes together with surrounding soil volume at PAS. (d) Laboratory set-up for calibration equation determination at the Soil Laboratory of Instituto de Ecología, A.C., Xalapa, Veracruz.

Table D1. Characteristics of soil horizons down to ~1.5 m. *K*sat = saturated hydraulic conductivity; FC = field capacity; PWP = permanent wilting point; NA = not available.

Site	Soil type [b]	Depth [cm]	Horizon	Bulk density [g cm^{-3}]	Total porosity [%]	*K*sat [cm h^{-1}]	θ at FC [cm^3 cm^{-3}]	θ at PWP [cm^3 cm^{-3}]	Roots [# cm^{-2}] [c]	dwu [cm] [d]
PAS [a]	Humic	5	Ah	0.42	72	1.87	0.53	0.41	2	NA
	Andisol	10	Ah	0.51	72	1.87	0.55	0.41	1.2	
		15	Ah	0.38	72	1.87	0.39	0.28	1.1	
		30	Bh	0.30	82	6.42	0.59	0.47	0.3	
		100	Bh	0.53	82	6.42	0.78	0.63	0.1	
YREF	Aluandic	5	A1	0.32	NA	NA	0.42	0.30	1.3	20-50
	Andosol	19	A2	0.33	86.1	65.4	0.42	0.30	0.8	
	Dystric	36	A3	0.28	85.3	22.88	0.53	0.46	0.8	
		70	Bw	0.28	87.4	38.22	0.54	0.49	0.5	
		123	BwC	0.33	85.7	14.05	0.63	0.58	0.2	
MREF1	Silandic	10	A1	0.57	75.6	12.03	0.45	0.35	1	20-50
	Andosol	35	A2	0.40	82.6	36.24	0.48	0.41	0.5	
	Dystric	58	A3-Bw	0.37	83.9	30.38	0.60	0.55	0.3	
		85	2A1	0.40	83.3	27.22	0.52	0.44	0.1	
		115	2Bw	0.41	82.9	11.66	0.54	0.46	0.02	
MREF2	Silandic	10	A1	0.56	77.0	27.2	0.41	0.26	1	20-50
	Andosol	25	2A1	0.42	82.6	24.22	0.41	0.26	0.5	
	Colluvic	40	2Bw	0.36	84.7	6.27	0.41	0.26	0.3	
	Dystric	87	3A1	0.43	82.3	5.2	0.60	0.54	0.05	
		115	3Bw	0.42	81.7	1.8	0.63	0.58	0	

[a] Soil type, horizon, total porosity and *K*sat from (Geris, 2007).
[b] (WRB, 2006)
[c] Count of fine roots (diameter < 2 mm) inside a 12 cm^2 frame randomly relocated three times per horizon on the clean wall of the pit.
[d] Depth of water uptake inferred from stable isotopes analyses of soil and xylem water (Goldsmith et al., 2012).

Table D2. Probe specific calibration equations to estimate volumetric soil water content (θ [cm^3 cm^{-3}]) from raw data (dielectric constant –K) measured with S616 probes (Campbell Scientific).

Site	Depth [cm]	Calibration equation	% bias [a]
PAS	5	$-3x10^{-4} K^3 + 3x10^{-2} K^2 - 1 K + 11.5$	-20%
	10	$1x10^{-4} K^3 - 0.01 K^2 + 0.3 K - 3.3$	-27%
	15	$-3x10^{-4} K^3 + 0.03 K^2 - 0.8 K + 9.2$	-28%
	30	$3x10^{-4} K^3 - 0.03 K^2 + 0.9 K - 10.2$	-26%
	100	$-3x10^{-4} K^3 + 0.03 K^2 - 0.9 K + 10.2$	-4%
YREF	5	$-2x10^{-4} K^3 + 2x10^{-2} K^2 - 0.7 K + 7.30$	-32%
	19	$-4x10^{-4} K^3 + 3x10^{-2} K^2 - 1.1 K + 11.30$	-31%
	36	$2x10^{-4} K^3 - 2x10^{-2} K^2 + 0.7 K - 8.88$	-33%
	70	$-6x10^{-5} K^3 + 6x10^{-3} K^2 - 0.1 K + 1.6$	-26%
	123	$3x10^{-4} K^3 - 3x10^{-2} K^2 + 1.0 K - 11.73$	-27%

[a] Mean bias from θ calculated with equation provided by manufacturer.

Table D3. Probe specific calibration equations to estimate volumetric soil water content (θ [cm^3 cm^{-3}]) from raw data (dielectric permittivity –RC) measured with EC5 probes (Decagon).

Site	Depth [cm]	Calibration equation	% bias [a]
MREF1	10	$4x10^{-9} RC^3 - 1x10^{-5} RC^2 + 1x10^{-2} RC - 4.9$	-38%
	35	$6x10^{-8} RC^3 - 2x10^{-4} RC^2 + 0.3 RC - 118.7$	-50%
	58	$2x10^{-8} RC^3 - 8x10^{-5} RC^2 + 0.1 RC - 51.0$	-43%
	85	$6x10^{-9} RC^3 - 2x10^{-5} RC^2 + 3x10^{-2} RC - 12.8$	-47%
	115	$7x10^{-8} RC^3 - 3x10^{-4} RC^2 + 0.4 RC - 188.8$	-47%
MREF2	10	$2x10^{-8} RC^3 - 7x10^{-5} RC^2 + 0.1 RC - 41.3$	-31%
	25	$-7x10^{-8} RC^3 + 3x10^{-4} RC^2 - 0.4 RC + 205.7$	-39%
	40	$3x10^{-8} RC^3 - 1x10^{-4} RC^2 + 0.1 RC - 66.0$	-21%
	87	$4x10^{-8} RC^3 - 2x10^{-4} RC^2 + 0.3 RC - 123.2$	-34%
	115	$2x10^{-8} RC^3 - 9x10^{-5} RC^2 + 0.1 RC - 59.6$	-39%

[a] Mean bias from θ calculated with equation provided by manufacturer.

APPENDIX E

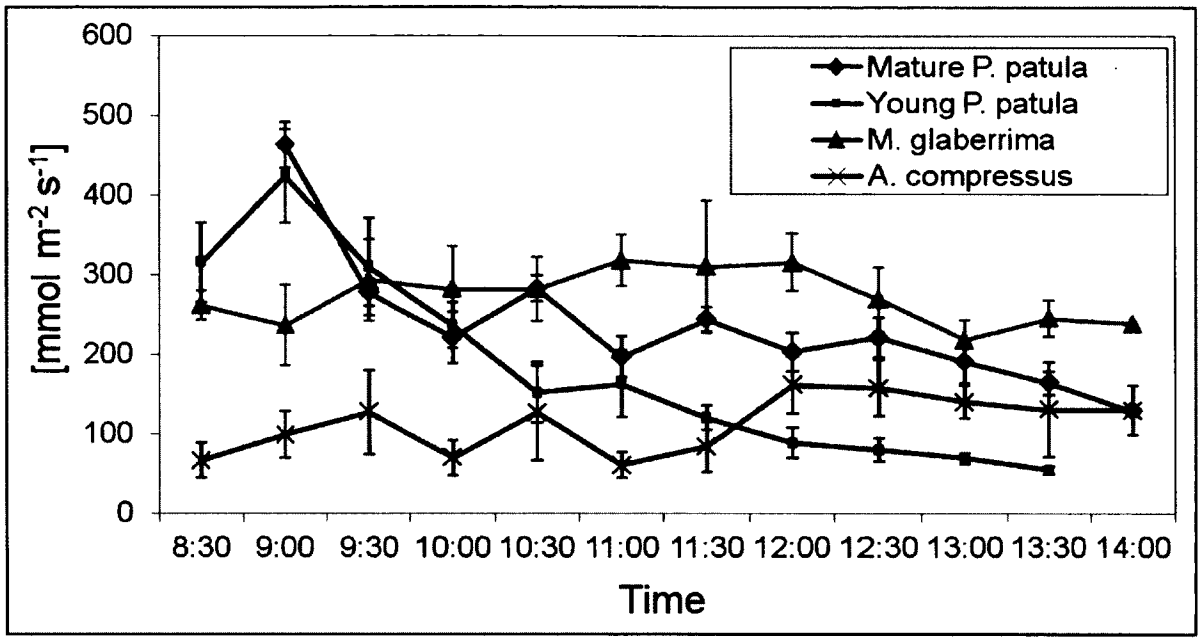

Figure E1. Hourly leaf-level stomatal conductance for young and mature *Pinus patula* trees, *Miconia glaberrima* shrubs (understory of the mature *P. patula* plantation) and *Axonopus compressus* (pasture) taken during dry-season days with clear sky. Symbols are mean (and error bars, standard error) of measurements on 5 individual trees/shrubs or 10 individual grass blades obtained with a SC-1 Leaf Porometer; Decagon. Selected *P. patula* needles were from exposed branches. The metallic tower installed at YREF was used for access to the top of the canopy. At MREF, access to the canopy at the site of sapflow monitoring was not possible. Therefore, sparse mature trees (with similar DBH ranges as sapflow sample trees) growing at a pasture site nearby (~200 m away from the sapflow plots) were measured.

APPENDIX F

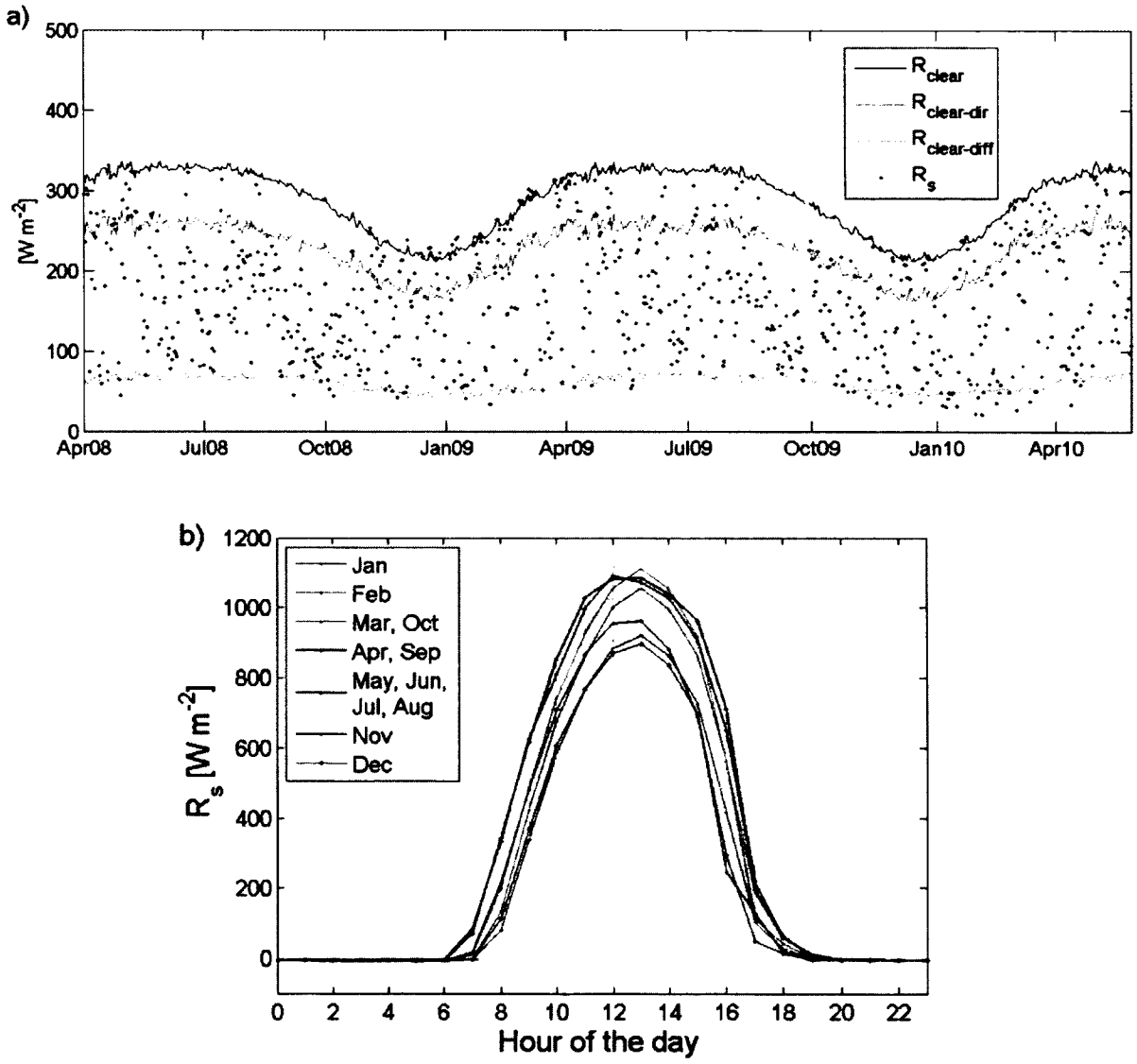

Figure E1. (a) Daily values of theoretical clear-sky incident short-wave radiation (R_{clear} [W m^{-2}]; cf. (Dingman, 2008)) disaggregated into direct and diffuse components ($R_{clear\text{-}dir}$ and $R_{clear\text{-}diff}$, respectively), and measured daily incoming short-wave radiation (R_s [W m^{-2}]) from April 2008 to May 2010 as observed at 2180 m a.s.l. in central Veracruz, Mexico (19.4931° N, 97.0422° W). (b) Month-specific mean diurnal courses of R_s as observed during clear-sky, or 'golden days' (i.e. days when $R_s \geq R_{clear}$). R_{s_golden} represents maximum hourly R_s expected for each month and used to compute hourly a relative cloudiness factor as: $(R_{s\_golden} - R_s) / R_{s\_golden}$. Error bars are one standard deviation.